UNIVERSITÀ
DI PARMA

UNIVERSITÀ DEGLI STUDI DI PARMA

DOTTORATO DI RICERCA IN

FISICA

CICLO XXXVI

Confronting Large Fluctuations in Numerical Stochastic Perturbation Theory

Coordinatore:

Prof.ssa Raffaella Burioni

Tutore:

Prof. Francesco Di Renzo

Dottorando:

Dott. Paolo Baglioni

Anni Accademici 2020/2021 – 2022/2023

Abstract

Perturbation theory is universally recognized as a fundamental tool in modern theoretical physics. In functional integral formalism, perturbation theory provides a method for studying field theories, offering both mathematical rigor and substantial physical insights. It is challenging to name an area of theoretical physics where perturbation theory does not play a fundamental role: even in theories specifically designed for a non-perturbative approach like lattice gauge theories, perturbation theory remains relevant and interesting. Lattice gauge theories offer a powerful framework for understanding non-perturbative aspects of quantum field theories. By discretizing space-time on a lattice, these theories enable detailed Monte Carlo simulations that are crucial for probing phenomena beyond the reach of perturbation theory, shedding light on subtle features such as quark confinement in QCD and many others. In the mid-1990s, a new method was developed that in a sense integrates traditional perturbation theory with Monte Carlo simulations of lattice field theories (in particular lattice gauge theories, for which traditional diagrammatic perturbation theory is cumbersome). This approach is known as Numerical Stochastic Perturbation Theory (NSPT). NSPT offers a fully automated stochastic method for calculating loop corrections in lattice field theories, using the power of Monte Carlo simulations. Its numerical implementation requires minimal changes with respect to traditional Monte Carlo simulations; (also due to this) NSPT enables the calculation of loop corrections at very high perturbative orders. The ease of implementation and advanced capability explain why NSPT has captured the attention of lattice practitioners.
A not-well-explored feature of NSPT is the freedom to choose any vacuum for calculating perturbation theory, in principle without encountering the intricacies of the diagrammatic perturbation theory. If one had to make a natural choice, low-dimensional models are the best candidates for exploratory analysis of the feasibility of perturbative expansions on top of non-trivial vacua. This way, one immediately encounters problems: it is known that NSPT simulations exhibit large fluctuations in low-dimensional models. As the perturbative order increases, huge fluctuations show up, completely obscuring the signal at even not-so-high perturbative orders.

In this thesis, we discuss NSPT simulations for a class of highly interesting low-dimensional models, the two-dimensional $O(N)$ Non-Linear Sigma Models (NLSMs). $O(N)$ non-linear sigma models can be regarded as a valuable theoretical laboratory in quantum field theory, as they display in a relatively simple framework interesting features like asymptotic freedom. From a more phenomenology-oriented point of view, NLSM proved to be effective in modeling different features in different contexts. As we will see, in this work our interest in $O(N)$ models is motivated by the possibility of tuning N. On general grounds, we expect that

huge fluctuations in simulations of low-dimensional models are somehow connected to the limited number of degrees of freedom. From this perspective, $O(N)$ NLSMs are an ideal laboratory: in fact we can modify the number of degrees of freedom by tuning the parameter N. Our numerical results show that in the large N limit NSPT simulations are not affected by the large fluctuations issue at high orders, in contrast to what occurs in the small N regime. Our conclusions are supported by extensive numerical studies of the properties of NSPT distributions as function of the perturbative order n and the parameter N. While a fundamental comprehension is admittedly lacking, we will consider different indicators for assessing if (and to what extent) large enough N computations are to be regarded as safe at a given perturbative order n. In particular, the study of relative errors has been particularly fruitful: in this context, the onset of fluctuations has been probed through violations of very generally expected scaling behaviors. Our numerical simulations strongly suggest that indeed for each perturbative order n, an NSPT computation in $O(N)$ can always be found safe with respect to fluctuations if we take a large enough N. As a result, the larger the value of N, the more perturbative corrections we could compute, significantly extending the previously known results from lattice diagrammatic perturbation theory.

Once for large enough N high perturbative orders can be safely computed, we expect we can explore the asymptotic behavior of perturbative expansions. In the context of lattice gauge theories, NSPT has proven to be effective in probing infrared renormalons. In the final part of the thesis, we discuss $O(N)$ renormalon effects in the large N limit. We will perform computations on a pretty small lattice size, but we will provide new insight on the role of finite-volume effects. In particular, by explicitly taking into account the infrared cutoff, we obtained an analytic (first-principles) estimate of finite-volume effects, assessing how they modify the factorial scaling of coefficients. Once we have such modeling, we can compare analytical predictions and numerical results, finding agreement in the asymptotic perturbative region. We stress that this will be a parameter-free comparison (there is no space for any parameter to adjust). Large N NSPT simulations for $O(N)$ models can also be regarded as a preliminary step towards going back to perturbative expansions around non-trivial vacua. Quite interestingly, such computations in the (quite close) $CP(N-1)$ models are connected to resurgence scenarios.

Contents

1 Introduction to NSPT **2**

1.1 Stochastic Quantization . . . 2

1.1.1 Fokker-Plank formulation . . . 4

1.1.2 Solution of the Fokker-Plank equation . . . 6

1.2 Stochastic Perturbation Theory . . . 7

1.2.1 Free scalar field theory . . . 8

1.2.2 Diagrammatic stochastic perturbation theory . . . 10

1.3 Numerical Stochastic Perturbation Theory . . . 12

1.3.1 Monte Carlo methods . . . 12

1.3.2 From SQ(PT) to NSPT . . . 14

1.4 Numerical integration . . . 17

1.4.1 Euler Integrator . . . 17

1.4.2 Runge-Kutta Integrator . . . 20

1.5 Continuum stochastic time extrapolations . . . 24

1.6 Autocorrelations and cross-correlations . . . 25

1.6.1 Gamma Function Method for NSPT . . . 25

1.6.2 Blocking Method for NSPT . . . 29

1.7 Implementation on the computer . . . 30

1.8 Other stochastic differential equations . . . 31

1.8.1 HMD based NSPT . . . 31

1.8.2 Kramers based NSPT . . . 33

2 NSPT around Instantons **35**

2.1 Non-perturbative corrections from Instantons . . . 35

2.2 The Double Well Potential case . . . 36

2.2.1 Extracting the energy splitting . . . 36
2.2.2 Path integral approach . . . 38
2.3 Two-loop correction from NSPT . . . 43
2.3.1 Minimum action solutions on the lattice . . . 43
2.3.2 Faddev-Popov regularization . . . 46
2.3.3 Perturbative Free Energy . . . 50
2.3.4 Numerical Results . . . 53
2.4 Higher-order corrections and discussions . . . 57

3 High-order NSPT computations for $O(N)$ in the large N limit 59
3.1 Introduction to the large fluctuations problem . . . 59
3.2 $O(N)$ Non-Linear Sigma Model . . . 60
3.3 Perturbation theory setup . . . 61
3.3.1 One-loop computation . . . 63
3.3.2 Two-loop computation . . . 64
3.4 Perturbative computations with NSPT . . . 65
3.4.1 Cumulative moving averages and standard deviations . . . 72
3.4.2 Large N and Large L . . . 76
3.4.3 Relative error scaling . . . 78

4 $O(N)$ NLSM renormalons in the Large N limit 82
4.1 Infrared renormalons . . . 82
4.2 Finite volume corrections to renormalons . . . 84
4.3 Probing renormalons for $O(N)$ at large N . . . 87

5 Conclusions 89

Appendices 98

A Kramers-Moyal expansion 98

B Complete expression for the energy splitting (continuum theory) 99

C First-order correction to the propagator 103

D Leading-order zero-mode regularization 106

E Infrared corrections to the renormalon scaling at two-loops **108**

Preface

Motivations

Numerical Stochastic Perturbation Theory (NSPT) [1] is a computational tool that uses stochastic methods to perform perturbative calculations in quantum field theory. This technique employs lattice simulations to systematically compute series expansions in the coupling constant, providing high loop-order results in theories for which traditional diagrammatic perturbation theory is cumbersome (this is the case for Lattice QCD). NSPT has emerged as a key tool to explore perturbative and non-perturbative aspects in quantum chromodynamics (QCD) and other field theories.

Thirty years after its first appearance [2, 3], today a lot of experience with NSPT simulations has been accumulated, with contributions coming from many lattice practitioners. Once the possibility to compute perturbative expansions using Monte Carlo techniques has been established, NSPT has been applied to many problems. In particular, NSPT has proven to be effective in studying observables for which a very limited number of perturbative coefficients were known [4–8]. It was noticed that the introduction of dynamical fermions in Lattice QCD [9] results in a far smaller computational overhead than for non-perturbative Monte Carlo simulations. Furthermore, significant applications of NSPT also involve Lattice QED [10], and many others [11, 12]. Later on, we will see how NSPT has been precious in probing the asymptotic behavior dictated by infrared renormalons. It is quite funny that one can directly inspect such an asymptotic effect in a perturbative scheme (the lattice) for which it has been traditionally thought that going to high-orders was impossible.

In recent years there has been a growing interest in the study of alternative underlying stochastic processes for NSPT simulations. Although historically NSPT has been formulated as the systematic order-by-order integration of a Langevin stochastic process, there are now many versions of NSPT based on different stochastic equations. Beyond the theoretical importance

of recognising different legitimate formulations, variants of NSPT aim to use the technology derived from state-of-the-art Monte Carlo algorithms for non-perturbative simulations, such as GHMD-based algorithms [8, 13]. Furthermore, NSPT has been in a sense reinterpreted in deep connection with Automatic Differentiation [14].

Despite the three-decade-long literature, there are specific features of NSPT that have not yet been fully understood. This is the case of high-order perturbative NSPT simulations for low-dimensional models. It is a well-known fact that significant fluctuations in high-orders NSPT simulations show up for *small* systems (let's say much smaller than Lattice QCD) [15]. As a matter of fact, the onset of large fluctuations prevents a systematic study of perturbative coefficients in the asymptotic region for low-dimensional models. Many of these models are interesting. For example, NSPT expansions around non-trivial vacua are intriguing (it should be possible to formulate a weak coupling perturbation theory in a much easier way than in diagrammatic perturbation theory). While NSPT appears to be an ideal tool for computing high-order corrections on top of non-trivial vacua (a similar case has been worked out for Lattice QCD in the Schrödinger functional formalism [16]), one would attack at first low dimensional problems displaying non-trivial vacua to start from. Because of the fluctuations issue we mentioned, we currently lack these high-order computations.

Furthermore, low-dimensional models can be asymptotically free, and it would be interesting to study the asymptotic perturbative behavior, to verify their fundamental properties numerically. Infrared renormalons [17] are among the most interesting. NSPT is an excellent numerical framework for the detection of renormalon scaling, since renormalon analysis provides predictions in the asymptotic limit, requiring calculations at very high perturbative orders. As a matter of fact, renormalons have been studied with fruitful results in SU(3) gluodynamics [18–20] and Lattice QCD with massless staggered fermions [21] by means of NSPT simulations. Despite some success claimed for $PC(N)$ models [22], there has been no systematic attempt at assessing how good the assessment of renormalon behavior can be with respect to the onset of fluctuations in low-dimensional models.

In this thesis, we study NSPT simulations in low-dimensional models. As expected, we will see that large fluctuations emerge at (not even that) high-orders when attempting to expand a theory around non-trivial vacua in low-dimensional models. For this reason, we moved to study the $O(N)$ non-linear sigma model. In this model we varied the number of degrees of freedom by tuning the parameter N. Using $O(N)$ NSLMs we can probe a general conjecture that we have fewer problems simulating more degrees of freedom. This seems to be further justified by

the fact that NSPT distributions exhibit a trend towards Gaussianity in the large N limit at lower orders, as detailed in [11]. Furthermore, since the $O(N)$ model is asymptotically free, we can study the asymptotic scaling of perturbative coefficients, hunting for infrared renormalons. It is worth noting that the $CP(N-1)$ model, a natural extension of the $O(N)$ sigma model, displays instantons [23]. For all these reasons it is expected that a comprehensive study of NSPT simulations for the $O(N)$ sigma models will lead to insights of general interest regarding new possible NSPT applications.

Thesis organization

This thesis is organized as follows. In Sec. 1 we introduce the main aspects related to Numerical Stochastic Perturbation Theory. We adhere to the historical path that led to the first implementation of NSPT, starting from the Stochastic Quantization. Special emphasis is given to the statistical analysis of data. At the end of the section, alternative approaches using different stochastic equations are briefly discussed. In Sec. 2 we present a first example of an unconventional application of NSPT, which involves weak coupling expansion around instantonic vacua for a $0+1$-dimensional field theory: the Double-Well Potential. We discuss all the key aspects of this method, critically analyzing its limitations in relation both to the continuum limit and to the emergence of fluctuations. In Sec. 3 we show NSPT results for the lattice $O(N)$ non-linear sigma model. Particular attention was given to the perturbation theory setup. In this context, high-order spikes and statistical distributions were studied and related to the parameter N, which represents the number of degrees of freedom. In Sec. 4 we present a direct application of what we have learned from $O(N)$ NSPT simulations: the study of renormalons in low-dimensional models. Finite volume effects have been taken into account by introducing a first-principles estimate of the infrared cutoff in the factorial scaling of loop corrections. In Sec. 5 we report our conclusions, discussing future prospects and new immediate applications.

List of publications

Part of this work has been published in

- **Proceeding**

  1. [24] - P. Baglioni and F. Di Renzo, *Numerical Stochastic Perturbation Theory around instantons*, in *PoS* LATTICE22 (2023) Vol. 430 [2212.11240]
  2. [25] - P. Baglioni and F. Di Renzo, *NSPT for $O(N)$ non-linear sigma model: the larger N the better*, in 40th International Symposium on Lattice Field Theory, (2023) [2401.11833]

- **Publications**

  1. [26] - P. Baglioni and F. Di Renzo, *Large fluctuations in NSPT computations: a lesson from $O(N)$ non-linear sigma models*, (2024) [2402.01322].
  2. [27] - P. Baglioni and F. Di Renzo, *Large order computations in $O(N)$ non-linear sigma models: renormalons, finite size effects and all that - in preparation.*

- **Other Publications**

  In the last year of my PhD program, my expertise in Langevin equation took me to study another subject; in collaboration with the Complex Systems group in Parma, we numerically studied the effectiveness of a Bayesian effective action in describing fully-connected one-hidden layer neural networks.

  1. [28] - P. Baglioni, R. Pacelli, R. Aiudi, F. Di Renzo, A. Vezzani, R. Burioni and P. Rotondo, *Predictive power of a Bayesian effective action for fully-connected one hidden layer neural networks in the proportional limit*, (2024) [2401.11004].

1 | Introduction to NSPT

1.1 Stochastic Quantization

Stochastic Quantization (SQ) represents *per se* an original approach to field theory quantization. It was introduced in an innovative article by Parisi and Wu [29]. Since then, the method has evolved into an effective instrument across various domains of quantum field theory. As said, it can be regarded as yet another brand-new quantization scheme. This is particularly interesting in the framework of gauge theories, since in this context one could in principle stay away from the theoretical issue of how gauge fixing interacts with the construction of the theory (think about Gribov copies) [30]. At the same time, the Langevin equation on which SQ is based has been regarded as an alternative to standard Monte Carlo methods in the non-perturbative study of lattice quantum field theories. As we will see, we will be mainly interested in yet another aspect, namely SQ gives rise to a novel approach to perturbation theory. For a quite old review, which is still very interesting, see [31]. For the purposes of this thesis, we present its formulation explicitly targeting Euclidean scalar field theories.

Following the historical introduction of SQ, the starting point is the notable parallel between Euclidean quantum field theory and statistical mechanics: in straightforward terms, the Euclidean path integral measure is intimately linked to a statistical system at the equilibrium in accordance with the Boltzmann distribution. It follows that n-points Euclidean Green functions in the Path Integral (PI) formalism

$$\langle\varphi(\boldsymbol{x}_1)\varphi(\boldsymbol{x}_2)\dots\varphi(\boldsymbol{x}_n)\rangle = \frac{1}{Z}\int D\varphi \exp\left(-\frac{1}{\hbar}S_E\right)\varphi(\boldsymbol{x}_1)\varphi(\boldsymbol{x}_2)\dots\varphi(\boldsymbol{x}_n) \tag{1}$$

can be deduced as correlation functions of statistical systems. In Eq. (1), S_E represents the Euclidean action. By setting $1/\hbar = 1/kT$, Eq. (1) can be interpreted as a statistical expectation value for a system in thermal equilibrium at temperature T. From now on, we consider physical units $\hbar = 1$.

Solving a Euclidean quantum field theory means knowing how to compute correlation func-

tions in Eq. (1). This is typically challenging and starting from the path integral one could think of providing solutions in a variety of ways, ranging from Perturbation Theory (PT) to numerical simulation of a Lattice Regularization (LR) version of the theory. Stochastic Quantization offers an alternative formulation of the problem. The starting point is the passage to a system with one more degree of freedom than the original problem

$$\varphi(\boldsymbol{x}) \to \varphi(\boldsymbol{x}, \tau)\,. \tag{2}$$

Thinking of this extra degree of freedom as a time, we will prescribe an evolution of the fields such that the system is led to an equilibrium distribution as *stochastic* time τ progresses. The evolution of the scalar field $\varphi(\boldsymbol{x}, \tau)$ through stochastic time is governed by a stochastic differential equation, namely the Langevin equation

$$\frac{\partial \varphi(\boldsymbol{x}, \tau)_\eta}{\partial \tau} = -\frac{\delta S_E}{\delta \varphi(\boldsymbol{x}, \tau)_\eta} + \eta(\boldsymbol{x}, \tau)\,. \tag{3}$$

We note that the vanishing of the first term in the RHS of Eq. (3)

$$\frac{\delta S_E}{\delta \varphi(\boldsymbol{x}, \tau)} = 0 \tag{4}$$

selects the classical field equations, altered only to include τ-dependency. The last term in Eq. (3) is a Gaussian white noise with defined correlations, namely

$$\langle \eta(\boldsymbol{x}_1, \tau_1)\eta(\boldsymbol{x}_2, \tau_2)\rangle_\eta = 2\delta^{(n)}(\boldsymbol{x}_1 - \boldsymbol{x}_2)\delta(\tau_1 - \tau_2) \tag{5}$$

and in general

$$\langle \eta(\boldsymbol{x}_1, \tau_1) \dots \eta(\boldsymbol{x}_{2k+1}, \tau_{2k+1})\rangle_\eta = 0\,, \tag{6}$$

$$\langle \eta(\boldsymbol{x}_1, \tau_1) \dots \eta(\boldsymbol{x}_{2k}, \tau_{2k})\rangle_\eta = \sum_W \prod \langle \eta(\boldsymbol{x}_i, \tau_i)\eta(\boldsymbol{x}_j, \tau_j)\rangle_\eta\,, \tag{7}$$

being W the set of all possible Wick contractions. In this context, the expectation values $\langle \dots \rangle_\eta$ are defined as averages over all possible noise realizations

$$\langle \dots \rangle_\eta = \frac{\int D\eta \exp\left[-\frac{1}{4}\int d\tau d\boldsymbol{x}\ \eta^2(\boldsymbol{x}, \tau)\right] \dots}{\int D\eta \exp\left[-\frac{1}{4}\int d\tau d\boldsymbol{x}\ \eta^2(\boldsymbol{x}, \tau)\right]}\,. \tag{8}$$

Fields evolving according with Eq. (3) depend on the white noise realization (this motivates the subscript notation $\varphi(\boldsymbol{x}, \tau)_\eta$) and for a given stochastic realization a formal solution of Eq. (3) has the form

$$\varphi(\boldsymbol{x}, \tau)_\eta = \varphi(\boldsymbol{x}, \tau_0) - \int_{\tau_0}^{\tau} d\tau' \frac{\delta S}{\delta \varphi(\boldsymbol{x}, \tau')} + \int_{\tau_0}^{\tau} d\tau' \eta(\boldsymbol{x}, \tau')\,. \tag{9}$$

The main assertion of stochastic quantization is that in the limit of τ approaching infinity, equilibrium is achieved, and the equal-time correlation functions converge to the corresponding Green's functions in Eq. (1), that is to say

$$\lim_{\tau\to\infty}\langle\varphi(\boldsymbol{x}_1,\tau)_\eta\varphi(\boldsymbol{x}_2,\tau)_\eta\dots\varphi(\boldsymbol{x}_n,\tau)_\eta\rangle_\eta=\langle\varphi(\boldsymbol{x}_1)\varphi(\boldsymbol{x}_2)\dots\varphi(\boldsymbol{x}_n)\rangle\,, \tag{10}$$

being the correlation functions defined as follows

$$\langle\varphi(\boldsymbol{x}_1,\tau)_\eta\dots\varphi(\boldsymbol{x}_n,\tau)_\eta\rangle_\eta=\frac{\int D\eta\exp\left[-\frac{1}{4}\int d\tau d\boldsymbol{x}\ \eta^2(\boldsymbol{x},\tau)\right]\varphi(\boldsymbol{x}_1,\tau)_\eta\dots\varphi(\boldsymbol{x}_n,\tau)_\eta}{\int D\eta\exp\left[-\frac{1}{4}\int d\tau d\boldsymbol{x}\ \eta^2(\boldsymbol{x},\tau)\right]}\,. \tag{11}$$

The statements suggest that the PI approach to field theories may be traded for a quantization scheme built on a nonlinear stochastic differential equation. For simplicity, from now on, we will omit the notation with the subscript $\varphi(\boldsymbol{x},\tau)_\eta$ assuming the dependence is understood.

Since the initial introduction of the Langevin equation in field theory applications, numerous developments have been achieved. On one hand, in the very original spirit, SQ was conceived for developing a perturbative evaluation of gauge theories without fixing the gauge. On the other hand, the Langevin equation has been widely employed as a simulation algorithm for non-perturbative calculations in lattice field (and in particular gauge) theories.

1.1.1 Fokker-Plank formulation

In Eq. (10) we are considering expectation values of fields, averaging over the white noise realizations. In general we can compute much more general functions of the fields in the SQ framework, namely

$$\langle A[\varphi(\boldsymbol{x}_1,\tau)\dots\varphi(\boldsymbol{x}_n,\tau)]\rangle_\eta=\int\mathcal{D}\eta\exp\left[-\frac{1}{4}\int d\tau d\boldsymbol{x}\ \eta^2(\boldsymbol{x},\tau)\right]A[\varphi(\boldsymbol{x}_1,\tau)\dots\varphi(\boldsymbol{x}_n,\tau)]\,, \tag{12}$$

where

$$\mathcal{D}\eta=\frac{D\eta}{\int D\eta\exp\left[-\frac{1}{4}\int d\tau d\boldsymbol{x}\ \eta^2(\boldsymbol{x},\tau)\right]} \tag{13}$$

is the normalized measure for the stochastic source.

One way to demonstrate the fundamental assertion in Eq. (10) is to study the (stochastic time dependent) probability distribution associated with a field configuration, which is dictated by the so-called Fokker-Planck (FP) formulation. Basically Eq. (12) can be rephrased as an average over the probability distribution $P[\varphi,\tau]$[1] according to

$$\langle A[\varphi(\tau)\dots\varphi(\boldsymbol{x}_n,\tau)]\rangle_\eta=\int D\varphi P[\varphi,\tau]A[\varphi(\boldsymbol{x}_1)\dots\varphi(\boldsymbol{x}_n)]\,. \tag{14}$$

[1]Formally, a formulation in terms of probability distribution $P[\varphi,\tau]$ is encoded in the relation $P[\varphi,\tau]=\langle\delta(\varphi-\varphi(\tau)_\eta)\rangle_\eta$

We are now interested in finding the equation that describes the dynamics of this probability distribution in the stochastic time and in evaluating its equilibrium solutions. The fundamental statement in Eq. (10) will thus be verified if a stationary solution can be found which corresponds precisely to the measure of the functional integral. First, consider the derivative with respect to stochastic time of Eq. (12) and Eq. (14):

$$\frac{d}{d\tau}\langle A[\varphi(\tau)]\rangle_\eta = \int D\varphi \frac{dP[\varphi,\tau]}{d\tau} A[\varphi]\,, \tag{15}$$

$$\begin{aligned}\frac{d}{d\tau}\langle A[\varphi]\rangle_\eta &= \int \mathcal{D}\eta \exp\left[-\frac{1}{4}\int d\tau d\boldsymbol{x}\ \eta^2(\boldsymbol{x},\tau)\right]\frac{dA[\varphi(\tau)]}{d\tau} \\ &= \int \mathcal{D}\eta \exp\left[-\frac{1}{4}\int d\tau d\boldsymbol{x}\ \eta^2(\boldsymbol{x},\tau)\right]\int d\boldsymbol{x}\frac{\delta A[\varphi]}{\delta\varphi(\boldsymbol{x},\tau)}\frac{d\varphi}{d\tau} \\ &= \int \mathcal{D}\eta \exp\left[-\frac{1}{4}\int d\tau d\boldsymbol{x}\ \eta^2(\boldsymbol{x},\tau)\right]\int d\boldsymbol{x}\frac{\delta A[\varphi]}{\delta\varphi(\boldsymbol{x},\tau)}\left(-\frac{\delta S_E}{\delta\varphi(\boldsymbol{x},\tau)_\eta}+\eta(\boldsymbol{x},\tau)\right),\end{aligned} \tag{16}$$

where in the last line of Eq. (16) we used Eq. (3). We can manage the second term in the last line of Eq. (16) as follow

$$\begin{aligned}&-2\int \mathcal{D}\eta \int d\boldsymbol{x}\left[\frac{\delta}{\delta\eta(\boldsymbol{x},\tau)}\exp\left(-\frac{1}{4}\int d\tau d\boldsymbol{x}\ \eta^2(\boldsymbol{x},\tau)\right)\right]\frac{\delta A[\varphi]}{\delta\varphi(\boldsymbol{x},\tau)} \\ =&2\int \mathcal{D}\eta \int d\boldsymbol{x}\int d\boldsymbol{y}\exp\left(-\frac{1}{4}\int d\tau d\boldsymbol{x}\ \eta^2(\boldsymbol{x},\tau)\right)\frac{\delta^2 A[\varphi]}{\delta\varphi(\boldsymbol{y},\tau)\delta\varphi(\boldsymbol{x},\tau)}\frac{\delta\varphi(\boldsymbol{y},\tau)}{\delta\eta(\boldsymbol{x},\tau)} \\ =&\int \mathcal{D}\eta \int d\boldsymbol{x}\exp\left(-\frac{1}{4}\int d\tau d\boldsymbol{x}\ \eta^2(\boldsymbol{x},\tau)\right)\frac{\delta^2 A[\varphi]}{\delta\varphi(\boldsymbol{x},\tau)^2}\,.\end{aligned} \tag{17}$$

We note that in the second line of Eq. (17) we use the formal solution in Eq. (9), namely

$$\frac{\delta\varphi(\boldsymbol{y},\tau)}{\delta\eta(\boldsymbol{x},\tau)} = \theta(0)\delta(\boldsymbol{x}-\boldsymbol{y})\,, \tag{18}$$

being $\theta(\tau)$ the Heaviside step function defined with the mid-point prescription rule $\theta(0) = 1/2$. We obtain

$$\begin{aligned}\frac{d}{d\tau}\langle A[\varphi]\rangle_\eta &= \int \mathcal{D}\eta \int d\boldsymbol{x}\exp\left[-\frac{1}{4}\int d\tau d\boldsymbol{x}\ \eta^2(\boldsymbol{x},\tau)\right]\left(-\frac{\delta S_E}{\delta\varphi(\boldsymbol{x},\tau)_\eta}\frac{\delta A[\varphi]}{\delta\varphi(\boldsymbol{x},\tau)}+\frac{\delta^2 A[\varphi]}{\delta\varphi(\boldsymbol{x},\tau)^2}\right) \\ &= \int D\varphi \int d\boldsymbol{x}\left(-\frac{\delta S_E}{\delta\varphi(\boldsymbol{x},\tau)_\eta}\frac{\delta A[\varphi]}{\delta\varphi(\boldsymbol{x},\tau)}+\frac{\delta^2 A[\varphi]}{\delta\varphi(\boldsymbol{x},\tau)^2}\right)P[\varphi,\tau] \\ &= \int D\varphi\ A[\varphi]\int d\boldsymbol{x}\frac{\delta}{\delta\varphi(\boldsymbol{x},\tau)}\left[\left(\frac{\delta S_E}{\delta\varphi(\boldsymbol{x},\tau)_\eta}+\frac{\delta}{\delta\varphi(\boldsymbol{x},\tau)}\right)P[\varphi,\tau]\right].\end{aligned} \tag{19}$$

By matching Eq. (15) and Eq. (19) we derive the Fokker-Plank equation

$$\frac{dP[\varphi,\tau]}{d\tau} = \int d\boldsymbol{x}\ \frac{\delta}{\delta\varphi(\boldsymbol{x},\tau)}\left[\left(\frac{\delta S_E}{\delta\varphi(\boldsymbol{x})}+\frac{\delta}{\delta\varphi(\boldsymbol{x},\tau)}\right)P[\varphi,\tau]\right]. \tag{20}$$

1.1.2 Solution of the Fokker-Plank equation

Eq. (20) prescribes the evolution of the probability density as the stochastic time progresses. Although we are only interested in the stationary solution, we show how this can be directly obtained from a more general solution, evaluated at $\tau \to \infty$. In our discussion, we will consider systems with a finite number of discrete degrees of freedom: it is not a restriction as we are interested in simulating the system on a computer. Nevertheless, generalizations to systems with infinite degrees of freedom are also possible [32, 33]. We now start from the Fokker-Plank equation

$$\frac{dP[\varphi,\tau]}{d\tau} = \frac{\partial}{\partial\varphi(\boldsymbol{x})}\left[\left(\frac{\delta S_E}{\delta\varphi(\boldsymbol{x})} + \frac{\delta}{\delta\varphi(\boldsymbol{x})}\right)P[\varphi,\tau]\right]. \tag{21}$$

We introduce the transformation

$$P[\varphi,\tau] = \psi(\varphi,\tau)e^{-\frac{S[\varphi]}{2}} \tag{22}$$

and the Fokker-Planck equation can be rewritten as

$$\dot{\psi}[\varphi,\tau]e^{-\frac{S[\varphi]}{2}} = \frac{\partial}{\partial\varphi(\boldsymbol{x})}\left[\frac{\partial\psi}{\partial\varphi(\boldsymbol{x})}e^{-\frac{S[\varphi]}{2}} + \frac{1}{2}\psi(\varphi,\tau)e^{-\frac{S[\varphi]}{2}}\frac{\partial S}{\partial\varphi(\boldsymbol{x})}\right]. \tag{23}$$

We can recast the equation as follow

$$\dot{\psi}[\varphi,\tau] = -2\left[-\frac{1}{2}\frac{\partial^2}{\partial\varphi(\boldsymbol{x})^2} - \frac{1}{4}\frac{\partial^2 S}{\partial\varphi(\boldsymbol{x})^2} + \frac{1}{8}\left(\frac{\partial S}{\partial\varphi(\boldsymbol{x})}\right)^2\right]\psi[\varphi,\tau]\,. \tag{24}$$

Setting

$$H = -\frac{1}{2}\frac{\partial^2}{\partial\varphi(\boldsymbol{x})^2} - \frac{1}{4}\frac{\partial^2 S}{\partial\varphi(\boldsymbol{x})^2} + \frac{1}{8}\left(\frac{\partial S}{\partial\varphi(\boldsymbol{x})}\right)^2, \tag{25}$$

we recognize the familiar Schröedinger equation

$$\dot{\psi} = -2H\psi\,. \tag{26}$$

By simplifying to a single degree of freedom (we can extend our conclusions also to more variables), we can assert that the Hamiltonian

$$H = -\frac{1}{2}\frac{\partial^2}{\partial x^2} - \frac{1}{4}\frac{\partial^2 S}{\partial x^2} + \frac{1}{8}\left(\frac{\partial S}{\partial x}\right)^2 = \frac{1}{2}\left(-\frac{\partial}{\partial x} + \frac{S'}{2}\right)\left(+\frac{\partial}{\partial x} + \frac{S'}{2}\right) \tag{27}$$

thus factorized, is self-adjoint and exhibits a non-negative spectrum. Furthermore, the spectrum is entirely discrete. The transformations in Eq. (22) can be expressed in the eigenstates basis as

$$\psi[\varphi,\tau] = \sum_{n=0}^{\infty} a_n\psi_n[\varphi]e^{-E_n\tau} = a_0\psi_0[\varphi] + \sum_{n=1}^{\infty} a_n\psi_n[\varphi]e^{-E_n\tau}\,, \tag{28}$$

being ψ_0 the zero-eigenvector of Hamiltonian in Eq. (27), namely

$$\psi_0[\varphi] = e^{-\frac{S[\varphi]}{2}} \,. \tag{29}$$

In the limit of large stochastic time we obtain

$$\lim_{\tau\to\infty} P[\varphi,\tau] = \lim_{\tau\to\infty} \psi(\varphi,\tau) e^{-\frac{S[\varphi]}{2}} = a_0 e^{-S[\varphi]} + \lim_{\tau\to\infty} \sum_{n=1}^{\infty} a_n \psi_n[\varphi] e^{-E_n\tau} e^{-\frac{S[\varphi]}{2}} = a_0 e^{-S[\varphi]} \,. \tag{30}$$

The normalization constant can be fixed by means of

$$\int d\varphi P[\varphi, \tau \to \infty] = 1 \,. \tag{31}$$

Stochastic Quantization thus leads in the limit of large stochastic times to probability distributions in agreement with Euclidean field theory. In other words, this can be considered as a demonstration of the equivalence between quantization via Path Integral and Stochastic Quantization.

Another way to prove this result goes through the expansion of the probability distribution into a power series in the coupling constant and writing the Fokker-Planck equation order-by-order [34]. One ends up with equations coupling the distribution at the k-th order with the distribution at the $k-1$ order. The proof then proceeds by induction, thus proving the equivalence at any fixed order. We can show the equivalence also using the formalism of the Langevin equation [35], again in the framework of perturbation theory, as we will see in the next section.

1.2 Stochastic Perturbation Theory

As anticipated, many results from the theory of Stochastic Quantization are closely related to perturbation theory. Indeed, the title of the original paper was "Perturbation theory without gauge fixing", highlighting the interest in perturbation theory for systems with gauge symmetry while avoiding the intricacies of Faddeev-Popov ghosts [29].

Perturbative expansions of the Langevin equation solutions are derived, as formal expansions in the coupling constant, from Eq. (3) through its recursive solution in the coupling constant itself. One of the simplest and paradigmatic examples, involving only scalar degrees of freedom, is the self-interacting theory defined by the action [31]

$$S = \int d\boldsymbol{x} \left[(\partial_\mu \varphi)(\partial_\mu \varphi) + m^2 \varphi^2 + \frac{\lambda}{3!} \varphi^3 \right] . \tag{32}$$

The associated Langevin equation follows straightforward

$$\frac{d}{d\tau}\varphi(\boldsymbol{x},\tau) = (\partial_\mu\partial_\mu - m^2)\varphi(\boldsymbol{x},\tau) - \frac{\lambda}{2}\varphi(\boldsymbol{x},\tau) + \eta(\boldsymbol{x},\tau)\,. \tag{33}$$

As usual, it is convenient to switch to momentum space via Fourier transformation (in the spatial variables only), through

$$\varphi(\boldsymbol{k},\tau) = \int d\boldsymbol{x}\; e^{i\boldsymbol{k}\cdot\boldsymbol{x}}\varphi(\boldsymbol{x},\tau) \tag{34}$$

and the equivalent of Eq. (33) in Fourier space reads

$$\frac{d}{d\tau}\varphi(\boldsymbol{k},\tau) = -(\boldsymbol{k}\cdot\boldsymbol{k} + m^2)\varphi(\boldsymbol{k},\tau) - \frac{\lambda}{2}\int \frac{d\boldsymbol{p}d\boldsymbol{q}}{(2\pi)^n}\varphi(\boldsymbol{p},\tau)\varphi(\boldsymbol{q},\tau)\delta(\boldsymbol{k}-\boldsymbol{p}-\boldsymbol{q}) + \eta(\boldsymbol{k},\tau)\,, \tag{35}$$

where now (the Fourier transform of a Gaussian noise in position space is still Gaussian in momentum space)

$$\langle\eta(\boldsymbol{k},\tau)\eta(\boldsymbol{k'},\tau')\rangle_\eta = 2(2\pi)^n\delta(\boldsymbol{k}-\boldsymbol{k'})\delta(\tau-\tau')\,. \tag{36}$$

From a practical point of view, Eq. (35) can be solved by iteration, obtaining an exact expression up to a fixed perturbative order.

1.2.1 Free scalar field theory

To construct solutions up to a generic perturbative order, it is necessary to first look at the basic building block, namely the free theory solution. As expected, the free Langevin equation

$$\frac{d}{d\tau}\varphi(\boldsymbol{k},\tau) = -(\boldsymbol{k}\cdot\boldsymbol{k} + m^2)\varphi(\boldsymbol{k},\tau) + \eta(\boldsymbol{k},\tau) \tag{37}$$

can be explicitly solved in the Green Functions (GF) formalism in Fourier space, namely

$$\frac{d}{d\tau}G(\boldsymbol{k},\tau) = -(\boldsymbol{k}\cdot\boldsymbol{k} - m^2)G(\boldsymbol{k},\tau) + \delta(\tau)\,, \qquad \text{with} \qquad G(\boldsymbol{k},\tau) = 0, \quad \tau < 0\,, \tag{38}$$

where the constraint in Eq. (38) selects only the retarded GFs. The solution of Eq. (38) is

$$G(\boldsymbol{k},\tau) = \exp\{-(\boldsymbol{k}\cdot\boldsymbol{k} + m^2)\tau\}\theta(\tau)\,. \tag{39}$$

The retarded GF in Eq. (39) can be used to construct the solution of Eq. (37) as follow

$$\varphi(\boldsymbol{k},\tau) = \int_{-\infty}^{\infty} d\tau' G(\boldsymbol{k},\tau-\tau')\eta(\boldsymbol{k},\tau') + a\exp\{-(\boldsymbol{k}\cdot\boldsymbol{k} + m^2)\tau\}\,, \tag{40}$$

where a is a constant fixed by the initial conditions. We can remove a evaluating the previous equation in $\tau = 0$

$$\varphi(\boldsymbol{k},0) = \varphi_0(\boldsymbol{k}) = \int_{-\infty}^{0} d\tau' \exp\{(\boldsymbol{k}\cdot\boldsymbol{k} + m^2)\tau'\}\eta(\boldsymbol{k},\tau') + a\,, \tag{41}$$

obtaining

$$a = \varphi_0(\boldsymbol{k}) - \int_{-\infty}^{0} d\tau' \exp\{(\boldsymbol{k}\cdot\boldsymbol{k} + m^2)\tau'\}\eta(\boldsymbol{k},\tau') \tag{42}$$

so that

$$\begin{aligned}\varphi(\boldsymbol{k},\tau) =& \int_{-\infty}^{\tau} d\tau' \exp\{-(\boldsymbol{k}\cdot\boldsymbol{k} + m^2)(\tau-\tau')\}\eta(\boldsymbol{k},\tau') \\ &+ \left(\varphi_0(\boldsymbol{k}) - \int_{-\infty}^{0} d\tau' \exp\{(\boldsymbol{k}\cdot\boldsymbol{k} + m^2)\tau'\}\eta(\boldsymbol{k},\tau')\right)\exp\{-(\boldsymbol{k}\cdot\boldsymbol{k} + m^2)\tau\} \\ =& \int_{0}^{\tau} d\tau' \exp\{-(\boldsymbol{k}\cdot\boldsymbol{k} + m^2)(\tau-\tau')\}\eta(\boldsymbol{k},\tau') + \varphi_0(\boldsymbol{k})\exp\{-(\boldsymbol{k}\cdot\boldsymbol{k} + m^2)\tau\}\,.\end{aligned}$$

Let us note that the dependence of the field at time τ on the field at time $\tau_0 = 0$ is exponentially suppressed, as expected. For this reason, for the sake of brevity, we can set the initial condition

$$\varphi_0(\boldsymbol{k}) = 0\,, \tag{43}$$

taking for granted that these terms cannot contribute in the evaluation of the correlation functions in the limit of large stochastic time. In this setting we obtain a simple expression for the stochastic free field

$$\varphi(\boldsymbol{k},\tau) = \int_{0}^{\tau} d\tau' \exp\{-(\boldsymbol{k}\cdot\boldsymbol{k} + m^2)(\tau-\tau')\}\eta(\boldsymbol{k},\tau') \tag{44}$$

and we are able to compute the free two-point function at different stochastic time

$$D(\boldsymbol{k},\boldsymbol{k}',\tau,\tau') = \langle\varphi(\boldsymbol{k},\tau)\varphi(\boldsymbol{k}',\tau')\rangle_\eta\,. \tag{45}$$

Inserting Eq. (44) in Eq. (45) we obtain

$$\begin{aligned}&\langle\int_{0}^{\tau} ds \exp\{-(\boldsymbol{k}\cdot\boldsymbol{k} + m^2)(\tau-s)\}\eta(\boldsymbol{k},s)\int_{0}^{\tau'} dt \exp\{-(\boldsymbol{k}'\cdot\boldsymbol{k}' + m^2)(\tau'-t)\}\eta(\boldsymbol{k}',t)\rangle_\eta \\ &= \int_{0}^{\tau} ds \int_{0}^{\tau'} dt \exp\{-(\boldsymbol{k}\cdot\boldsymbol{k} + m^2)(\tau-s)\}\exp\{-(\boldsymbol{k}'\cdot\boldsymbol{k}' + m^2)(\tau'-t)\}\langle\eta(\boldsymbol{k},s)\eta(\boldsymbol{k}',t)\rangle_\eta \\ &= \int_{0}^{\tau}\int_{0}^{\tau'} ds\; dt \exp\{(\boldsymbol{k}\cdot\boldsymbol{k} + m^2)(s-\tau)\}\exp\{(\boldsymbol{k}'\cdot\boldsymbol{k}' + m^2)(t-\tau')\}2(2\pi)^n\delta(\boldsymbol{k}-\boldsymbol{k}')\delta(s-t)\,,\end{aligned} \tag{46}$$

where in the last line we use Eq. (36). Integrating in the stochastic time we obtain

$$\begin{aligned}D(\boldsymbol{k},\boldsymbol{k}',\tau,\tau') =& 2(2\pi)^n\int_{0}^{\min(\tau,\tau')} ds \exp\{(\boldsymbol{k}\cdot\boldsymbol{k} + m^2)(2s-\tau-\tau')\}\delta(\boldsymbol{k}-\boldsymbol{k}') \\ =& (2\pi)^n\frac{\exp\{-(\boldsymbol{k}\cdot\boldsymbol{k} + m^2)(\tau+\tau')\}\left(\exp\{2(\boldsymbol{k}\cdot\boldsymbol{k} + m^2)\min(\tau,\tau')\} - 1\right)}{(\boldsymbol{k}\cdot\boldsymbol{k} + m^2)}\delta(\boldsymbol{k}-\boldsymbol{k}')\,.\end{aligned} \tag{47}$$

We note that

$$\exp\{-(\boldsymbol{k}\cdot\boldsymbol{k}+m^2)(\tau+\tau'-2\min(\tau,\tau'))\}=\exp\{-(\boldsymbol{k}\cdot\boldsymbol{k}+m^2)(\tau-\tau')\}\,,\qquad \tau>\tau'\,, \tag{48}$$

$$\exp\{-(\boldsymbol{k}\cdot\boldsymbol{k}+m^2)(\tau+\tau'-2\min(\tau,\tau'))\}=\exp\{-(\boldsymbol{k}\cdot\boldsymbol{k}+m^2)(\tau'-\tau)\}\,,\qquad \tau'>\tau\,, \tag{49}$$

and we can write

$$\exp\{-(\boldsymbol{k}\cdot\boldsymbol{k}+m^2)(\tau+\tau'-2\min(\tau,\tau'))\}=\exp\{-(\boldsymbol{k}\cdot\boldsymbol{k}+m^2)|\tau-\tau'|\}\,. \tag{50}$$

In the end, the two point propagator reads

$$D(\boldsymbol{k},\boldsymbol{k}',\tau,\tau')=(2\pi)^n\Big(\exp\{-(\boldsymbol{k}\cdot\boldsymbol{k}+m^2)|\tau-\tau'|\}-\exp\{-(\boldsymbol{k}\cdot\boldsymbol{k}+m^2)(\tau+\tau')\}\Big)\frac{\delta(\boldsymbol{k}-\boldsymbol{k'})}{\boldsymbol{k}\cdot\boldsymbol{k}+m^2}\,. \tag{51}$$

Additionally, Eq. (51) highlights the property

$$D(\boldsymbol{k},\boldsymbol{k}',\tau,\tau')=D(\boldsymbol{k},\tau,\tau')\,. \tag{52}$$

Given the propagator in Eq. (51), we can provide an explicit proof of the statement in Eq. (10) for the free theory. Indeed, we note that the propagator can be evaluated at equal stochastic time, providing

$$D(\boldsymbol{k},\tau)=(2\pi)^n\Big(1-\exp\{-2(\boldsymbol{k}\cdot\boldsymbol{k}+m^2)\tau\}\Big)\frac{\delta(\boldsymbol{k}-\boldsymbol{k'})}{\boldsymbol{k}\cdot\boldsymbol{k}+m^2}\,, \tag{53}$$

and we can calculate the limit for large stochastic times as follows

$$\lim_{\tau\to\infty}D(\boldsymbol{k},\tau)=\langle\varphi(\boldsymbol{k},\tau)\varphi(\boldsymbol{k},\tau)\rangle_\eta=(2\pi)^n\frac{\delta(\boldsymbol{k}-\boldsymbol{k'})}{\boldsymbol{k}\cdot\boldsymbol{k}+m^2}\,, \tag{54}$$

reproducing, as expected, the well-known propagator of the associated Euclidean theory [36].

1.2.2 Diagrammatic stochastic perturbation theory

The free solution in Eq. (44) can be naturally seen as a solution of the interacting theory up to an $O(\lambda)$. The underlying idea of Stochastic Perturbation Theory is to substitute this solution in the formal solution of Eq. (35), namely

$$\varphi(\boldsymbol{k},\tau)=\int_0^\tau d\tau'\exp\{-(\boldsymbol{k}\cdot\boldsymbol{k}+m^2)(\tau-\tau')\}\Big[\eta(\boldsymbol{k},\tau')-\frac{\lambda}{2}\int\frac{d\boldsymbol{p}d\boldsymbol{q}}{(2\pi)^n}\varphi(\boldsymbol{p},\tau')\varphi(\boldsymbol{q},\tau')\delta(\boldsymbol{k}-\boldsymbol{p}-\boldsymbol{q})\Big]\,. \tag{55}$$

The solution in Eq. (55) is obtained noting that Eq. (35) is equivalent to Eq. (37) after the replacement of

$$\eta(\boldsymbol{k},\tau')\to\eta(\boldsymbol{k},\tau')-\frac{\lambda}{2}\int\frac{d\boldsymbol{p}d\boldsymbol{q}}{(2\pi)^n}\varphi(\boldsymbol{p},\tau')\varphi(\boldsymbol{q},\tau')\delta(\boldsymbol{k}-\boldsymbol{p}-\boldsymbol{q})\,. \tag{56}$$

A solution can be constructed from Eq. (44) using the same replacement as before. By substituting the free solution in Eq. (55) we generate a solution to Eq. (35) up to $O(\lambda^2)$. Furthermore, one can think of continuing in this manner with the newly found solution, and generate a solution up to $O(\lambda^3)$. Iteratively, solutions can be constructed in principle up to a fixed order. The solutions obtained are naturally written as power series in the coupling constant up to a fixed order. Here we present an outline of the procedure.

Writing symbolically the zero-order solution

$$\varphi^0 = \int (G\eta)\,, \tag{57}$$

where the superscript i indicates the order of the recursion procedure, we can construct by means of Eq. (55) a first-order solution

$$\varphi^1 = \int (G\eta) - \frac{\lambda}{2} \int G \int \varphi^0 \varphi^0 = \int G\eta - \frac{\lambda}{2} \int \int \int G(G\eta)(G\eta) \tag{58}$$

and a second-order solution

$$\varphi^2 = \int G\eta - \frac{\lambda}{2} \int \int \int G(G\eta)(G\eta) + \frac{\lambda^2}{2} \int \int \int \int \int G(G\eta)G(G\eta)(G\eta) \tag{59}$$

and so on up to a desired order. Typically a graphical representation is given for the perturbative series in Eq. (59) [31]. These are diagrams very similar to the Feynman diagrams

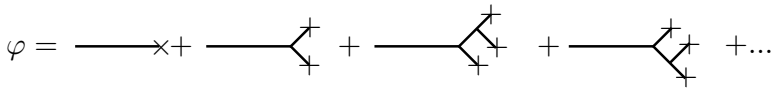

In this description, we characterize G by a line and η by a cross. The process involves integrating over the momenta at the connection points and considering the fictitious times at both the junctions and the cross points. The Diagrammatic Stochastic Perturbation Theory proceeds in building the two-point correlation function from the diagrams presented above. In particular, for the action in Eq. (32) we have the following stochastic diagrams

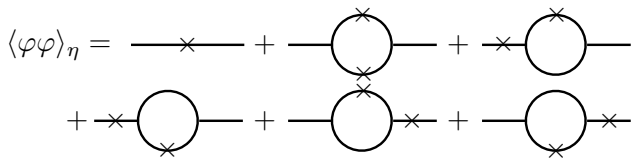

where the symbol "×" denotes the average over the gaussian white noise. Each of these stochastic diagrams resemble a typical Feynman diagram, with the exception of crosses marking the conjunction of two stochastic noises on the lines.

On the other hand for each Feynman diagram a set of stochastic diagrams sharing the same structure exists. Additionally, it can be shown that the sum of all the stochastic diagrams of a given topology reconstructs exactly, in the limit of large stochastic time $\tau \to \infty$, the contribution of the Feynman diagram with that topology [35]. Of course, this can be considered as an additional perturbative proof of the equivalence between Stochastic Quantization and Canonical Quantization. For a more complete presentation of the Diagrammatic Stochastic Perturbation Theory we refer the reader to the review [31] or the original work of Parisi and Wu [29].

1.3 Numerical Stochastic Perturbation Theory

As said, Stochastic Quantization provides an alternative to Canonical Quantization. In this framework the evaluation of the functional integral in Eq. (1) is traded for a new stochastic dynamics taking place in the fictitious time τ, recovering all the well-known results of Euclidean field theory in the (equilibrium) limit of $\tau \to \infty$, after averaging over all possible realizations of stochastic noise.

Notably, the perspective of solving a stochastic differential equation fits particularly well to a Monte Carlo implementation: averages over the distribution defined by the path integral are traded for time averages of expressions built out of solution of the Langevin equation, evaluated in the asymptotic time limit, in which we recover the functional integral measure as the equilibrium distribution of the stochastic process. From this viewpoint, the Langevin dynamics has been implemented in what is now called Langevin Monte Carlo, providing an alternative tool in numerical simulations of statistical systems [37–39]. Moreover, these algorithms have been also used for simulations of Lattice Gauge Theories (LGT) [40–42]. Given the close relationship with Monte Carlo, we digress briefly and discuss the latter.

1.3.1 Monte Carlo methods

Monte Carlo simulations are a computational technique used to approximate multi-dimensional integrals [43, 44], especially in cases where analytical solutions are difficult to obtain. These simulations utilize random sampling to estimate the properties of complex systems. The main goal

of a Monte Carlo simulation is the evaluation of an observable $A[\varphi_1, \ldots, \varphi_n]$ for a system with degrees of freedom $\{\varphi_1, \ldots, \varphi_n\}$ distributed according to the probability density $P(\varphi_1, \ldots, \varphi_n)$. Basically we want an estimate of

$$\langle A \rangle = \int d\varphi_1 \ldots d\varphi_n \; A[\varphi_1, \ldots, \varphi_n] \; P(\varphi_1, \ldots, \varphi_n) \, . \tag{60}$$

For what we are mainly interested in, the probability density is expressed as (Z is the partition function)

$$P(\varphi_1, \ldots, \varphi_n) = \frac{e^{-S(\varphi_1, \ldots, \varphi_n)}}{Z} \, , \tag{61}$$

where $S(\varphi_1, \ldots, \varphi_n)$ is the action describing the system. The partition function is given by

$$Z = \int d\varphi_1 \ldots d\varphi_n \; e^{-S(\varphi_1, \ldots, \varphi_n)} \, , \tag{62}$$

in which we sum over all possible configurations of the system.

To compute the expectation value of $A[\varphi_1, \ldots, \varphi_n]$, a Monte Carlo simulation generates a sequence of states

$$\{\varphi_1, \ldots, \varphi_n\}_1 \to \{\varphi_1, \ldots, \varphi_n\}_2 \to \ldots \to \{\varphi_1, \ldots, \varphi_n\}_m \to \ldots \, , \tag{63}$$

sampled according to the probability density in Eq. (61): this is known as *importance sampling*. If importance sampling is guaranteed, as a simple application of the law of large numbers the expectation value in Eq. (60) can be approximated by the average over the sample

$$\langle A \rangle \approx \frac{1}{N} \sum_{i=1}^{N} A[\{\varphi_1, \ldots, \varphi_n\}_i] \, , \tag{64}$$

where N is the total number of sampled states and $A[\{\varphi_1, \ldots, \varphi_n\}_i]$ is the value of the observable $A[\varphi_1, \ldots, \varphi_n]$ computed on the i-th configuration. As N grows, the Monte Carlo estimate converges to the true expectation value, with the statistical error diminishing as $1/\sqrt{N}$. In a sense, we have simply traded the original problem with that of implementing importance sampling. In practice, all the Monte Carlo methods that are extensively used are built out of stochastic processes (Markov processes, actually), the requirement being that asymptotically the process is distributed according to the probability distribution we want to sample. There are various algorithms implementing stochastic processes with the desired property we have just described. The Metropolis–Hastings algorithm [45, 46] is to some extent a prototype (this is true in a quite sad sense, with many people actually thinking of Metropolis as Monte Carlo *tout court*). In more recent years, newer and more efficient algorithms have been introduced, such

as Hybrid Monte Carlo (HMC)[47], which is probably the preferred choice in most interesting cases (including Lattice QCD). Notice that taking for stochastic sampling the solution of a stochastic differential equation is another natural choice. With this respect, Langevin is one of the possibilities: as seen, after equilibrium is reached, the configurations are distributed according to the probability measure in Eq. (61). We should now point out that we have till now discussed the analytic solution of Langevin equation. When it comes to its implementation in the sense of a Monte Carlo, the Langevin equation requires numerical integration: this means discretizing the stochastic time in discrete steps, so that evolution over a given stochastic time extent is given by $\tau = N_{\text{steps}}\Delta\tau$. We indicate the value of $\Delta\tau$ as stochastic time step. The simplest discretized Langevin equation (Euler scheme) reads

$$\varphi(\boldsymbol{x}, \tau_0 + \Delta\tau) = \varphi(\boldsymbol{x}, \tau_0) - \Delta\tau \frac{\partial S}{\partial \varphi(\boldsymbol{x}, \tau_0)} + \sqrt{2\Delta\tau}\eta(\boldsymbol{x}, \tau_0)\,, \tag{65}$$

being now the Gaussian white noise normalized with zero mean and unit standard deviation

$$\langle \eta(\boldsymbol{x}, \tau_0) \rangle = 0\,, \qquad \langle \eta(\boldsymbol{x}, \tau_0)\eta(\boldsymbol{y}, \tau_1) \rangle = \delta(\boldsymbol{x} - \boldsymbol{y})\delta_{\tau_0,\tau_1}\,. \tag{66}$$

We note that in Eq. (65) we replaced functional derivatives in Eq. (3) with partial derivatives: this is because in order to solve the Eq. (65) on the computer, we will discretize the degrees of freedom and place them in a finite volume, thus obtaining a finite number of degrees of freedom.

Solutions to Eq. (65) no longer satisfy the Fokker-Planck equation introduced in Eq. (20) [41]. Discretised Langevin equation (here we are talking of the discretization in terms of stochastic time steps) introduces systematic effects (typically in the form of polynomial correction in the stochastic time step $\Delta\tau$) that need to be removed. Since these technical details are common to NSPT simulations, all aspects will be treated in detail in the NSPT section.

1.3.2 From SQ(PT) to NSPT

Numerical Stochastic Perturbation Theory (NSPT) roughly lies at the midpoint between Stochastic Perturbation Theory and non-perturbative Monte Carlo Langevin methods. First introduced by the pioneering works of the lattice group of Parma University [1], it has evolved significantly over the years, becoming nowadays one of the main numerical tools for calculations in perturbation theory. In our discussion, we will only present NSPT in its position space formulation (which is typically used in Monte Carlo simulations). We omit the presentation in Fourier space, which does not present any difference.

We consider a generic action of a Euclidean field theory $S[\varphi]$, in a simplified setting in which the action contains only one coupling constant g and a scalar field $\varphi(\boldsymbol{x})$ (these conditions are not

at all stringent; they only simplify the notation)[2]. In the framework of Stochastic Quantization, the degrees of freedom are promoted to depend on stochastic time $\varphi(\boldsymbol{x}) \to \varphi(\boldsymbol{x}, \tau)$ and evolved according to the Langevin equation

$$\frac{\partial \varphi(\boldsymbol{x}, \tau)}{\partial \tau} = -\frac{\delta S}{\delta \varphi(\boldsymbol{x}, \tau)} + \eta(\boldsymbol{x}, \tau)\,. \tag{67}$$

The key element of Numerical Stochastic Perturbation Theory is that at each fixed stochastic time it is always possible to expand the fields in a formal power series in the coupling constant, namely

$$\varphi(\boldsymbol{x}, \tau) = \varphi^{(0)}(\boldsymbol{x}, \tau) + g\varphi^{(1)}(\boldsymbol{x}, \tau) + g^2\varphi^{(2)}(\boldsymbol{x}, \tau) + \ldots = \varphi^{(0)}(\boldsymbol{x}, \tau) + \sum_{n=1}^{\infty} g^n \varphi^{(n)}(\boldsymbol{x}, \tau)\,. \tag{68}$$

We can insert the series expansion given by Eq. (68) in the Langevin equation. We make the point that the expansion is a formal one: no particular value of the coupling will be considered at any time, but everything will be expanded order by order in the coupling. We note that this is exactly what happens in the standard approach to perturbation theory. This means that we can reorganize the Langevin dynamics into a tower of differential equations, each for any given perturbative order. Let us introduce a convenient notation: let

$$\left.\frac{\delta S}{\delta \varphi(\boldsymbol{x}, \tau)}\right|_{\sum_{n=0}^{\infty} g^n \varphi^{(n)}(\boldsymbol{x}, \tau)} = \sum_{n=0}^{\infty} g^n \Sigma^{(n)}(\boldsymbol{x}, \tau)\,, \tag{69}$$

where we mean that the gradient of the action should be calculated on the field and then the field should be substituted with its series expansion in Eq. (68). We can then organise all operations on fields as order-by-order operations; for example

$$\begin{aligned} \varphi_a(\boldsymbol{x}, \tau) + \varphi_b(\boldsymbol{x}, \tau) = \Big(\varphi_a^{(0)}(\boldsymbol{x}, \tau) + \varphi_b^{(0)}(\boldsymbol{x}, \tau)\Big) + g\Big(\varphi_a^{(1)}(\boldsymbol{x}, \tau) + \varphi_b^{(1)}(\boldsymbol{x}, \tau)\Big) \\ + g^2\Big(\varphi_a^{(2)}(\boldsymbol{x}, \tau) + \varphi_b^{(2)}(\boldsymbol{x}, \tau)\Big) + \ldots\,, \end{aligned} \tag{70}$$

$$\begin{aligned} \varphi_a(\boldsymbol{x}, \tau) \cdot \varphi_b(\boldsymbol{x}, \tau) = \varphi_a^{(0)}(\boldsymbol{x}, \tau)\varphi_b^{(0)}(\boldsymbol{x}, \tau) + g\Big(\varphi_a^{(0)}(\boldsymbol{x}, \tau)\varphi_b^{(1)}(\boldsymbol{x}, \tau) + \varphi_a^{(1)}(\boldsymbol{x}, \tau)\varphi_b^{(0)}(\boldsymbol{x}, \tau)\Big) \\ + g^2\Big(\varphi_a^{(0)}(\boldsymbol{x}, \tau)\varphi_b^{(2)}(\boldsymbol{x}, \tau) + \varphi_a^{(1)}(\boldsymbol{x}, \tau)\varphi_b^{(1)}(\boldsymbol{x}, \tau) + \varphi_a^{(2)}(\boldsymbol{x}, \tau)\varphi_b^{(0)}(\boldsymbol{x}, \tau)\Big)\,, \end{aligned} \tag{71}$$

As seen, the gradient of the action itself is expanded in power series of the coupling constant with coefficients $\Sigma^{(n)}(\boldsymbol{x}, \tau)$. To clarify the meaning of Eq. (69), we observe that for every theory

[2]It can be shown that we can very well consider more than one coupling constant and several degrees of freedom (scalars, matrices, fermions and so on) simultaneously.

whose action can be decomposed into a free part and an interacting part proportional to the coupling constant

$$S = S_0 + gS_I\,, \tag{72}$$

the coefficients in Eq. (69) take the form:

$$\Sigma^{(n)}(\boldsymbol{x},\tau) = G_0^{-1}\varphi^{(n)}(\boldsymbol{x},\tau) - D^{(n)}(\varphi^{(0)}(\boldsymbol{x},\tau),\varphi^{(1)}(\boldsymbol{x},\tau),\dots,\varphi^{(n-1)}(\boldsymbol{x},\tau))\,, \tag{73}$$

where $D^{(n)}(\varphi^{(0)}(\boldsymbol{x},\tau),\dots,\varphi^{(n-1)}(\boldsymbol{x},\tau))$ is a source term that couples different perturbative orders and changes with the considered order n. $D^{(n)}$ depends only on the values of the fields at perturbative orders $m < n$. In Eq. (73) G_0^{-1} is the free propagator of the theory, namely:

$$\left.\frac{\delta S_0}{\delta\varphi(\boldsymbol{x},\tau)}\right|_{\varphi^{(n)}(\boldsymbol{x},\tau)} = G_0^{-1}\varphi^{(n)}(\boldsymbol{x},\tau)\,, \tag{74}$$

and its structure is independent of the considered perturbative order. Moreover, it does not mix different orders.

Given the decomposition in Eq. (73), inserting the series expansion of Eq. (68) in the Langevin Eq. (67) we obtain a set of hierarchical stochastic differential equations, namely

$$\begin{aligned}
\frac{\partial\varphi^{(0)}(\boldsymbol{x},\tau)}{\partial\tau} &= -G_0^{-1}\varphi^{(0)}(\boldsymbol{x},\tau) + \eta(\boldsymbol{x},\tau)\,,\\
\frac{\partial\varphi^{(1)}(\boldsymbol{x},\tau)}{\partial\tau} &= -G_0^{-1}\varphi^{(1)}(\boldsymbol{x},\tau) + D^{(1)}(\varphi^{(0)}(\boldsymbol{x},\tau))\,,\\
\frac{\partial\varphi^{(2)}(\boldsymbol{x},\tau)}{\partial\tau} &= -G_0^{-1}\varphi^{(2)}(\boldsymbol{x},\tau) + D^{(2)}(\varphi^{(0)}(\boldsymbol{x},\tau),\varphi^{(1)}(\boldsymbol{x},\tau))\,,\\
&\dots\\
\frac{\partial\varphi^{(n)}(\boldsymbol{x},\tau)}{\partial\tau} &= -G_0^{-1}\varphi^{(n)}(\boldsymbol{x},\tau) + D^{(n)}(\varphi^{(0)}(\boldsymbol{x},\tau),\varphi^{(1)}(\boldsymbol{x},\tau),\dots,\varphi^{(n-1)}(\boldsymbol{x},\tau))\,,\\
&\dots
\end{aligned} \tag{75}$$

We emphasize that only the first equation (the free theory equation) is a properly stochastic equation, containing the dependence on the realization of the stochastic noise. The other equations contain the stochastic source by means of the dependence on the zero-order. Furthermore we note that the set of equations is exact at any fixed truncation in perturbation theory (in particular this will be the case whenever we consider numerical simulations): given a truncation order n, all the equations depend only on fields defined at orders $m \leq n$.

Numerical Stochastic Perturbation Theory consists in integrating Eq. (75) on the computer, effectively outlining a strategy for a *perturbative Monte Carlo*. A key practical feature of this approach is its implementation ease, requiring minimal changes to existing non-perturbative Monte Carlo routines (see also Sec. 1.7).

We have discussed the perturbative expansion of the Langevin equation. It is important to note that also other stochastic equations can be used [8, 13] (we discuss two of them in the following sections). However, no accept/reject Metropolis update algorithms can be implemented. This is inherent in the nature of the perturbative expansion mechanism: the latter makes sense only provided an analytic solution exists, which is unavoidably lost in a process like an accept/reject mechanism. As a matter of fact, this consideration has to do with the "exactness" of NSPT simulations, which is still under debate.

In NSPT obtaining the perturbative expansion of a given generic observable $A[\varphi]$ is pretty simple

$$\begin{aligned} A[\varphi] &= A[\sum_{n=0}^{\infty} g^n \varphi^{(n)}] = A^{(0)}[\varphi^{(0)}] + gA^{(1)}[\varphi^{(0)}, \varphi^{(1)}] + g^2 A^{(2)}[\varphi^{(0)}, \varphi^{(1)}, \varphi^{(2)}] \\ &= \sum_{n=0}^{\infty} g^n A^{(n)}[\varphi^{(0)}, \ldots, \varphi^{(n)}] \,, \end{aligned} \tag{76}$$

being the $A^{(n)}$ the coefficients we are interested in.

1.4 Numerical integration

The NSPT program proceeds by numerically integrating the Eq. (75). From now on, we switch from the continuous space-time notation to the lattice notation

$$\varphi(\boldsymbol{x}, \tau) \to \varphi_{\boldsymbol{i}}(\tau) \tag{77}$$

and we will imply that perturbative operations are performed up to a fixed order, discarding contributions of higher order.

1.4.1 Euler Integrator

The simplest choice is to use the Euler scheme. In this case, one obtains

$$\begin{aligned} \varphi_{\boldsymbol{i}}^{(0)}(\tau + \Delta\tau) &= \varphi_{\boldsymbol{i}}^{(0)}(\tau) - \Delta\tau G_0^{-1} \varphi_{\boldsymbol{i}}^{(0)}(\tau) + \sqrt{2\Delta\tau}\eta_{\boldsymbol{i}}(\tau) \,, \\ \varphi_{\boldsymbol{i}}^{(1)}(\tau + \Delta\tau) &= \varphi_{\boldsymbol{i}}^{(1)}(\tau) - \Delta\tau G_0^{-1} \varphi_{\boldsymbol{i}}^{(1)}(\tau) + \Delta\tau D^{(1)}(\varphi^{(0)}(\tau)) \,, \\ \varphi_{\boldsymbol{i}}^{(2)}(\tau + \Delta\tau) &= \varphi_{\boldsymbol{i}}^{(2)}(\tau) - \Delta\tau G_0^{-1} \varphi_{\boldsymbol{i}}^{(2)}(\tau) + \Delta\tau D^{(2)}(\varphi^{(0)}(\tau), \varphi^{(1)}(\tau)) \,, \\ &\ldots \\ \varphi_{\boldsymbol{i}}^{(n)}(\tau + \Delta\tau) &= \varphi_{\boldsymbol{i}}^{(n)}(\tau) - \Delta\tau G_0^{-1} \varphi_{\boldsymbol{i}}^{(n)}(\tau) + \Delta\tau D^{(n)}(\varphi^{(0)}(\tau), \varphi^{(1)}(\tau), \ldots, \varphi^{(n)}(\tau)) \,. \end{aligned} \tag{78}$$

The discretization of the stochastic time $\tau = n_{\text{steps}}\Delta\tau$ implies that the evolution in Eq. (78) no longer satisfies the Fokker-Planck equation. The stochastic process can still be considered as a stationary process, because the corrections to the Fokker-Planck equation can be obtained from the leading order Fokker-Planck equation with a redefinition of the action.

A Langevin discrete dynamics can be written as

$$\varphi_{\boldsymbol{i}}(\tau + \Delta\tau) = \varphi_{\boldsymbol{i}}(\tau) - F_{\boldsymbol{i}}(\tau)\,, \tag{79}$$

where $F_{\boldsymbol{i}}(\tau)$ is a scheme-dependent function. We consider the Kramers-Moyal asymptotic expansion (see App. A for a hint of the proof)

$$\frac{P[\varphi, \tau + \Delta\tau] - P[\varphi, \tau]}{\Delta\tau} = \frac{1}{\Delta\tau}\sum_{n=1}^{\infty}\frac{1}{n!}\frac{\partial^n}{\partial\varphi_{\boldsymbol{i}_1}\dots\partial\varphi_{\boldsymbol{i}_n}}\Big[\langle F_{\boldsymbol{i}_1}(\tau)\dots F_{\boldsymbol{i}_n}(\tau)\rangle P[\varphi,\tau]\Big]\,. \tag{80}$$

For a stochastic dynamics at the equilibrium, the LHS of Eq. (80) vanishes for each value of $\Delta\tau$

$$\frac{1}{\Delta\tau}\sum_{n=1}^{\infty}\frac{1}{n!}\frac{\partial^n}{\partial\varphi_{\boldsymbol{i}_1}\dots\partial\varphi_{\boldsymbol{i}_n}}\Big[\langle F_{\boldsymbol{i}_1}\dots F_{\boldsymbol{i}_n}\rangle P[\varphi]\Big] = 0\,, \tag{81}$$

where we dropped the trivial dependence on the stochastic time. In the Euler scheme we have

$$F_{\boldsymbol{i}}(\tau) = \Delta\tau\frac{\partial S}{\partial\varphi_{\boldsymbol{i}}(\tau)} - \sqrt{2\Delta\tau}\eta_{\boldsymbol{i}}(\tau)\,. \tag{82}$$

The idea is to evaluate the first correction in $\Delta\tau$ to Eq. (81), so that expectation values up to the second order need to be computed:

$$\begin{aligned}
\langle F_{\boldsymbol{i}_1}\rangle &= \Delta\tau\frac{\partial S}{\partial\varphi_{\boldsymbol{i}_1}}\,,\\
\langle F_{\boldsymbol{i}_1}F_{\boldsymbol{i}_2}\rangle &= \Delta\tau^2\frac{\partial S}{\partial\varphi_{\boldsymbol{i}_1}}\frac{\partial S}{\partial\varphi_{\boldsymbol{i}_2}} + 2\Delta\tau\delta_{\boldsymbol{i}_1\boldsymbol{i}_2}\,,\\
\langle F_{\boldsymbol{i}_1}F_{\boldsymbol{i}_2}F_{\boldsymbol{i}_3}\rangle &= 2\Delta\tau^2\left(\frac{\partial S}{\partial\varphi_{\boldsymbol{i}_1}}\delta_{\boldsymbol{i}_2\boldsymbol{i}_3} + \frac{\partial S}{\partial\varphi_{\boldsymbol{i}_2}}\delta_{\boldsymbol{i}_3\boldsymbol{i}_1} + \frac{\partial S}{\partial\varphi_{\boldsymbol{i}_3}}\delta_{\boldsymbol{i}_2\boldsymbol{i}_1}\right) + O(\Delta\tau^3)\,,\\
\langle F_{\boldsymbol{i}_1}F_{\boldsymbol{i}_2}F_{\boldsymbol{i}_3}F_{\boldsymbol{i}_4}\rangle &= 4\Delta\tau^2(\delta_{\boldsymbol{i}_1\boldsymbol{i}_2}\delta_{\boldsymbol{i}_3\boldsymbol{i}_4} + \delta_{\boldsymbol{i}_1\boldsymbol{i}_3}\delta_{\boldsymbol{i}_2\boldsymbol{i}_4} + \delta_{\boldsymbol{i}_1\boldsymbol{i}_4}\delta_{\boldsymbol{i}_2\boldsymbol{i}_3}) + O(\Delta\tau^3)\,.
\end{aligned} \tag{83}$$

Inserting Eq. (83) in the expansion (81) we obtain

$$
\begin{aligned}
&\frac{\partial}{\partial\varphi_{i_1}}\Big[\langle F_{i_1}\rangle P\Big]+\frac{1}{2}\frac{\partial^2}{\partial\varphi_{i_1}\partial\varphi_{i_2}}\Big[\langle F_{i_1}F_{i_2}\rangle P\Big]+\frac{1}{6}\frac{\partial^3}{\partial\varphi_{i_1}\partial\varphi_{i_2}\partial\varphi_{i_3}}\Big[\langle F_{i_1}F_{i_2}F_{i_3}\rangle P\Big]+\\
&+\frac{1}{24}\frac{\partial^4}{\partial\varphi_{i_1}\partial\varphi_{i_2}\partial\varphi_{i_3}\partial\varphi_{i_4}}\Big[\langle F_{i_1}F_{i_2}F_{i_3}F_{i_4}\rangle P\Big]\\
=&\frac{\partial}{\partial\varphi_{i_1}}\left[\frac{\partial S}{\partial\varphi_{i_1}}P\right]+\frac{1}{2}\frac{\partial^2}{\partial\varphi_{i_1}\partial\varphi_{i_2}}\left[\left(\Delta\tau\frac{\partial S}{\partial\varphi_{i_1}}\frac{\partial S}{\partial\varphi_{i_2}}+2\delta_{i_1i_2}\right)P\right]\\
&+\frac{1}{3}\frac{\partial^3}{\partial\varphi_{i_1}\partial\varphi_{i_2}\partial\varphi_{i_3}}\left[\Delta\tau\left(\frac{\partial S}{\partial\varphi_{i_1}}\delta_{i_2i_3}+\frac{\partial S}{\partial\varphi_{i_2}}\delta_{i_3i_1}+\frac{\partial S}{\partial\varphi_{i_3}}\delta_{i_2i_1}\right)P\right]\\
&+\frac{1}{6}\frac{\partial^4}{\partial\varphi_{i_1}\partial\varphi_{i_2}\partial\varphi_{i_3}\partial\varphi_{i_4}}\Big[\Delta\tau(\delta_{i_1i_2}\delta_{i_3i_4}+\delta_{i_1i_3}\delta_{i_2i_4}+\delta_{i_1i_4}\delta_{i_2i_3})P\Big]\\
=&\frac{\partial}{\partial\varphi_{i_1}}\left[\frac{\partial S}{\partial\varphi_{i_1}}P\right]+\frac{1}{2}\frac{\partial^2}{\partial\varphi_{i_1}\partial\varphi_{i_2}}\left[\left(\Delta\tau\frac{\partial S}{\partial\varphi_{i_1}}\frac{\partial S}{\partial\varphi_{i_2}}+2\delta_{i_1i_2}\right)P\right]\\
&+\frac{\partial^3}{\partial\varphi_{i_1}\partial\varphi_{i_2}\partial\varphi_{i_2}}\left[\Delta\tau\left(\frac{\partial S}{\partial\varphi_{i_1}}\right)P\right]+\frac{1}{2}\frac{\partial^4}{\partial\varphi_{i_1}\partial\varphi_{i_1}\partial\varphi_{i_2}\partial\varphi_{i_2}}\Big[\Delta\tau P\Big]+O(\Delta\tau^2)=0\,.
\end{aligned}
\tag{84}
$$

The leading order Kramers-Moyal expansions gives

$$
\frac{\partial}{\partial\varphi_{i_1}}\left[\frac{\partial S}{\partial\varphi_{i_1}}P\right]+\frac{\partial^2}{\partial\varphi_{i_1}\partial\varphi_{i_1}}\Big[P\Big]=0\,,
\tag{85}
$$

which is the Fokker-Planck equation introduced in Eq. (20) for the Langevin discrete dynamics. The first-order correction is

$$
\begin{aligned}
&\Delta\tau\Big\{\frac{1}{2}\frac{\partial}{\partial\varphi_{i_1}}\left[\left(\frac{\partial^2 S}{\partial\varphi_{i_2}\partial\varphi_{i_1}}\right)\left(\frac{\partial S}{\partial\varphi_{i_2}}\right)P+\left(\frac{\partial S}{\partial\varphi_{i_1}}\right)\left(\frac{\partial^2 S}{\partial\varphi_{i_2}\partial\varphi_{i_2}}\right)P-\left(\frac{\partial S}{\partial\varphi_{i_1}}\right)\left(\frac{\partial S}{\partial\varphi_{i_2}}\right)^2P\right]\\
&\qquad+\frac{\partial^3}{\partial\varphi_{i_1}\partial\varphi_{i_2}\varphi_{i_2}}\left[\left(\frac{\partial S}{\partial\varphi_{i_1}}\right)P\right]+\frac{1}{2}\frac{\partial^4}{\partial\varphi_{i_1}^2\partial\varphi_{i_2}^2}P\Big\}\\
=\Delta\tau&\Big\{\frac{1}{2}\frac{\partial}{\partial\varphi_{i_1}}\left[\left(\frac{\partial^2 S}{\partial\varphi_{i_2}\partial\varphi_{i_1}}\right)\left(\frac{\partial S}{\partial\varphi_{i_2}}\right)P+\left(\frac{\partial S}{\partial\varphi_{i_1}}\right)\left(\frac{\partial^2 S}{\partial\varphi_{i_2}\partial\varphi_{i_2}}\right)P-\left(\frac{\partial S}{\partial\varphi_{i_1}}\right)\left(\frac{\partial S}{\partial\varphi_{i_2}}\right)^2P\right]\\
&\qquad+\frac{1}{2}\frac{\partial^3}{\partial\varphi_{i_1}\partial\varphi_{i_2}\varphi_{i_2}}\left[\left(\frac{\partial S}{\partial\varphi_{i_1}}\right)P\right]\Big\}\\
=\Delta\tau&\Big\{\frac{1}{2}\frac{\partial}{\partial\varphi_{i_1}}\left[\left(\frac{\partial^2 S}{\partial\varphi_{i_2}\partial\varphi_{i_1}}\right)\left(\frac{\partial S}{\partial\varphi_{i_2}}\right)P+\left(\frac{\partial S}{\partial\varphi_{i_1}}\right)\left(\frac{\partial^2 S}{\partial\varphi_{i_2}\partial\varphi_{i_2}}\right)P-\left(\frac{\partial S}{\partial\varphi_{i_1}}\right)\left(\frac{\partial S}{\partial\varphi_{i_2}}\right)^2P\right]\\
&+\frac{1}{2}\frac{\partial}{\partial\varphi_{i_1}}\left[\left(\frac{\partial^3 S}{\partial\varphi_{i_1}\partial\varphi_{i_2}\partial\varphi_{i_2}}\right)P-\left(\frac{\partial^2 S}{\partial\varphi_{i_1}\partial\varphi_{i_2}}\right)\left(\frac{\partial S}{\partial\varphi_{i_2}}\right)P-\left(\frac{\partial^2 S}{\partial\varphi_{i_1}\partial\varphi_{i_2}}\right)\left(\frac{\partial S}{\partial\varphi_{i_2}}\right)P\right.\\
&\left.-\left(\frac{\partial S}{\partial\varphi_{i_1}}\right)\left(\frac{\partial^2 S}{\partial\varphi_{i_2}\partial\varphi_{i_2}}\right)P+\left(\frac{\partial S}{\partial\varphi_{i_1}}\right)\left(\frac{\partial S}{\partial\varphi_{i_2}}\right)^2P\right]\Big\}\\
&=\frac{\Delta\tau}{2}\left\{\frac{\partial}{\partial\varphi_{i_1}}\left[\left(\frac{\partial^3 S}{\partial\varphi_{i_1}\partial\varphi_{i_2}\partial\varphi_{i_2}}\right)P-\left(\frac{\partial S}{\partial\varphi_{i_1}}\right)\left(\frac{\partial^2 S}{\partial\varphi_{i_2}\partial\varphi_{i_2}}\right)P\right]\right\},
\end{aligned}
\tag{86}
$$

where we use the relation

$$
\frac{\partial S}{\partial\varphi_{i_1}}P=-\frac{\partial P}{\partial\varphi_{i_1}}+O(\Delta\tau)\,,
\tag{87}
$$

obtained from the leading order term in Eq. (85). The same leading correction can be obtained starting directly from Eq. (85) and considering the modified action

$$S \to S + \Delta\tau \bar{S}\,, \tag{88}$$

where

$$\bar{S} = -\frac{1}{4}\left[\left(\frac{\partial S}{\partial \varphi_{\boldsymbol{i}_1}}\right)^2 - 2\left(\frac{\partial^2 S}{\partial \varphi_{\boldsymbol{i}_1}\partial \varphi_{\boldsymbol{i}_1}}\right)\right]. \tag{89}$$

As a consequence, the observables display leading $\Delta\tau$ corrections, namely

$$\langle A\rangle_{\Delta\tau} = \frac{\int D\varphi\ A[\varphi]\ e^{-(S+\Delta\tau\bar{S})}}{\int D\varphi\ e^{-(S+\Delta\tau\bar{S})}} = \frac{\int D\varphi\ A[\varphi]\ e^{-S}(1-\Delta\tau\bar{S})}{\int D\varphi\ e^{-S}(1-\Delta\tau\bar{S})} = \langle A\rangle + O(\Delta\tau)\,, \tag{90}$$

approaching the correct expectation value for the continuous stochastic process $\Delta\tau \to 0$.

We note that in this context stochastic equations differ significantly from partial differential equations. In the stochastic case we are not interested in the single update step being executed with a chosen precision $O(\Delta\tau^n)$. In contrast, given such an integrator, we look at corrections to the Fokker-Planck equation. This is quite different compared to partial differential equations, where different integration schemes can be implemented requiring a fixed single-step precision.

1.4.2 Runge-Kutta Integrator

We can build for the Langevin equation a second-order scheme. In this section we consider the same analysis as before but changing the function $F_{\boldsymbol{i}}(\tau)$. While there is no systematic study to date in terms of high-order integrators for stochastic equations, we can derive a second-order integrator taking inspiration from the general structure of Runge-Kutta integrators.

We consider the following discrete Langevin parametric equation

$$\varphi_{\boldsymbol{i}}(\tau+\Delta\tau) = \varphi_{\boldsymbol{i}}(\tau) - \Delta\tau\left[a\left(\frac{\partial S}{\partial \varphi_{\boldsymbol{i}}}\right)_{\tau} + b\left(\frac{\partial S}{\partial \varphi_{\boldsymbol{i}}}\right)_{\tau+\Delta\tau k}\right] + \sqrt{2\Delta\tau}\eta_{\boldsymbol{i}}(\tau)\,, \tag{91}$$

where the subscript τ means that the gradient is computed on $\varphi(\tau)$ and the subscript $\tau+\Delta\tau k$ means that the gradient is computed on $\varphi(\tau+\Delta\tau k)$, updated with a parametric Euler step, *i.e.*

$$\left(\frac{\partial S}{\partial \varphi_{\boldsymbol{i}}}\right)_{\tau+\Delta\tau k} = \left(\frac{\partial S}{\partial \varphi_{\boldsymbol{i}}}\right)\left(\varphi(\tau) - k\Delta\tau(\nabla S)_{\tau} + \sigma\sqrt{2\Delta\tau}\eta(\tau)\right). \tag{92}$$

We can consider the Taylor expansion of Eq. (92), namely

$$\begin{aligned}\left(\frac{\partial S}{\partial\varphi_{\boldsymbol{i}_1}}\right)_{\tau+\Delta\tau k}=&\left(\frac{\partial S}{\partial\varphi_{\boldsymbol{i}_1}}\right)_{\tau}+\left(\frac{\partial^2 S}{\partial\varphi_{\boldsymbol{i}_1}\partial\varphi_{\boldsymbol{i}_2}}\right)_{\tau}\left[-k\Delta\tau\left(\frac{\partial S}{\partial\varphi_{\boldsymbol{i}_2}}\right)_{\tau}-\sigma\sqrt{2\Delta\tau}\eta_{\boldsymbol{i}_2}(\tau)\right]+\\
+\frac{1}{2}\left(\frac{\partial^3 S}{\partial\varphi_{\boldsymbol{i}_1}\partial\varphi_{\boldsymbol{i}_2}\partial\varphi_{\boldsymbol{i}_3}}\right)_{\tau}&\left[-k\Delta\tau\left(\frac{\partial S}{\partial\varphi_{\boldsymbol{i}_2}}\right)_{\tau}-\sigma\sqrt{2\Delta\tau}\eta_{\boldsymbol{i}_2}(\tau)\right]\left[-k\Delta\tau\left(\frac{\partial S}{\partial\varphi_{\boldsymbol{i}_3}}\right)_{\tau}-\sigma\sqrt{2\Delta\tau}\eta_{\boldsymbol{i}_3}(\tau)\right]+O(\Delta\tau^{\frac{3}{2}})\\
=&\left(\frac{\partial S}{\partial\varphi_{\boldsymbol{i}_1}}\right)_{\tau}-k\Delta\tau\left(\frac{\partial^2 S}{\partial\varphi_{\boldsymbol{i}_1}\partial\varphi_{\boldsymbol{i}_2}}\right)_{\tau}\left(\frac{\partial S}{\partial\varphi_{\boldsymbol{i}_2}}\right)_{\tau}-\sigma\sqrt{2\Delta\tau}\eta_{\boldsymbol{i}_2}(\tau)\left(\frac{\partial^2 S}{\partial\varphi_{\boldsymbol{i}_1}\partial\varphi_{\boldsymbol{i}_2}}\right)_{\tau}+\\
&+\left(\frac{\partial^3 S}{\partial\varphi_{\boldsymbol{i}_1}\partial\varphi_{\boldsymbol{i}_2}\partial\varphi_{\boldsymbol{i}_3}}\right)_{\tau}\sigma^2\Delta\tau\eta_{\boldsymbol{i}_2}(\tau)\eta_{\boldsymbol{i}_3}(\tau)+O(\Delta\tau^{\frac{3}{2}})\,.\end{aligned}\tag{93}$$

Inserting Eq. (93) in Eq. (91) we obtain an explicit form for $F_{\boldsymbol{i}}(\tau)$ up to $O(\Delta\tau^{\frac{5}{2}})$ correction as follows

$$\begin{aligned}F_{\boldsymbol{i}_1}=&\Delta\tau\left[a\left(\frac{\partial S}{\partial\varphi_{\boldsymbol{i}_1}}\right)+b\left(\frac{\partial S}{\partial\varphi_{\boldsymbol{i}_1}}\right)-bk\Delta\tau\left(\frac{\partial^2 S}{\partial\varphi_{\boldsymbol{i}_1}\partial\varphi_{\boldsymbol{i}_2}}\right)\left(\frac{\partial S}{\partial\varphi_{\boldsymbol{i}_2}}\right)-b\sigma\sqrt{2\Delta\tau}\eta_{\boldsymbol{i}_2}\left(\frac{\partial^2 S}{\partial\varphi_{\boldsymbol{i}_1}\partial\varphi_{\boldsymbol{i}_2}}\right)\right.\\
&\left.+\Delta\tau b\sigma^2\left(\frac{\partial^3 S}{\partial\varphi_{\boldsymbol{i}_1}\partial\varphi_{\boldsymbol{i}_2}\partial\varphi_{\boldsymbol{i}_3}}\right)\eta_{\boldsymbol{i}_2}\eta_{\boldsymbol{i}_3}\right]+\sqrt{2\Delta\tau}\eta_{\boldsymbol{i}_1}+O(\Delta\tau^{\frac{5}{2}})\,.\end{aligned}\tag{94}$$

We set

$$a+b=1\tag{95}$$

for first-order consistency. In this case Eq. (94) simplifies to

$$\begin{aligned}F_{\boldsymbol{i}_1}=&\Delta\tau\left(\frac{\partial S}{\partial\varphi_{\boldsymbol{i}_1}}\right)-bk\Delta\tau^2\left(\frac{\partial^2 S}{\partial\varphi_{\boldsymbol{i}_1}\partial\varphi_{\boldsymbol{i}_2}}\right)\left(\frac{\partial S}{\partial\varphi_{\boldsymbol{i}_2}}\right)-b\sigma\sqrt{2}(\Delta\tau)^{\frac{3}{2}}\eta_{\boldsymbol{i}_2}\left(\frac{\partial^2 S}{\partial\varphi_{\boldsymbol{i}_1}\partial\varphi_{\boldsymbol{i}_2}}\right)&(96)\\
&+\Delta\tau^2 b\sigma^2\left(\frac{\partial^3 S}{\partial\varphi_{\boldsymbol{i}_1}\partial\varphi_{\boldsymbol{i}_2}\partial\varphi_{\boldsymbol{i}_3}}\right)\eta_{\boldsymbol{i}_2}\eta_{\boldsymbol{i}_3}+\sqrt{2\Delta\tau}\eta_{\boldsymbol{i}_1}+O(\Delta\tau^{\frac{5}{2}})\,.&(97)\end{aligned}$$

As before, we need to compute the expectation values over the gaussian white noise, namely

$$\langle F_{\boldsymbol{i}_1}\rangle=\Delta\tau\left(\frac{\partial S}{\partial\varphi_{\boldsymbol{i}_1}}\right)-k\Delta\tau^2 b\left(\frac{\partial^2 S}{\partial\varphi_{\boldsymbol{i}_1}\partial\varphi_{\boldsymbol{i}_2}}\right)\left(\frac{\partial S}{\partial\varphi_{\boldsymbol{i}_2}}\right)+\Delta\tau^2 b\sigma^2\left(\frac{\partial^3 S}{\partial\varphi_{\boldsymbol{i}_1}\partial\varphi_{\boldsymbol{i}_2}\partial\varphi_{\boldsymbol{i}_2}}\right)+O(\Delta\tau^{\frac{5}{2}})\,,\tag{98}$$

$$\langle F_{\boldsymbol{i}_1}F_{\boldsymbol{i}_2}\rangle=\Delta\tau^2\left(\frac{\partial S}{\partial\varphi_{\boldsymbol{i}_1}}\right)\left(\frac{\partial S}{\partial\varphi_{\boldsymbol{i}_2}}\right)-4b\sigma\Delta\tau^2\left(\frac{\partial^2 S}{\partial\varphi_{\boldsymbol{i}_1}\partial\varphi_{\boldsymbol{i}_2}}\right)+2\Delta\tau\delta_{\boldsymbol{i}_1\boldsymbol{i}_2}+O(\Delta\tau^{\frac{5}{2}})\,,\tag{99}$$

$$\langle F_{\boldsymbol{i}_1}F_{\boldsymbol{i}_2}F_{\boldsymbol{i}_3}\rangle=2\Delta\tau^2\left[\left(\frac{\partial S}{\partial\varphi_{\boldsymbol{i}_1}}\right)\delta_{\boldsymbol{i}_2\boldsymbol{i}_3}+\left(\frac{\partial S}{\partial\varphi_{\boldsymbol{i}_2}}\right)\delta_{\boldsymbol{i}_1\boldsymbol{i}_3}+\left(\frac{\partial S}{\partial\varphi_{\boldsymbol{i}_3}}\right)\delta_{\boldsymbol{i}_1\boldsymbol{i}_2}\right]+O(\Delta\tau^{\frac{5}{2}})\,,\tag{100}$$

$$\langle F_{\boldsymbol{i}_1}F_{\boldsymbol{i}_2}F_{\boldsymbol{i}_3}F_{\boldsymbol{i}_4}\rangle=4\Delta\tau^2\left[\delta_{\boldsymbol{i}_1\boldsymbol{i}_2}\delta_{\boldsymbol{i}_3\boldsymbol{i}_4}+\delta_{\boldsymbol{i}_1\boldsymbol{i}_3}\delta_{\boldsymbol{i}_2\boldsymbol{i}_4}+\delta_{\boldsymbol{i}_1\boldsymbol{i}_4}\delta_{\boldsymbol{i}_2\boldsymbol{i}_3}\right]+O(\Delta\tau^{\frac{5}{2}})\,,\tag{101}$$

$$\langle F_{i_1} F_{i_2} F_{i_3} F_{i_4} F_{i_5} \ldots \rangle = O(\Delta\tau^{\frac{5}{2}}) \,. \tag{102}$$

Using the Kramers-Moyal expansion[3] in Eq. (81) we recover the leading order equation

$$\frac{\partial}{\partial\varphi_{i_1}}\left[\left(\frac{\partial S}{\partial\varphi_{i_1}}\right)P\right] + \frac{\partial^2}{\partial\varphi_{i_1}\partial\varphi_{i_2}}\left[\delta_{i_1 i_2} P\right] = 0 \,. \tag{103}$$

Additionally, the first-order correction to Eq. (103) reads

$$\begin{aligned}
&\frac{\partial}{\partial\varphi_{i_1}}\left[-kb\left(\frac{\partial^2 S}{\partial\varphi_{i_1}\partial\varphi_{i_3}}\right)\left(\frac{\partial S}{\partial\varphi_{i_3}}\right)P + b\sigma^2\left(\frac{\partial^3 S}{\partial\varphi_{i_3}\partial\varphi_{i_3}\partial\varphi_{i_1}}\right)P\right] + \\
&+\frac{1}{2}\frac{\partial}{\partial\varphi_{i_1}}\left[\left(\frac{\partial^2 S}{\partial\varphi_{i_2}\partial\varphi_{i_1}}\right)\left(\frac{\partial S}{\partial\varphi_{i_2}}\right)P + \left(\frac{\partial S}{\partial\varphi_{i_1}}\right)\left(\frac{\partial^2 S}{\partial\varphi_{i_2}\partial\varphi_{i_2}}\right)P - \left(\frac{\partial S}{\partial\varphi_{i_1}}\right)\left(\frac{\partial S}{\partial\varphi_{i_2}}\right)^2 P - \right. \\
&\left. - 4b\sigma\left(\frac{\partial^3 S}{\partial\varphi_{i_1}\partial\varphi_{i_2}\partial\varphi_{i_2}}\right)P + 4b\sigma\left(\frac{\partial^2 S}{\partial\varphi_{i_1}\partial\varphi_{i_2}}\right)\left(\frac{\partial S}{\partial\varphi_{i_2}}\right)P\right] \\
&+\frac{\partial^3}{\partial\varphi_{i_1}\partial\varphi_{i_2}^2}\left[\left(\frac{\partial S}{\partial\varphi_{i_1}}\right)P\right] + \frac{1}{2}\frac{\partial^4}{\partial\varphi_{i_1}^2\partial\varphi_{i_2}^2}P \,.
\end{aligned} \tag{104}$$

As before, we can use Eq. (87) to handle the last equation

$$\begin{aligned}
&\frac{\partial}{\partial\varphi_{i_1}}\left[-kb\left(\frac{\partial^2 S}{\partial\varphi_{i_1}\partial\varphi_{i_3}}\right)\left(\frac{\partial S}{\partial\varphi_{i_3}}\right)P + b\sigma^2\left(\frac{\partial^3 S}{\partial\varphi_{i_3}\partial\varphi_{i_3}\partial\varphi_{i_1}}\right)P\right] + \\
&+\frac{1}{2}\frac{\partial}{\partial\varphi_{i_1}}\left[\left(\frac{\partial^2 S}{\partial\varphi_{i_2}\partial\varphi_{i_1}}\right)\left(\frac{\partial S}{\partial\varphi_{i_2}}\right)P + \left(\frac{\partial S}{\partial\varphi_{i_1}}\right)\left(\frac{\partial^2 S}{\partial\varphi_{i_2}\partial\varphi_{i_2}}\right)P - \left(\frac{\partial S}{\partial\varphi_{i_1}}\right)\left(\frac{\partial S}{\partial\varphi_{i_2}}\right)^2 P - \right. \\
&\left. - 4b\sigma\left(\frac{\partial^3 S}{\partial\varphi_{i_1}\partial\varphi_{i_2}\partial\varphi_{i_2}}\right)P + 4b\sigma\left(\frac{\partial^2 S}{\partial\varphi_{i_1}\partial\varphi_{i_2}}\right)\left(\frac{\partial S}{\partial\varphi_{i_2}}\right)P\right] + \frac{1}{2}\frac{\partial^3}{\partial\varphi_{i_1}\partial\varphi_{i_2}^2}\left[\left(\frac{\partial S}{\partial\varphi_{i_1}}\right)P\right] \\
&= \frac{\partial}{\partial\varphi_{i_1}}\left[-kb\left(\frac{\partial^2 S}{\partial\varphi_{i_1}\partial\varphi_{i_3}}\right)\left(\frac{\partial S}{\partial\varphi_{i_3}}\right)P + b\sigma^2\left(\frac{\partial^3 S}{\partial\varphi_{i_3}\partial\varphi_{i_3}\partial\varphi_{i_1}}\right)P\right] + \\
&+\frac{\partial}{\partial\varphi_{i_1}}\left[\frac{1}{2}\left(\frac{\partial^2 S}{\partial\varphi_{i_2}\partial\varphi_{i_1}}\right)\left(\frac{\partial S}{\partial\varphi_{i_2}}\right)P + \frac{1}{2}\left(\frac{\partial S}{\partial\varphi_{i_1}}\right)\left(\frac{\partial^2 S}{\partial\varphi_{i_2}\partial\varphi_{i_2}}\right)P - \frac{1}{2}\left(\frac{\partial S}{\partial\varphi_{i_1}}\right)\left(\frac{\partial S}{\partial\varphi_{i_2}}\right)^2 P - \right. \\
&\left. - 2b\sigma\left(\frac{\partial^3 S}{\partial\varphi_{i_1}\partial\varphi_{i_2}\partial\varphi_{i_2}}\right)P + 2b\sigma\left(\frac{\partial^2 S}{\partial\varphi_{i_1}\partial\varphi_{i_2}}\right)\left(\frac{\partial S}{\partial\varphi_{i_2}}\right)P\right] + \\
&+\underbrace{\frac{1}{2}\frac{\partial^2}{\partial\varphi_{i_1}\partial\varphi_{i_2}}\left[\left(\frac{\partial^2 S}{\partial\varphi_{i_1}\partial\varphi_{i_2}}\right)P - \left(\frac{\partial S}{\partial\varphi_{i_1}}\right)\left(\frac{\partial S}{\partial\varphi_{i_2}}\right)P\right]}_{=A} \,.
\end{aligned} \tag{105}$$

The last term can be written as

$$\begin{aligned}
A =& \frac{1}{2}\frac{\partial^2}{\partial\varphi_{i_1}\partial\varphi_{i_2}}\left[\left(\frac{\partial^2 S}{\partial\varphi_{i_1}\partial\varphi_{i_2}}\right)P - \left(\frac{\partial S}{\partial\varphi_{i_1}}\right)\left(\frac{\partial S}{\partial\varphi_{i_2}}\right)P\right] \\
=& \frac{1}{2}\frac{\partial}{\partial\varphi_{i_1}}\left[\left(\frac{\partial^3 S}{\partial\varphi_{i_2}\partial\varphi_{i_2}\partial\varphi_{i_1}}\right)P - \left(\frac{\partial^2 S}{\partial\varphi_{i_1}\partial\varphi_{i_2}}\right)\left(\frac{\partial S}{\partial\varphi_{i_2}}\right)P - \left(\frac{\partial^2 S}{\partial\varphi_{i_2}\partial\varphi_{i_1}}\right)\left(\frac{\partial S}{\partial\varphi_{i_2}}\right)P - \right. \\
&\left. - \left(\frac{\partial S}{\partial\varphi_{i_1}}\right)\left(\frac{\partial^2 S}{\partial\varphi_{i_2}\partial\varphi_{i_2}}\right)P + \left(\frac{\partial S}{\partial\varphi_{i_1}}\right)\left(\frac{\partial S}{\partial\varphi_{i_2}}\right)^2 P\right] \,.
\end{aligned} \tag{106}$$

[3] We note that Eq. (81) holds for every discrete stochastic process.

Considering the previous equation, the first-order correction reads

$$\begin{aligned}
&\frac{\partial}{\partial\varphi_{\boldsymbol{i}_1}}\Big[-kb\Big(\frac{\partial^2 S}{\partial\varphi_{\boldsymbol{i}_1}\partial\varphi_{\boldsymbol{i}_3}}\Big)\Big(\frac{\partial S}{\partial\varphi_{\boldsymbol{i}_3}}\Big)P+b\sigma^2\Big(\frac{\partial^3 S}{\partial\varphi_{\boldsymbol{i}_3}\partial\varphi_{\boldsymbol{i}_3}\partial\varphi_{\boldsymbol{i}_1}}\Big)P\Big]+\\
&+\frac{\partial}{\partial\varphi_{\boldsymbol{i}_1}}\Big[\frac{1}{2}\Big(\frac{\partial^2 S}{\partial\varphi_{\boldsymbol{i}_2}\partial\varphi_{\boldsymbol{i}_1}}\Big)\Big(\frac{\partial S}{\partial\varphi_{\boldsymbol{i}_2}}\Big)P+\frac{1}{2}\Big(\frac{\partial S}{\partial\varphi_{\boldsymbol{i}_1}}\Big)\Big(\frac{\partial^2 S}{\partial\varphi_{\boldsymbol{i}_2}\partial\varphi_{\boldsymbol{i}_2}}\Big)P-\frac{1}{2}\Big(\frac{\partial S}{\partial\varphi_{\boldsymbol{i}_1}}\Big)\Big(\frac{\partial S}{\partial\varphi_{\boldsymbol{i}_2}}\Big)^2P-\\
&-2b\sigma\Big(\frac{\partial^3 S}{\partial\varphi_{\boldsymbol{i}_1}\partial\varphi_{\boldsymbol{i}_2}\partial\varphi_{\boldsymbol{i}_2}}\Big)P+2b\sigma\Big(\frac{\partial^2 S}{\partial\varphi_{\boldsymbol{i}_1}\partial\varphi_{\boldsymbol{i}_2}}\Big)\Big(\frac{\partial S}{\partial\varphi_{\boldsymbol{i}_2}}\Big)P\Big]+\\
&\frac{\partial}{\partial\varphi_{\boldsymbol{i}_1}}\Big[\frac{1}{2}\Big(\frac{\partial^3 S}{\partial\varphi_{\boldsymbol{i}_2}\partial\varphi_{\boldsymbol{i}_2}\partial\varphi_{\boldsymbol{i}_1}}\Big)P-\frac{1}{2}\Big(\frac{\partial^2 S}{\partial\varphi_{\boldsymbol{i}_1}\partial\varphi_{\boldsymbol{i}_2}}\Big)\Big(\frac{\partial S}{\partial\varphi_{\boldsymbol{i}_2}}\Big)P-\frac{1}{2}\Big(\frac{\partial^2 S}{\partial\varphi_{\boldsymbol{i}_2}\partial\varphi_{\boldsymbol{i}_1}}\Big)\Big(\frac{\partial S}{\partial\varphi_{\boldsymbol{i}_2}}\Big)P-\\
&-\frac{1}{2}\Big(\frac{\partial S}{\partial\varphi_{\boldsymbol{i}_1}}\Big)\Big(\frac{\partial^2 S}{\partial\varphi_{\boldsymbol{i}_2}\partial\varphi_{\boldsymbol{i}_2}}\Big)P+\frac{1}{2}\Big(\frac{\partial S}{\partial\varphi_{\boldsymbol{i}_1}}\Big)\Big(\frac{\partial S}{\partial\varphi_{\boldsymbol{i}_2}}\Big)^2P\Big]\\
&=\frac{\partial}{\partial\varphi_{\boldsymbol{i}_1}}\Big[\Big(\frac{\partial^2 S}{\partial\varphi_{\boldsymbol{i}_1}\partial\varphi_{\boldsymbol{i}_3}}\Big)\Big(\frac{\partial S}{\partial\varphi_{\boldsymbol{i}_3}}\Big)P\Big(-kb+2b\sigma-\frac{1}{2}\Big)+\Big(\frac{\partial^3 S}{\partial\varphi_{\boldsymbol{i}_3}\partial\varphi_{\boldsymbol{i}_3}\partial\varphi_{\boldsymbol{i}_1}}\Big)P\Big(b\sigma^2-2b\sigma+\frac{1}{2}\Big)\Big]\,.
\end{aligned}\tag{107}$$

We can set the parameters to cancel the first-order correction in the time step. The equations to be solved are

$$\begin{cases}
a+b=1\\
-kb+2b\sigma-\dfrac{1}{2}=0\\
b\sigma^2-2b\sigma+\dfrac{1}{2}=0\,.
\end{cases}\tag{108}$$

In the standard Runge-Kutta methods one sets [48]

$$b=\frac{1}{2}\qquad\rightarrow\qquad a=\frac{1}{2}\,,\qquad k=1\,,\qquad \sigma=1\,.\tag{109}$$

The corresponding discrete Langevin dynamics reads

$$\varphi_{\boldsymbol{i}}(\tau+\Delta\tau)=\varphi_{\boldsymbol{i}}(\tau)-\frac{\Delta\tau}{2}\Big[\Big(\frac{\partial S}{\partial\varphi_{\boldsymbol{i}}}\Big)_{\tau}+\Big(\frac{\partial S}{\partial\varphi_{\boldsymbol{i}}}\Big)_{\tau+\Delta\tau}\Big]+\sqrt{2\Delta\tau}\eta_{\boldsymbol{i}}(\tau)\,,\tag{110}$$

where the second gradient in Eq. (110) is calculated in the *tentative* update

$$\tilde{\varphi}(\tau)=\varphi(\tau)-\Delta\tau(\nabla S)_{\tau}+\sqrt{2\Delta\tau}\eta(\tau)\,.\tag{111}$$

In this way we obtain vanishing corrections in $\Delta\tau$, yielding

$$\langle A\rangle_{\Delta\tau}=\frac{\int D\varphi\ A[\varphi]\ e^{-(S+\Delta\tau^2\bar{S})}}{\int D\varphi\ e^{-(S+\Delta\tau^2\bar{S})}}=\frac{\int D\varphi\ A[\varphi]\ e^{-S}(1-\Delta\tau^2\bar{S})}{\int D\varphi\ e^{-S}(1-\Delta\tau^2\bar{S})}=\langle A\rangle+O(\Delta\tau^2)\,.\tag{112}$$

Eq. (112) shows that for a fixed tiny stochastic time step, the systematic effects using Runge-Kutta integrator can be *in principle* smaller compared to the Euler integrator. However, Runge-Kutta scheme requires extra calculations of the gradient. In the case we presented, the computational cost doubles for each Monte Carlo step.

1.5 Continuum stochastic time extrapolations

We consider NSPT measurements of an observable A, namely

$$A^{(n)}_{\Delta\tau,i}\,, \qquad i=1,\ldots,N_{\text{samples}}\,, \tag{113}$$

where n is the perturbative order and $\Delta\tau$ is the time step. The best estimate for A is the mean

$$\langle A^{(n)}\rangle_{\Delta\tau} = \frac{1}{N_{\text{samples}}}\sum_{i=1}^{N_{\text{samples}}} A^{(n)}_{\Delta\tau,i}\,. \tag{114}$$

Furthermore, we can define the covariance matrix

$$\Sigma_{\Delta\tau,\Delta\tau'}(n,m) = \text{cov}(A^{(n)}_{\Delta\tau}, A^{(m)}_{\Delta\tau'})\,, \tag{115}$$

being $\text{cov}(A^{(n)}_{\Delta\tau}, A^{(m)}_{\Delta\tau'})$ the covariance of the mean. In this section we will not consider autocorrelated or cross-correlated data. In the next section we discuss how to introduce autocorrelations and cross-correlations in the matrix element of Eq. (115). Moreover we are always implying that measurements are taken on thermalized histories, excluding configurations in the transient region.

Being the samples uncorrelated for different time steps, the matrix in Eq. (115) is a block diagonal matrix, namely

$$\Sigma_{\Delta\tau,\Delta\tau'}(n,m) = \delta_{\Delta\tau,\Delta\tau'}\Sigma_{\Delta\tau}(n,m) = \delta_{\Delta\tau,\Delta\tau'}\text{cov}(A^{(n)}_{\Delta\tau}, A^{(m)}_{\Delta\tau})\,. \tag{116}$$

Extrapolations to vanishing time step can be obtained considering a dedicated χ^2. Using first-order scheme such as the Euler scheme, we consider the minimum of the function [21]

$$\chi^2_{gen} = \sum_{n,m}^{n_{\text{max}}}\sum_{\Delta\tau}\big(\langle A^{(n)}\rangle_{\Delta\tau} - \alpha_n\Delta\tau - \beta_n\big)\Sigma^{-1}_{\Delta\tau}(n,m)\big(\langle A^{(m)}\rangle_{\Delta\tau} - \alpha_m\Delta\tau - \beta_m\big) \tag{117}$$

in terms of the parameters α_n and β_n. It is evident then the order-by-order identification

$$\langle A^{(n)}\rangle = \beta_n\,. \tag{118}$$

If there is sufficient statistic to also consider higher-order corrections, the previous formula can be extended as

$$\chi^2_{gen} = \sum_{n,m,\Delta\tau}\big(\langle A^{(n)}\rangle_{\Delta\tau} - \gamma_n\Delta\tau^2 - \alpha_n\Delta\tau - \beta_n\big)\Sigma^{-1}_{\Delta\tau}(n,m)\big(\langle A^{(m)}\rangle_{\Delta\tau} - \gamma_m\Delta\tau^2 - \alpha_m\Delta\tau - \beta_m\big)\,. \tag{119}$$

Second-order schemes like the Runge-Kutta scheme display second-order corrections. In this case the extrapolation can be obtained considering the minimum of the function

$$\chi^2_{gen} = \sum_{n,m}^{n_{\max}} \sum_{\Delta\tau} \left(\langle A^{(n)}\rangle_{\Delta\tau} - \alpha_n \Delta\tau^2 - \beta_n\right) \Sigma^{-1}_{\Delta\tau}(n,m) \left(\langle A^{(m)}\rangle_{\Delta\tau} - \alpha_m \Delta\tau^2 - \beta_m\right), \tag{120}$$

where the linear correction terms have been set to zero. We can introduce also cubic correction to Eq. (120), obtaining

$$\chi^2_{gen} = \sum_{n,m}^{n_{\max}} \sum_{\Delta\tau} \left(\langle A^{(n)}\rangle_{\Delta\tau} - \gamma_n \Delta\tau^3 - \alpha_n \Delta\tau^2 - \beta_n\right) \Sigma^{-1}_{\Delta\tau}(n,m) \left(\langle A^{(m)}\rangle_{\Delta\tau} - \gamma_m \Delta\tau^3 - \alpha_m \Delta\tau^2 - \beta_m\right). \tag{121}$$

Error propagation does not present particular subtleties once the parameters in Eqs. (117) - (119) - (120) - (121) have been determined. We use the Gaussian sampling method. With this tool we generate a sampling of the data using a standard multivariate distribution with covariance matrix $\Sigma_{\Delta\tau}(n,m)$. For each sample, we perform an order-by-order polynomial fit in $\Delta\tau$, obtaining a distribution of values for each parameter. Fitted quantities and errors are the mean and the standard deviation of the respective distributions.

Other methods are available, such as error propagation through Automatic Differentiation methods [49–51]. Some checks have been carried out at low perturbative orders, showing agreement with Gaussian sampling.

1.6 Autocorrelations and cross-correlations

When generating configurations with a stochastic differential equation, in order to correctly compute errors we need to compute and take into account the autocorrelations characteristic of the Monte Carlo process. In addition, NSPT simulations also require evaluating cross-correlations at different perturbative orders. We describe our methodology, based on the Gamma Function Method [52] and the Blocking Method [53].

1.6.1 Gamma Function Method for NSPT

This method is used to estimate the autocorrelation time τ_{int}. We present below an extended version to consider also cross-correlations. We discuss only the single-replica ensemble case, while the extension to multiple replicas ensemble for autocorrelations is presented in [54]. We present the Gamma Function Method using the language of NSPT simulations, *i.e.* taking into account different perturbative orders.

Consider an ensemble of measurements

$$\{A_1^{(n)}, A_2^{(n)}, A_3^{(n)}, \ldots, A_N^{(n)}\} = \{A_i^{(n)}\}\,, \tag{122}$$

with defined average $\mu_A^{(n)}$, where the superscript n indicates the perturbative order. As before, the best estimate we can assign to the variable is the mean

$$\bar{A}^{(n)} = \sum_{i=1}^{N} A_i^{(n)} \tag{123}$$

and we are interested in its variance. In particular, we noted that

$$\begin{aligned}
\mathrm{Var}(\bar{A}^{(n)}) &= \langle (\bar{A}^{(n)} - \mu_A^{(n)})(\bar{A}^{(n)} - \mu_A^{(n)}) \rangle = \frac{1}{N^2} \sum_{t=1}^{N} \sum_{s=1}^{N} \Big[\langle A_t^{(n)} A_s^{(n)} \rangle - (\mu_A^{(n)})^2 \Big] \\
&= \frac{1}{N^2} \sum_{t,s=1}^{N} \Big[\langle A_t^{(n)} A_{t+(s-t)}^{(n)} \rangle - (\mu_A^{(n)})^2 \Big] \\
&= \frac{1}{N^2} \sum_{t,s=1}^{N} C_{A^{(n)} A^{(n)}}(s-t)\,,
\end{aligned} \tag{124}$$

where we defined the unnormalized autocorrelation function

$$C_{A^{(n)} A^{(n)}}(t) = \langle A_s^{(n)} A_{s+t}^{(n)} \rangle - (\mu_A^{(n)})^2\,. \tag{125}$$

Being the unnormalized autocorrelation function dependent only on index differences, it is possible to change the summation variables:

$$\begin{aligned}
\mathrm{Var}(\bar{A}^{(n)}) &= \frac{1}{N^2} \sum_{t,s=1}^{N} C_{A^{(n)} A^{(n)}}(s-t) \\
&= \frac{1}{N^2} \sum_{t=-(N-1)}^{+(N-1)} C_{A^{(n)} A^{(n)}}(t)(N - |t|) \\
&= \frac{1}{N} \sum_{t=-(N-1)}^{+(N-1)} C_{A^{(n)} A^{(n)}}(t) \left(1 - \frac{|t|}{N}\right) \\
&= \frac{\mathrm{Var}(A^{(n)})}{N} \sum_{t=-(N-1)}^{+(N-1)} \rho_{A^{(n)} A^{(n)}}(t) \left(1 - \frac{|t|}{N}\right),
\end{aligned} \tag{126}$$

where we introduced the normalized autocorrelation function

$$\rho_{A^{(n)} A^{(n)}}(t) = \frac{C_{A^{(n)} A^{(n)}}(t)}{C_{A^{(n)} A^{(n)}}(0)} = \frac{C_{A^{(n)} A^{(n)}}(t)}{\mathrm{Var}(A^{(n)})}\,. \tag{127}$$

We note that in the case of correlated samples, the variance of the mean is corrected with respect to the uncorrelated samples by a factor

$$\sum_{t=-(N-1)}^{+(N-1)} \rho_{A^{(n)} A^{(n)}}(t) \left(1 - \frac{|t|}{N}\right). \tag{128}$$

From the properties

$$\rho_{A^{(n)}A^{(n)}}(t) = \rho_{A^{(n)}A^{(n)}}(-t) \tag{129}$$

and

$$\rho_{A^{(n)}A^{(n)}}(0) = 1\,, \tag{130}$$

we can further simplify the expression to

$$\begin{aligned}\mathrm{Var}(\bar{A}^{(n)}) &= \frac{\mathrm{Var}(A^{(n)})}{N}\left\{2\sum_{t=1}^{(N-1)}\rho_{A^{(n)}A^{(n)}}(t)\left(1-\frac{|t|}{N}\right)+1\right\} \\ &= \frac{2\mathrm{Var}(A^{(n)})}{N}\left\{\sum_{t=1}^{(N-1)}\rho_{A^{(n)}A^{(n)}}(t)\left(1-\frac{|t|}{N}\right)+\frac{1}{2}\right\}.\end{aligned} \tag{131}$$

The normalized autocorrelation function decays such that it is negligible for $t > \hat{t}$; then for $N >> \hat{t}$ we notice that the second term in the parentheses can be neglected. We obtain

$$\mathrm{Var}(\bar{A}^{(n)}) = \frac{2\mathrm{Var}(A^{(n)})}{N}\left\{\sum_{t=1}^{(N-1)}\rho_{A^{(n)}A^{(n)}}(t)+\frac{1}{2}\right\} \simeq \frac{\mathrm{Var}(A^{(n)})}{N/2\tau_{\mathrm{int,A^{(n)}}}}\,, \tag{132}$$

where we have introduced the so-called integrated autocorrelation time

$$\tau^{(n)}_{\mathrm{int,f}} = \sum_{t=1}^{\infty}\rho_{ff}(t)+\frac{1}{2}\,. \tag{133}$$

In the framework of Eqs. (117) - (121) we set

$$\Sigma_{\Delta\tau}(n,n) = \frac{\mathrm{Var}(A^{(n)})}{N/2\tau^{(n)}_{\mathrm{int,A^{(n)}}}}\,. \tag{134}$$

We have now only computed diagonal contributions entering any of Eqs. (117) - (121), so we move on and consider two different perturbative order

$$\{A^{(n)}_1, A^{(n)}_2, A^{(n)}_3, \ldots, A^{(n)}_N\} = \{A^{(n)}_i\}\,, \tag{135}$$

$$\{A^{(m)}_1, A^{(m)}_2, A^{(m)}_3, \ldots, A^{(m)}_N\} = \{A^{(m)}_i\}\,, \tag{136}$$

with averages $\mu^{(n)}_A$ and $\mu^{(m)}_A$. We can compute

$$\begin{aligned}\mathrm{Cov}(\bar{A}^{(n)},\bar{A}^{(m)}) &= \langle(\bar{A}^{(n)}-\mu^{(n)}_A)(\bar{A}^{(m)}-\mu^{(m)}_A)\rangle = \frac{1}{N^2}\sum_{t=1}^{N}\sum_{s=1}^{N}\left[\langle A^{(n)}_t A^{(m)}_s\rangle - \mu^{(n)}_A\mu^{(m)}_A\right] \\ &= \frac{1}{N^2}\sum_{t,s=1}^{N}\left[\langle A^{(n)}_t A^{(m)}_{t+(s-t)}\rangle - \mu^{(n)}_A\mu^{(m)}_A\right] \\ &= \frac{1}{N^2}\sum_{t,s=1}^{N} C_{A^{(n)}A^{(m)}}(s-t)\,,\end{aligned} \tag{137}$$

where we defined the unnormalized cross-correlation function

$$C_{A^{(n)}A^{(m)}}(t) = \langle A_s^{(n)} A_{s+t}^{(m)} \rangle - \mu_A^{(n)} \mu_A^{(m)} \,. \tag{138}$$

As before, we can perform a change of variable $t = t - s$ obtaining

$$\begin{aligned}
\frac{1}{N^2} \sum_{t,s=0}^{N} C_{A^{(n)}A^{(m)}}(s-t) &= \frac{1}{N^2} \Bigg[\sum_{t=1}^{N-1} C_{A^{(n)}A^{(m)}}(t)(1-t) + \sum_{t=1}^{N-1} C_{A^{(m)}A^{(n)}}(t)(1-t) \\
&\qquad + N C_{A^{(n)}A^{(m)}}(0) \Bigg] \\
&= \frac{1}{N} \Bigg[\sum_{t=1}^{N-1} C_{A^{(n)}A^{(m)}}(t) \left(1 - \frac{t}{N}\right) + \sum_{t=1}^{N-1} C_{A^{(m)}A^{(n)}}(t) \left(1 - \frac{t}{N}\right) \\
&\qquad + C_{A^{(n)}A^{(m)}}(0) \Bigg] \,.
\end{aligned} \tag{139}$$

Introducing the two normalized cross-correlation functions

$$\begin{aligned}
\rho_{A^{(n)}A^{(m)}}(t) &= \frac{C_{A^{(n)}A^{(m)}}(t)}{C_{A^{(n)}A^{(m)}}(0)} = \frac{C_{A^{(n)}A^{(m)}}(t)}{\mathrm{Cov}(A^{(n)}, A^{(m)})} \,, \\
\rho_{A^{(m)}A^{(a)}}(t) &= \frac{C_{A^{(m)}A^{(n)}}(t)}{C_{A^{(m)}A^{(n)}}(0)} = \frac{C_{A^{(m)}A^{(n)}}(t)}{\mathrm{Cov}(A^{(m)}, A^{(n)})} \,,
\end{aligned} \tag{140}$$

we finally obtain

$$\begin{aligned}
\mathrm{Cov}(\bar{A}^{(n)}, \bar{A}^{(m)}) &= \frac{\mathrm{Cov}(A^{(n)}, A^{(m)})}{N} \Bigg[\sum_{t=1}^{N-1} \rho_{A^{(n)}A^{(m)}}(t) \left(1 - \frac{t}{N}\right) \\
&\qquad + \sum_{t=1}^{N-1} \rho_{A^{(m)}A^{(n)}}(t) \left(1 - \frac{t}{N}\right) + 1 \Bigg] \\
&= \frac{\mathrm{Cov}(A^{(n)}, A^{(m)})}{N} \left[\sum_{t=1}^{N-1} \rho_{A^{(n)}A^{(m)}}(t) + \frac{1}{2} + \sum_{t=1}^{N-1} \rho_{A^{(m)}A^{(n)}}(t) + \frac{1}{2} \right] ,
\end{aligned} \tag{141}$$

having neglected the t/N terms as before. In the end we end up with

$$\mathrm{Cov}(\bar{A}^{(n)}, \bar{A}^{(m)}) \simeq \frac{\mathrm{Cov}(A^{(n)}, A^{(m)})}{N} \left[\tau_{\mathrm{int}}^{(A^{(n)}, A^{(m)})} + \tau_{\mathrm{int}}^{(A^{(m)}, A^{(n)})} \right] , \tag{142}$$

where

$$\tau_{\mathrm{int}}^{(f,g)} = \sum_{t=1}^{\infty} \rho_{f,g}(t) + \frac{1}{2} \,. \tag{143}$$

We now have an expression for non-diagonal contributions entering any of Eqs. (117) - (121), namely

$$\Sigma_{\Delta\tau}(n,m) = \frac{\mathrm{Cov}(A^{(n)}, A^{(m)})}{N} \left[\tau_{\mathrm{int}}^{(A^{(n)}, A^{(m)})} + \tau_{\mathrm{int}}^{(A^{(m)}, A^{(n)})} \right] . \tag{144}$$

From a numerical point of view, the sum in Eq. (133) and in Eq. (143) need to be truncated: indeed, the larger t, the fewer data are available, possibly resulting in a noisy signal. Automatic windowing procedures (based on specific criteria) are usually adopted [54]. In this thesis we used a hard cut. All the autocorrelations and cross-correlations functions have been checked, ensuring their reliability.

1.6.2 Blocking Method for NSPT

Besides the Gamma Function Method, error estimation can go through the so-called Blocking Method. As before, we consider an ensemble of measurements

$$\{A_1^{(n)}, A_2^{(n)}, A_3^{(n)}, \dots, A_N^{(n)}\} = \{A_i^{(n)}\}\,. \tag{145}$$

Again, neglecting autocorrelations, the naive estimation of the error would be

$$\sigma^2_{\text{naive},A^{(n)}} = \frac{\text{Var}(A^{(n)})}{N}\,. \tag{146}$$

Now we can divide the set of measurements into blocks of arbitrary size L. For example, we can set $L = 2$. We perform the average in each block, obtaining a new ensemble of $\tilde{N} = N/2$ elements

$$\{\underbrace{A_1^{(n)}, A_2^{(n)}}_{\text{block 1}}, \underbrace{A_3^{(n)}, A_4^{(n)}}_{\text{block 2}}, \dots, A_N^{(n)}\} \quad \to \quad \{\tilde{A}_1^{(n)}, \tilde{A}_2^{(n)}, \tilde{A}_3^{(n)}, \dots, \tilde{A}_{\tilde{N}}^{(n)}\}\,. \tag{147}$$

The new naive estimation of the variance is

$$\sigma^2_{\text{size}=2,A^{(n)}} = \frac{\text{Var}(\tilde{A}^{(n)})}{\tilde{N}}\,. \tag{148}$$

Notice that if data were uncorrelated, the variance in Eq. (148) would be the same as that given by Eq. (146). We can repeat the procedure for increasing block size, for example setting $L = 4$. We obtain a new dataset with $\bar{N} = N/4$ elements. The new estimation of the error is

$$\sigma^2_{\text{size}=4,A^{(n)}} = \frac{\text{Var}(\bar{A}^{(n)})}{\bar{N}}\,. \tag{149}$$

This process can be repeated an arbitrary number of times for increasing block sizes. If data were uncorrelated, at each step the variance of the blocked data should decrease as the inverse of the block size, compensating the decreasing number of samples (which are now the blocked data). Because of autocorrelation effects, the different estimations of the variance will monotonically increase, till blocked variables eventually are uncorrelated and we reach a plateau. The value of the plateau provides the value of the error to be associated with the measurements.

In the case of two different perturbative orders

$$\{A_1^{(n)}, A_2^{(n)}, A_3^{(n)}, \ldots, A_N^{(n)}\} = \{A_i^{(n)}\}\,, \tag{150}$$

$$\{A_1^{(m)}, A_2^{(m)}, A_3^{(m)}, \ldots, A_N^{(m)}\} = \{A_i^{(m)}\}\,, \tag{151}$$

Eq. (142) suggests that a naive values of the covariance of the mean can be computed as

$$\sigma_{\text{naive},A^{(n)}A^{(m)}} = \frac{\text{Cov}(A^{(n)}, A^{(m)})}{N}\,. \tag{152}$$

Now we implement again the blocking procedure, starting for example with block size $L = 2$. Computing the average in each block, we have a new ensemble of $\tilde{N} = N/2$ elements

$$\{\underbrace{A_1^{(n)}, A_2^{(n)}}_{\text{block 1}}, \underbrace{A_3^{(n)}, A_4^{(n)}}_{\text{block 2}}, \ldots, A_N^{(n)}\} \quad \to \quad \{\tilde{A}_1^{(n)}, \tilde{A}_2^{(n)}, \tilde{A}_3^{(n)}, \ldots, \tilde{A}_{\tilde{N}}^{(n)}\}\,, \tag{153}$$

$$\{\underbrace{A_1^{(m)}, A_2^{(m)}}_{\text{block 1}}, \underbrace{A_3^{(m)}, A_4^{(m)}}_{\text{block 2}}, \ldots, A_N^{(m)}\} \quad \to \quad \{\tilde{A}_1^{(m)}, \tilde{A}_2^{(m)}, \tilde{A}_3^{(m)}, \ldots, \tilde{A}_{\tilde{N}}^{(m)}\}\,. \tag{154}$$

The new estimation of the covariance is

$$\sigma_{\text{size}=2,A^{(n)}A^{(m)}} = \frac{\text{Cov}(\tilde{A}^{(n)}, \tilde{A}^{(m)})}{\tilde{N}}\,. \tag{155}$$

We repeat the procedure until we reach a plateau. For the corresponding block size, we have a statistically independent dataset. The value of the covariance at the plateau is the value of the covariance matrix element $\Sigma_{\Delta\tau}(m, n)$.

1.7 Implementation on the computer

One of the fundamental properties of NSPT is the ability to implement all the order-by-order computations automatically. In a real NSPT simulation, in a sense what we need to implement is something very close to the non-perturbative Langevin equation. Thanks to operator overloading, what is actually implemented is an automatic coding of all the different perturbative equations.

To be more precise, we note that by redefining operations as order-by-order operations in the following way

$$\begin{aligned} a = b + c \qquad &\to \qquad a^{(n)} = b^{(n)} + c^{(n)}\,, \\ a = b \cdot c \qquad &\to \qquad a^{(n)} = \sum_{i=0}^{n} b^{(i)} c^{(n-i)}\,, \end{aligned} \tag{156}$$

every non-perturbative Monte Carlo is automatically converted into its NSPT counterpart, almost without further modifications. Using Eq. (156), all types of interactions can be implemented, including logarithms, square roots and so on, which are defined through their Taylor series expansion up to a fixed order.

Of course, this order-by-order machinery results in increasing memory demand and computational cost as the perturbative order grows. Given the computing resources available today, this is not a big problem. Neglecting autocorrelations, the computational cost scales linearly with the volume and quadratically with the perturbative order [9], namely

$$T_{\rm NSPT} \approx L^d \left(\frac{n_{\rm max}^2 - n_{\rm max}}{2} \right) , \tag{157}$$

where d is the dimension of the lattice.

1.8 Other stochastic differential equations

The mechanism underlying NSPT is actually more general and can be implemented starting from many stochastic differential equations. With this respect, NSPT can benefit from state-of-the-art non-perturbative algorithms, improving efficiency. In non-perturbative simulations Generalized Hybrid Molecular Dynamics (GHMD) algorithms have proven to be more effective than Langevin algorithms. It is therefore not surprising that this has in recent years attracted attention, resulting in variants of NSPT.

The approach can be interesting given the lack of high-order schemes for the Langevin dynamics. On the contrary, for GHMD-type dynamics, based on the integration of Hamiltonian equations, it is possible to systematically implement integrators of increasingly higher-orders [55]: among these, to date the most used are symplectic integrators. Moreover, efficiently implementing these integrators is often not so difficult [56].

We present NSPT implementations based on HMD dynamics [47] and Kramers dynamics [57, 58], also referred to as HSPT and KSPT [13].

1.8.1 HMD based NSPT

HSPT is built on top of the Hybrid Molecular Dynamics (HMD) equations [59]. The general idea is to move from the action relevant to our problem to a fictitious Hamiltonian

$$S[\varphi] \qquad \rightarrow \qquad H[\pi, \varphi] = \frac{1}{2} \sum_{\boldsymbol{i}} \pi_{\boldsymbol{i}}^2 + S[\varphi] \, , \tag{158}$$

where the fictitious momenta $\pi_{\boldsymbol{i}}$ are extracted according to a normal distribution

$$P[\pi] = \frac{1}{N} \exp\left(-\frac{1}{2}\sum_{\boldsymbol{i}} \pi_{\boldsymbol{i}}^2\right). \tag{159}$$

Fields and momenta are evolved from a time τ_0 to a time $\tau_0 + \tau$ according to the Hamilton equations

$$\begin{aligned} \frac{d\pi_{\boldsymbol{i}}}{d\tau} &= -\frac{\partial H[\varphi,\pi]}{\partial \varphi_{\boldsymbol{i}}} = -\frac{\partial S[\varphi]}{\partial \varphi_{\boldsymbol{i}}}\,, \\ \frac{d\varphi_{\boldsymbol{i}}}{d\tau} &= \frac{\partial H[\varphi,\pi]}{\partial \pi_{\boldsymbol{i}}} = \pi_{\boldsymbol{i}}\,. \end{aligned} \tag{160}$$

To ensure ergodicity, at the end of the trajectory we need to refresh the momenta, again according to the distribution in Eq. (159) . All in all, we need to numerically integrate the equations of motion with a given integrator. Since once again we cannot rely on an *accept-reject* step, we will once again end up with an inexact algorithm, much the same as for the Langevin equation.

In the NSPT spirit, to get HSPT out of Eq. (160), fields and momenta are to be understood as expanded in power series of the coupling

$$\begin{aligned} \varphi_{\boldsymbol{i}}(\tau) \quad &\to \quad \varphi_{\boldsymbol{i}}^{(0)}(\tau) + \sum_{n=1}^{n_{\max}} g^n \varphi_{\boldsymbol{i}}^{(n)}(\tau)\,, \\ \pi_{\boldsymbol{i}}(\tau) \quad &\to \quad \pi_{\boldsymbol{i}}^{(0)}(\tau) + \sum_{n=1}^{n_{\max}} g^n \pi_{\boldsymbol{i}}^{(n)}(\tau)\,. \end{aligned} \tag{161}$$

At the beginning of each numerical integration of a trajectory, the momenta must be refreshed: the perturbative field $\pi_{\boldsymbol{i}}^{(n)}(\tau)$ is initialized to zeros and only the leading order component is assigned a random Gaussian variable following the distribution in Eq. (159). During the evolution, all the perturbative components of the momenta produce non-zero values through the integration of Eq. (160) which propagate the stochastic source to all orders. Chosen a trajectory length, let's say τ, the system is numerically integrated by implementing a designated discrete step $\tau = n_{\text{steps}}\Delta\tau$. In this case, several symplectic integrators are available: usually, the fourth-order integrator OMF4 [55] is used. Let us note that HSPT algorithm as discussed so far lacks ergodicity at the leading order. A straightforward remedy is to randomize the trajectory length τ [60].

Implementing HSPT with high-order integration schemes is interesting because one could think of treating systematic errors differently. In particular, it has been noted that instead of simulating the theory for different values of $\Delta\tau$ and then extrapolating to vanishing time step, one can choose a high-order integrator and simulate the theory for a very small time step [13]. In this case, extrapolation may not be necessary as the systematic errors are less than the

statistical errors. This is a claim that should be taken with great care, in particular if one is interested in high orders: the latter can hold surprises (and in general they do).

1.8.2 Kramers based NSPT

KSPT is formulated starting from the Kramers equation [57, 58], which is a second-order stochastic differential equation. We can define the Stochastic Molecular Dynamics (SMD) equation as

$$\frac{d^2\varphi_{\boldsymbol{i}}(\tau)}{d\tau^2} + \gamma\frac{d\varphi_{\boldsymbol{i}}(\tau)}{d\tau} = -\frac{\partial S}{\partial\varphi_{\boldsymbol{i}}(\tau)} + \eta_{\boldsymbol{i}}(\tau)\,. \tag{162}$$

Introducing the momentum $\pi_{\boldsymbol{i}}(\tau)$, one can trade the second-order equation Eq. (162) for a system of two coupled first-order equations, namely

$$\begin{aligned}\frac{d\varphi_{\boldsymbol{i}(\tau)}}{d\tau} &= \pi_{\boldsymbol{i}}(\tau)\,,\\ \frac{d\pi_{\boldsymbol{i}(\tau)}}{d\tau} &= -\gamma\pi_{\boldsymbol{i}}(\tau) - \frac{\partial S}{\partial\varphi_{\boldsymbol{i}}(\tau)} + \eta_{\boldsymbol{i}}(\tau)\,,\end{aligned} \tag{163}$$

where γ is a free parameter and $\eta_{\boldsymbol{i}}(\tau)$ is a Gaussian white noise with the following normalization

$$\langle\eta_{\boldsymbol{i}}(\tau)\rangle_\eta = 0\,, \qquad \langle\eta_{\boldsymbol{i}}(\tau)\eta_{\boldsymbol{j}}(\tau')\rangle_\eta = 2\gamma\delta_{\boldsymbol{ij}}\delta(\tau-\tau')\,. \tag{164}$$

We note that performing the substitution

$$\tau \qquad \to \qquad \gamma\tau \tag{165}$$

and considering the limit of $\gamma\to\infty$, Eq. (162) is equivalent to the Langevin equation [61]. In addition, for $\gamma = 0$ we recover the ordinary Molecular Dynamics.

The numerical integration of Eq. (163) displays interesting peculiarities. Consider a stochastic time step $\Delta\tau$. With a given integration scheme, we perform a single integration step in the limit of $\gamma = 0$, that is to say the system is driven forward in time ($\tau_0 \to \tau_0 + \Delta\tau$) using non-stochastic MD equations. At the end of the first integration step we introduce a refresh of the momenta according to

$$\pi'_{\boldsymbol{i}}(\tau_0+\Delta\tau) = \exp\left(-\gamma\Delta\tau\right)\pi_{\boldsymbol{i}}(\tau_0+\Delta\tau) + \sqrt{1-\exp\left(-2\gamma\Delta\tau\right)}\eta_{\boldsymbol{i}}(\tau_0+\Delta\tau)\,, \tag{166}$$

being now the Gaussian white noise normalized as follows

$$\langle\eta_{\boldsymbol{i}}(\tau_0)\eta_{\boldsymbol{j}}(\tau_1)\rangle_\eta = \delta_{\boldsymbol{ij}}\delta_{\tau_0\tau_1}\,. \tag{167}$$

This two-step procedure are iterated and this defines the Monte Carlo dynamics.

It is interesting to point out that the stochastic update in Eq. (166) is exact. Consequently, systematics coming from numerical integration is only given by the order of the integrator used for the integration of the Molecular Dynamics equations [57].

The KSPT implementation proceeds in analogy with HSPT: first, the formal expansion in power series of the coupling for fields and momenta is considered. As before, Eq. (163) is interpreted as an order-by-order dynamical evolution. Eq. (166) shows that the refresh of momenta in the KSPT language acts in a double way: on one hand, the field is rescaled by a constant factor at each perturbative order; on the other hand, the stochastic noise is added only to the leading perturbative order.

2 | NSPT around Instantons

2.1 Non-perturbative corrections from Instantons

In theoretical physics, instantons provide a valuable approach for studying non-perturbative effects. These are classical solutions of the euclidean equations of motion and are shown up in barrier-penetration processes, often assumed to play a fundamental role in determining the ground-state structure of theories such as QCD [62].

Perturbative expansions on instantonic solutions have become quite interesting also due to their connection with Resurgence Theory (RT) [63–65]. In this mathematical framework perturbative series are understood as "generalized series", offering the possibility to include even non-perturbative effects. The new series, called Trans-series, has the form (we refer the reader to [66] for an introduction to the subject)

$$A(g) = \sum_{n=0}^{\infty} g^n A_0^{(n)} + \sum_i e^{-\frac{S_i}{g}} \sum_{n=0}^{\infty} g^n A_i^{(n)} \,. \tag{168}$$

Note that factors like $e^{-\frac{S_i}{g}}$ are genuine non-perturbative effects which can not be detected with standard (small g) perturbation theory.

One way to physically explain the structure outlined in Eq. (168) is to consider it as perturbative corrections on top of saddle-point solutions. In the traditional perturbation theory, the saddle-point solutions are minima of the Euclidean action related to constant configurations. We can expand the action around a minimum, obtaining second-order fluctuations (*i.e.* the Gaussian theory) and higher-order contributions (perturbative loop corrections). In these cases the action computed at the minimum vanishes, so that we obtain the standard perturbative series (*i.e.* the first series in Eq. (168)). However, in some special theories not all the saddle-points are related to constant field configurations. Actually some of them can lead to finite-action configurations [67]. In such cases we talk about Instanton configurations, which were first introduced by A. Polyakov [68]. Instantonic configurations produce new genuinely

non-perturbative terms in front of the usual perturbative series and for this reason are expected to be related to non-perturbative physics. Quite interestingly, it is possible to formulate a perturbation theory on top of the instantons. In analogy with the standard perturbation theory, we can expand the action around the (non-constant) solution, obtaining the Gaussian theory from the second-order fluctuations and interaction terms from high-order corrections. The resulting perturbation theory is cumbersome: complicated propagators and vertices do not allow for high perturbative orders to be reached, even in the case of Quantum Mechanics.

The mathematical framework of RT has been developed to naturally include the singularities of the series in Eq. (168) and to study its asymptotic nature. In this work, however, we are interested in providing a stochastic calculation for the coefficients $A_i^{(n)}$ in Eq. (168). In particular, we will focus on one-instanton corrections $A_1^{(n)}$, neglecting multi-instanton contributions.

As a matter of fact, we have not made any assumptions about the nature of the minimum action solution around which the perturbative expansion is computer by means of NSPT. We notice that NSPT calculations have already been used to evaluate perturbative series around non-trivial vacua in the so-called Schrödinger functional formulation [16].

2.2 The Double Well Potential case

In this section we will discuss the Double Well Potential (DWP) for which instantons have the key-property of resolving degeneracies in the framework of perturbation theory. We consider the potential

$$V(x) = \lambda(x^2 - x_0^2)^2 \tag{169}$$

represented in Fig. 1. Naively, the DWP has two ground states, each centered around one of the two classically degenerate minima. This notably leads to the spontaneous breaking of parity symmetry in perturbation theory. However, from basic quantum mechanics principles, the spectrum of the Schrödinger operator is expected to be discrete, with a symmetric ground-state wavefunction. Furthermore energy difference between the ground state and the first excited state (*i.e.* the energy splitting) scales as $e^{-1/\lambda}$ [67].

2.2.1 Extracting the energy splitting

Let us consider the Hamiltonian operator

$$\hat{H} = \frac{\hat{p}^2}{2m} + \lambda(\hat{x}^2 - x_0^2)^2 \,. \tag{170}$$

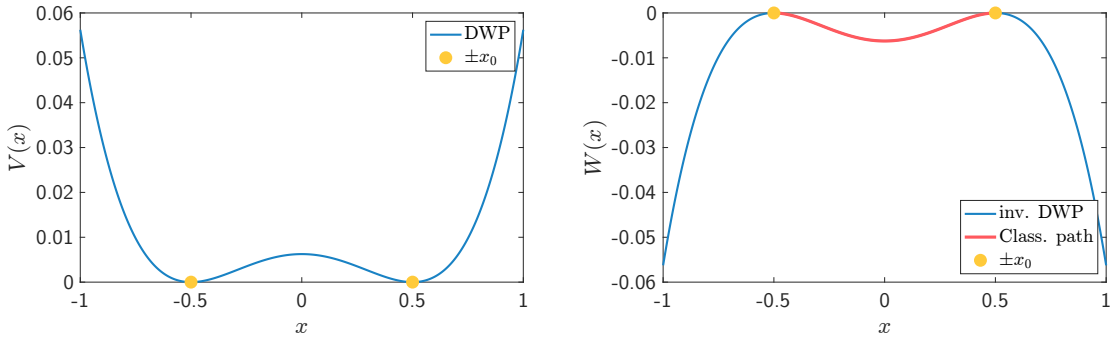

Figure 1: Left plot: Graphical representation of the Double Well Potential of Eq. (169) with $\lambda = 0.1$ and $x_0 = 0.5$ (blue line). The minima are indicated with yellow circles. Right plot: representation of the inverted potential with $\lambda = 0.1$ and $x_0 = 0.5$ (blue line). The maxima are indicated with yellow circles, while the continuous red line indicates the Euclidean potential hole related to the energy tunneling solution given in Eq. (184).

This commutes with the Parity operator $\hat{P}$ in the coordinate space:

$$[\hat{H}, \hat{P}] = 0\,. \tag{171}$$

As a consequence we can construct a basis of eigenvectors for the Hamiltonian with two quantum numbers (n, s), such that the following eigenvalue equations hold

$$\hat{H}\psi_{n,s}(x) = E_{n,s}\psi_{n,s}(x)\,, \qquad \hat{P}\psi_{n,s}(x) = s\psi_{n,s}(x)\,, \tag{172}$$

where $s = \pm 1$. The ground state energy is expected to be in the form [67]

$$E_{0,\pm} = E_0 \mp \frac{\Delta E}{2}\,, \tag{173}$$

where the first term E_0 results from the standard perturbative expansion (which is usually called the expansion in the zero-instanton sector), while ΔE denotes the energy splitting. Considering corrections coming only from the one-instanton sector, the energy splitting comes out to be proportional to $e^{-\frac{1}{\lambda}}$ [67], and thus becomes increasingly smaller as the coupling approaches zero. Given the definition of the partition function

$$Z(\beta) = \mathrm{Tr}\left[e^{-\beta\hat{H}}\right], \tag{174}$$

the ground state can be studied in the limit of $\beta \to \infty$. As a matter of fact, the partition function of the system in the limit of large β and small coupling constant reads

$$\begin{aligned}
\lim_{\beta\to\infty} Z(\beta) &= \lim_{\beta\to\infty} \mathrm{Tr}\big[e^{-\beta\hat{H}}\big] = \lim_{\beta\to\infty} \sum_{n,s=\pm} \langle n,s|e^{-\beta\hat{H}}|n,s\rangle = \lim_{\beta\to\infty} \sum_{n,s=\pm} e^{-\beta E_{n,s}} \\
&\approx e^{-\beta E_{0,+}} + e^{-\beta E_{0,-}} \\
&\approx e^{-\frac{\beta}{2}(E_{0,+}+E_{0,-})}\Big(e^{-\frac{\beta}{2}(E_{0,+}-E_{0,-})} + e^{\frac{\beta}{2}(E_{0,+}-E_{0,-})}\Big) \\
&\approx 2e^{-\frac{\beta}{2}(E_{0,+}+E_{0,-})}\cosh\frac{\beta}{2}(E_{0,+}-E_{0,-}) \\
&\approx 2e^{-\frac{\beta}{2}(E_{0,+}+E_{0,-})}\cosh\beta\frac{\Delta E}{2}\,.
\end{aligned} \tag{175}$$

We note that the partition function given in Eq. (175) is dominated by the purely zero-instanton sector. Conversely, the twisted partition function [67]

$$Z_a(\beta) = \mathrm{Tr}\big[\hat{P}e^{-\beta\hat{H}}\big] \tag{176}$$

displays a non-vanishing contribution from the one-instanton sectors. In fact, Eq. (176) in the limit of $\beta \to \infty$ and $g \to 0$ reads

$$\begin{aligned}
\lim_{\beta\to\infty} Z_a(\beta) &= \lim_{\beta\to\infty} \mathrm{Tr}\big[\hat{P}e^{-\beta\hat{H}}\big] = \lim_{\beta\to\infty} \sum_{n,s=\pm} \langle n,s|\hat{P}e^{-\beta\hat{H}}|n,s\rangle = \lim_{\beta\to\infty} \sum_{n,s=\pm} e^{-\beta E_{n,s}}s \\
&\approx e^{-\beta E_{0,+}} - e^{-\beta E_{0,-}} \\
&\approx e^{-\frac{\beta}{2}(E_{0,+}+E_{0,-})}\Big(e^{-\frac{\beta}{2}(E_{0,+}-E_{0,-})} - e^{\frac{\beta}{2}(E_{0,+}-E_{0,-})}\Big) \\
&\approx -2e^{-\frac{\beta}{2}(E_{0,+}+E_{0,-})}\sinh\frac{\beta}{2}(E_{0,+}-E_{0,-}) \\
&\approx 2e^{-\frac{\beta}{2}(E_{0,+}+E_{0,-})}\sinh\beta\frac{\Delta E}{2}\,.
\end{aligned} \tag{177}$$

We immediately notice that taking the ratio of the partition functions given in Eq. (176) and Eq. (175) we get the energy splitting ΔE

$$\lim_{\beta\to\infty} \frac{Z_a(\beta)}{Z(\beta)} \approx \beta\frac{\Delta E}{2}\,. \tag{178}$$

2.2.2 Path integral approach

The partition function in Eq. (174) can be represented using the path integral formalism

$$Z(\beta) = \int_{PBC} Dx\; e^{-S[x]}\,, \tag{179}$$

where $S[x]$ is the Euclidean action and PBC indicates that we are integrating over periodic paths, for which the following condition is imposed

$$x(-\beta/2) = x(\beta/2)\,. \tag{180}$$

On the other hand, the twisted partition function in Eq. (176) admits a representation in terms of integrals over antiperiodic paths

$$Z_a(\beta) = \int dx\ \langle x|\hat{P}e^{-\beta\hat{H}}|x\rangle = \int dx\ \langle -x|e^{-\beta\hat{H}}|x\rangle = \int_{ABC} Dx\ e^{-S[x]}\,, \tag{181}$$

where $\int_{ABC}$ denotes integration over paths that satisfy

$$x(-\beta/2) = -x(\beta/2)\,. \tag{182}$$

The Euclidean action can be always written in the Lagrangian formalism, where the new potential function $W(x)$ is given by

$$W(x) = -V(x)\,. \tag{183}$$

In Fig. 1 we display the new potential $W(x)$ for the DWP case. Since we are interested in evaluating the functional integral saddle-points, which correspond to the minima of the Euclidean action, we need to solve the classical equations of motion in the new inverted potential, in the limit of $\beta \to \infty$, considering periodic and antiperiodic boundary conditions. It is trivial to verify that for periodic boundary conditions the only solutions are configurations of constant field. On the other hand, for antiperiodic configurations we obtain the following solutions for the saddles-points

$$x_c^{\pm}(t) = \pm x_0 \tanh\left[\frac{\omega}{2}(t-t_0)\right], \qquad \omega = \sqrt{\frac{8\lambda x_0^2}{m}}\,, \tag{184}$$

where t_0 parametrizes the family of solutions[4]. In Fig. 2 we show the solutions shown Eq. (184).

Let us assume that we are looking for minima of the action (179) for finite β and anti-periodic boundary conditions. We denote this solution by $q_c(t)$. Using the saddle-point approximation, it follows

$$\begin{aligned} Z_a(\beta) &= \int_{ABC} Dx\ e^{-S[x]} \\ &= \int_{ABC} Dx\ \exp\left(-S[q_c] - \frac{1}{2}\int dt \int dt' (x(t)-q_c(t)) \left.\frac{\delta^2 S}{\delta x(t)\delta x(t')}\right|_{q_c} (x(t')-q_c(t')) + \dots\right) \\ &= e^{-S[q_c]} \int_{ABC} Dr\ \exp\left(-\frac{1}{2}\int dt \int dt' r(t) M(t,t') r(t') + \dots\right), \end{aligned} \tag{185}$$

where we have set

$$r(t) = x(t) - q_c(t) \tag{186}$$

[4]The two solutions $x_c^{\pm}(t)$ are equivalent. In the following we consider only $x_c^{+}(t)$, remembering at the end of the calculation to add a factor of 2 to the integrals approximated with the saddle-points.

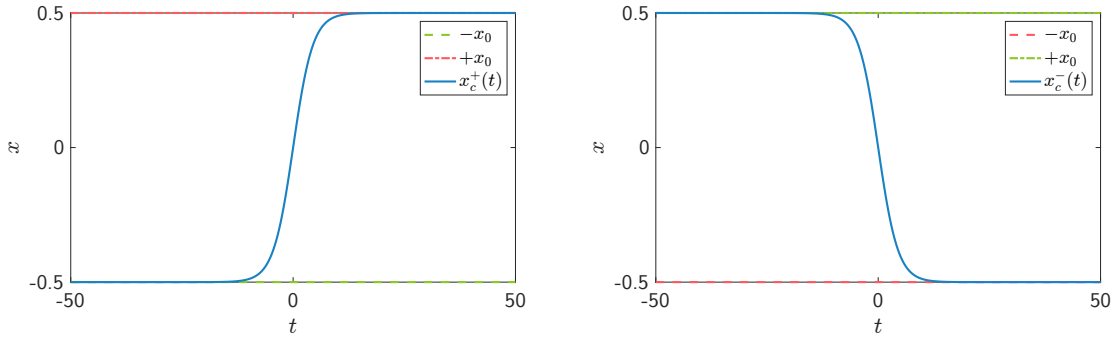

Figure 2: Graphical representation of $x_c^{\pm}(t)$, see Eq. (184). Left plot: we display with a blue solid line the instantonic solution $x_c^+(t)$, with a green (red) dashed line the starting (ending) minimum. Right plot: we display with a blue solid line the anti-instantonic solution $x_c^-(t)$, with a green (red) dashed line the starting (ending) minimum. In both figures we use $t_0 = 0$, $m = 1$, $x_0 = 1/2$, $\lambda = 0.1$.

for the (antiperiodic) fluctuations and

$$M(t,t') = \frac{\delta^2 S}{\delta x(t)\delta x(t')}\bigg|_{q_c} = \delta(t-t')\left[-\frac{d^2}{dt^2} - W''(q_c(t))\right]. \tag{187}$$

We note that in Eq. (185) the dots indicate higher-order corrections. As for now, we will only consider second-order Gaussian fluctuations, which are usually referred in the literature as 1-loop corrections. Following the approach discussed in [67], fluctuations are given in terms of expansions of the form

$$r(t) = \sum_{n\geq 0} c_n q_n(t) \tag{188}$$

where $q_n(t)$ are the eigenvectors of the kernel matrix, *i.e.* they satisfy

$$M q_n(t) = \lambda_n q_n(t)\,. \tag{189}$$

We can compute formally the Gaussian integral, obtaining

$$\begin{aligned} Z_a(\beta) &\approx e^{-S[q_c]} \int_{ABC} Dr\ \exp\left(-\frac{1}{2}\int dt \int dt' r(t) M(t,t') r(t')\right) \\ &\approx e^{-S[q_c]} \mathcal{N} \int \prod_{n\geq 0} \frac{dc_n}{\sqrt{2\pi}} \exp\left(-\frac{1}{2}\sum_{n\geq 0} c_n \lambda_n c_n\right) \\ &\approx e^{-S[q_c]} \mathcal{N} \prod_{n\geq 0} \lambda_n^{-\frac{1}{2}} \\ &\approx e^{-S[q_c]} \mathcal{N} \big(\det M\big)^{-\frac{1}{2}}\,, \end{aligned} \tag{190}$$

where we have used the standard convention

$$Dr = \mathcal{N} \prod_{n \geq 0} \frac{dc_n}{\sqrt{2\pi}} \,, \tag{191}$$

where $\mathcal{N}$ will be defined below. It is immediate to verify that the determinant in Eq. (190) requires regularization. Indeed, by differentiating the equations of motion with respect to t, one obtains

$$\left[-\frac{d^2}{dt^2} - W''(q_c) \right] \dot{q}_c(t) = M \dot{q}_c(t) = 0 \,, \tag{192}$$

from which it can be deduced that $\dot{q}_c(t)$ is an eigenvector with vanishing eigenvalue. We will refer to the normalized function

$$q_0(t) = \dot{q}_c(t) / ||\dot{q}_c|| \tag{193}$$

as the zero-mode of the theory. In Eq. (193) the symbol $||\dots||$ denotes

$$||\dot{q}_c||^2 = \int_{-\beta/2}^{\beta/2} dt \; \dot{q}_c(t)^2 \,. \tag{194}$$

The zero-mode can be treated separately by writing

$$Z_a(\beta) = e^{-S[q_c]} \mathcal{N} \big(\det M' \big)^{-\frac{1}{2}} \int_{-\infty}^{\infty} \frac{dc_0}{\sqrt{2\pi}} \,, \tag{195}$$

where higher-order corrections are neglected and

$$\big(\det M' \big)^{-\frac{1}{2}} = \prod_{n \neq 0} \lambda_n^{-\frac{1}{2}} \,. \tag{196}$$

The divergence of the zero-mode is usually expressed as [5]

$$\int_{-\infty}^{\infty} \frac{dc_0}{\sqrt{2\pi}} = \frac{\beta ||\dot{q}_c||}{\sqrt{2\pi}} \,. \tag{197}$$

As a final step, we need to define the path integral measure, $\mathcal{N}$. This can be achieved using the harmonic oscillator with $m = \omega = 1$. The corresponding thermal partition function reads

$$Z_G(\beta) = \mathcal{N} (\det M_0)^{-\frac{1}{2}} \,, \tag{198}$$

where

$$M_0 = -\frac{d^2}{dt^2} + 1 \,. \tag{199}$$

Thanks to Eq. (198), the twisted partition function becomes

$$Z_a(\beta) = e^{-S[q_c]} Z_G(\beta) \left(\frac{\det M'}{\det M_0} \right)^{-\frac{1}{2}} \frac{\beta ||\dot{q}_c||}{\sqrt{2\pi}} \,. \tag{200}$$

[5] This result can be demostrated by interpreting any variation δc_0 as a variation δt_0 [67]. In fact the presence of the zero-mode is closely related to the invariance under reparameterization of the solution $x_c^+(t)$ shown in Eq. (184).

In the limit of $\beta \to \infty$ and $m = \omega = 1$, for the saddle-point solution $x_c^+(t)$ we have

$$\begin{aligned}
q_c(t) \quad &\to \quad x_c^+(t)\,, \\
S[q_c] \quad &\to \quad S[x_c^+] = \frac{m^2\omega^3}{12\lambda} = \frac{1}{12\lambda}\,, \\
Z_G(\beta) \quad &\to \quad Z_G(\beta\to\infty) = e^{-\beta E_0} = e^{-\frac{\beta}{2}}\,, \\
\frac{\det M'}{\det M_0} \quad &\to \quad \frac{1}{12}\,, \\
||\dot{q}_c|| \quad &\to \quad \sqrt{\frac{\omega^2 x_0^2}{4}\int_{-\infty}^{\infty} dt\,\mathrm{sech}^4\left(\frac{\omega(t-t_0)}{2}\right)} = \sqrt{\frac{\omega^3 m^2}{12\lambda}} = \frac{1}{\sqrt{12\lambda}}\,,
\end{aligned} \tag{201}$$

where for the ratio of determinants (see fourth equation from above) the general result for Pöschl–Teller operators has been used [67]. By also inserting the factor 2 owing to the presence of a second saddle-point solution $x_c^-(t)$ one obtains

$$Z_a(\beta) = 2e^{-\frac{1}{12\lambda}} e^{-\frac{\beta}{2}} \beta \frac{1}{\sqrt{2\pi\lambda}}\,. \tag{202}$$

The above result indicates the presence of a purely non-perturbative contribution to the twisted partition function. By forming the ratio of the twisted partition function of Eq. (202) and the standard leading-order partition function given by

$$Z(\beta\to\infty) = 2e^{-\beta/2} \tag{203}$$

we get

$$\frac{Z_a(\beta)}{Z(\beta)} = e^{-\frac{1}{12\lambda}} \beta \frac{1}{\sqrt{2\pi\lambda}}\,. \tag{204}$$

Therefore, by means of Eq. (178) we obtain the energy splitting that reads

$$\Delta E = 2e^{-\frac{1}{12\lambda}} \frac{1}{\sqrt{2\pi\lambda}} \big(1 + O(\lambda)\big)\,, \tag{205}$$

recovering thus the one-loop contribution shown in [69] and [70]. Moreover, we can consider also higher-orders in the Taylor series expansion of the action, which are evaluated on the Gaussian instantonic theory, yielding perturbative correction in the energy splitting. This scheme has been implemented in [69] and [70], where two- and three-loop corrections are computed with the use of diagrammatic perturbation theory and the Faddeev-Popov regularization (more details about this computation is given in App. B). In that case one gets

$$\begin{aligned}
\Delta E &= 2e^{-\frac{1}{12\lambda}} \frac{1}{\sqrt{2\pi\lambda}} \left[1 + (12\lambda) z^{(1)} + (12\lambda)^2 z^{(2)} + O(\lambda)^3\right], \\
z^{(1)} &= -\frac{71}{72}\,, \\
z^{(2)} &= -\frac{9299}{10368}\,.
\end{aligned} \tag{206}$$

2.3 Two-loop correction from NSPT

It is well-known that the continuum action

$$S_{\rm cont}[x] = \int dt \left[\frac{1}{2} m\dot{x}^2 + \lambda(x^2 - x_0^2)^2\right], \tag{207}$$

that describes a simple quantum mechanical system, can be regarded as a field theory in $0+1$ dimensions which can be studied with lattice tools [71]. In this framework one can implement a naive discretization of the derivative and the action becomes

$$S_{\rm latt}[x] = \sum_i a\left[\frac{1}{2} m\Big(\frac{x_{i+1} - x_i}{a}\Big)^2 + \lambda(x_i^2 - x_0^2)^2\right], \tag{208}$$

where $x(ia) = x_i$. The interpretation after the discretization of the path is as follows: a generic path of length T (a configuration, in the language of field theory) is sampled at discrete times that are multiples of the lattice spacing a. The number of sites L scales with the lattice spacing such that $T = L \cdot a$. Definition of dimensionless quantities on the lattice require the following relationship

$$\begin{aligned} am &= \tilde{m} \\ x_i/a &= \tilde{x}_i \\ a^5\lambda &= \tilde{\lambda} \\ x_0/a &= \tilde{x}_0\,, \end{aligned} \tag{209}$$

where we have set $\hbar = c = 1$. It is possible now to rewrite the lattice action in terms of the above dimensionless quantities

$$S_{\rm latt}[\tilde{x}] = \sum_i \left[\frac{1}{2}\tilde{m}(\tilde{x}_{i+1} - \tilde{x}_i)^2 + \tilde{\lambda}(\tilde{x}_i^2 - \tilde{x}_0^2)^2\right]. \tag{210}$$

Notice that the definition of $\tilde{x}_i$ in the second of Eq. (209) fixes the dimensions of the coupling $\tilde{\lambda}$ (see third of Eq. (209)), which is now also dimensionless. Therefore, it is expected that all the perturbative corrections have the same physical dimensions. For notation simplicity in the following we will write $S_{\rm latt}[\tilde{x}] \equiv S[\tilde{x}]$.

2.3.1 Minimum action solutions on the lattice

We are interested in the minimum solutions $\tilde{x}^*$ of the action given in Eq. (208), *i.e.* we are looking for solutions of

$$\delta S[\tilde{x}]\big|_{\tilde{x}^*} = 0 \tag{211}$$

in order to use the saddle-point approximation. In general, the minimum action configurations for the discretized theory will be different from those of the continuum theory, although we expect that in the limit of vanishing lattice spacing the former will approach the latter. The minimum action solutions are not known analytically for the lattice Double Well Potential, but they can be derived numerically. A possible choice is to use the Steepest Descent Method (also known as Gradient Descent) [72]. In the Steepest Descent Method one considers an arbitrary initial configuration $\tilde{x}_i(0)$ and evolves it according to the equation

$$\dot{\tilde{x}}_i = -\frac{\partial S}{\partial \tilde{x}_i} \,. \tag{212}$$

The previous equation is implemented numerically introducing a small parameter ϵ

$$\tilde{x}_i(j+1) = \tilde{x}_i(j) - \epsilon \frac{\partial S}{\partial \tilde{x}_i}\bigg|_{\tilde{x}(j)} \tag{213}$$

and the evolution in ϵ goes on until a stationary point is reached, where the derivatives of the action are zero. In Fig. 3 we display the solution found with this procedure. We note that the lattice instanton differs from the continuum one by $O(a)$ corrections. Additionally, the Steepest Descent algorithm depends on the particular choice of the initial configuration. However, we have verified that this does not change the shape of the minimum solution at all, but it only yields different transition points. In what follows, the initial configuration will be always chosen in such a way that the transition point coincides with the center of the lattice. In addition, we rescale the stationary solution according to

$$\tilde{x}_i^* = \tilde{x}_0 \cdot \bar{x}_i \,. \tag{214}$$

Let us emphasize that the boundary conditions, either periodic or antiperiodic, enter into the minimization of the action (213) by establishing that

$$\begin{aligned} \text{PBC} &: \tilde{x}_{i+L} = \tilde{x}_i \,, \\ \text{ABC} &: \tilde{x}_{i+L} = -\tilde{x}_i \,. \end{aligned} \tag{215}$$

Once the minimum action solution is identified through the Steepest Descent Method, we are allowed to work in terms of the fluctuations. We introduce the dimensionless local fluctuations as

$$\tilde{x}_i = \tilde{x}_i^* + \tilde{\xi}_i = \tilde{x}_0 \cdot \bar{x}_i + \tilde{\xi}_i \tag{216}$$

and we can write the corresponding action in the following form

$$\begin{aligned}
&\frac{1}{2}\tilde{m}(\tilde{\xi}_{i+1}-\tilde{\xi}_i)^2+\tilde{m}(\tilde{x}^*_{i+1}-\tilde{x}^*_i)(\tilde{\xi}_{i+1}-\tilde{\xi}_i)\\
&\qquad+\tilde{\lambda}(\tilde{x}_i^{*^2}-\tilde{x}_0^2)^2+\tilde{\lambda}(\tilde{\xi}_i^2+2\tilde{\xi}_i\tilde{x}^*_i)^2+2\tilde{\lambda}(\tilde{x}_i^{*^2}-\tilde{x}_0^2)(\tilde{\xi}_i^2+2\tilde{\xi}_i\tilde{x}^*_i)\Big]\\
&=S[\tilde{x}^*]+\sum_i\Big[\frac{1}{2}\tilde{m}(\tilde{\xi}_{i+1}-\tilde{\xi}_i)^2+\tilde{m}(\tilde{x}^*_{i+1}-\tilde{x}^*_i)(\tilde{\xi}_{i+1}-\tilde{\xi}_i)+\tilde{\lambda}(\tilde{\xi}_i^2+2\tilde{\xi}_i\tilde{x}^*_i)^2\\
&\qquad+2\tilde{\lambda}(\tilde{x}_i^{*^2}-\tilde{x}_0^2)(\tilde{\xi}_i^2+2\tilde{\xi}_i\tilde{x}^*_i)\Big]\,.
\end{aligned}\tag{217}$$

The previous formula can be simplified with the use of equations of motion. In fact, from

$$\left.\frac{\partial\mathcal{S}_E}{\partial\tilde{x}_j}\right|_{\tilde{x}^*}=0$$

we derive

$$\sum_i\Big[\tilde{m}(\tilde{x}^*_{i+1}-\tilde{x}^*_i)(\delta_{i+1,j}-\delta_{i,j})+2\tilde{\lambda}(\tilde{x}_i^{*^2}-\tilde{x}_0^2)2\tilde{x}^*_i\delta_{i,j}\Big]=0\,,\tag{218}$$

so that

$$\tilde{m}(2\tilde{x}^*_j-\tilde{x}^*_{j+1}-\tilde{x}^*_{j-1})=-4\tilde{\lambda}\tilde{x}^*_j(\tilde{x}_j^{*^2}-\tilde{x}_0^2)\,.\tag{219}$$

We now notice that the mixed velocity term in the action (217) is written up to boundary terms as

$$\sum_i\tilde{m}(\tilde{x}^*_{i+1}-\tilde{x}^*_i)(\tilde{\xi}_{i+1}-\tilde{\xi}_i)=\sum_i\tilde{m}(2\tilde{x}^*_i-\tilde{x}^*_{i-1}-\tilde{x}^*_{i+1})\tilde{\xi}_i\tag{220}$$

which, with the use of Eq. (219), becomes

$$\sum_i\tilde{m}(\tilde{x}^*_{i+1}-\tilde{x}^*_i)(\tilde{\xi}_{i+1}-\tilde{\xi}_i)=-\sum_j4\tilde{\lambda}\tilde{x}^*_j(\tilde{x}_j^{*^2}-\tilde{x}_0^2)\tilde{\xi}_j\,.$$

The RHS of the above equation cancels out a part of the potential, so that the action becomes

$$\begin{aligned}
S[\tilde{x}]&=S[\tilde{x}^*]+\sum_i\Big[\frac{1}{2}\tilde{m}(\tilde{\xi}_{i+1}-\tilde{\xi}_i)^2+\tilde{\lambda}(\tilde{\xi}_i^2+2\tilde{\xi}_i\tilde{x}^*_i)^2+2\tilde{\lambda}(\tilde{x}_i^{*^2}-\tilde{x}_0^2)\tilde{\xi}_i^2\Big]\\
&=S[\tilde{x}^*]+\sum_i\Big[\frac{1}{2}\tilde{m}(\tilde{\xi}_{i+1}-\tilde{\xi}_i)^2+\tilde{\lambda}\tilde{\xi}_i^4+\tilde{\lambda}4\tilde{x}_i^{*^2}\tilde{\xi}_i^2+4\tilde{\lambda}\tilde{x}^*_i\tilde{\xi}_i^3+2\tilde{\lambda}(\tilde{x}^{*^2}-\tilde{x}_0^2)\tilde{\xi}_i^2\Big]\\
&=S[\tilde{x}^*]+\sum_i\Big[\frac{1}{2}\tilde{m}(\tilde{\xi}_{i+1}-\tilde{\xi}_i)^2+\tilde{\lambda}\tilde{\xi}_i^4+\tilde{\lambda}\tilde{x}_0^2(6\bar{x}_i^2-2)\tilde{\xi}_i^2+4\tilde{\lambda}\tilde{x}_0\bar{x}_i\tilde{\xi}_i^3\Big]\,.
\end{aligned}\tag{221}$$

Following the convention in [70], it is customary to set

$$4\tilde{\lambda}\tilde{x}_0^2=\frac{1}{2}\tilde{m}\tilde{\omega}^2\tag{222}$$

in order to recover the action of the harmonic oscillator as free theory for PBC. Indeed, given that the minimum solution of the action with periodic boundary conditions is

$$\tilde{x}^* = x_0 \tag{223}$$

from which

$$\bar{x}_i = 1\,, \tag{224}$$

it follows that

$$S_{\rm PBC}[\tilde{x}] = 0 + \sum_i \Big[\frac{1}{2}\tilde{m}(\tilde{\xi}_{i+1} - \tilde{\xi}_i)^2 + \frac{1}{2}\tilde{m}\tilde{\omega}^2\tilde{\xi}^2 + \sqrt{2\tilde{\lambda}\tilde{m}\tilde{\omega}^2}\tilde{\xi}^3 + \tilde{\lambda}\tilde{\xi}_i^4\Big] \tag{225}$$

In that way the usual theory with cubic and quartic vertex interactions is recovered. In the case of solutions where antiperiodic boundary conditions have been employed (*i.e.* instantons) the general action reads

$$\begin{aligned} S_{\rm ABC}[\tilde{x}] &= S[\tilde{x}^*] + \sum_i \Big[\frac{1}{2}\tilde{m}(\tilde{\xi}_{i+1} - \tilde{\xi}_i)^2 + \frac{1}{2}\tilde{m}\tilde{\omega}^2\Big(\frac{3}{2}\bar{x}_i^2 - \frac{1}{2}\Big)\tilde{\xi}_i^2 + \sqrt{2\tilde{\lambda}\tilde{m}\tilde{\omega}^2}\bar{x}_i\tilde{\xi}_i^3 + \tilde{\lambda}\tilde{\xi}_i^4\Big] \\ &= S[\tilde{x}^*] + S[\tilde{\xi}] \end{aligned} \tag{226}$$

where it can be noticed that, in addition to a much more complicated free theory, the cubic interaction term depends on the site where the interaction occurs. This is actually one of the reasons for which it is difficult to treat diagrammatically the perturbation theory of the instantons.

2.3.2 Faddev-Popov regularization

The kinetic matrix defined by the action in Eq. (226)

$$K_{ij} = \frac{\partial^2 S_{\rm ABC}[\tilde{\xi}]}{\partial\tilde{\xi}_i\partial\tilde{\xi}_j}\Big|_{\tilde{\xi}=0} \tag{227}$$

among else has a zero-mode. In the right panel of Fig. 3 the eigenvalues of the kinetic matrix are plotted. In analogy to the continuous theory, the twisted partition function is thus ill-defined and requires regularization. We regularize the zero-mode by implementing the Faddeev-Popov (FP) procedure [6]. Essentially, the idea is to use a convenient rewriting of the identity. Indicating with t_0 the transition point for the instantonic lattice solution, we can write

$$\int dt_0\ \delta(t_0 - t_0^*) = 1\,, \tag{228}$$

[6] For the FP implementation in the lattice theory, we took inspiration from the continuum case presented in [73].

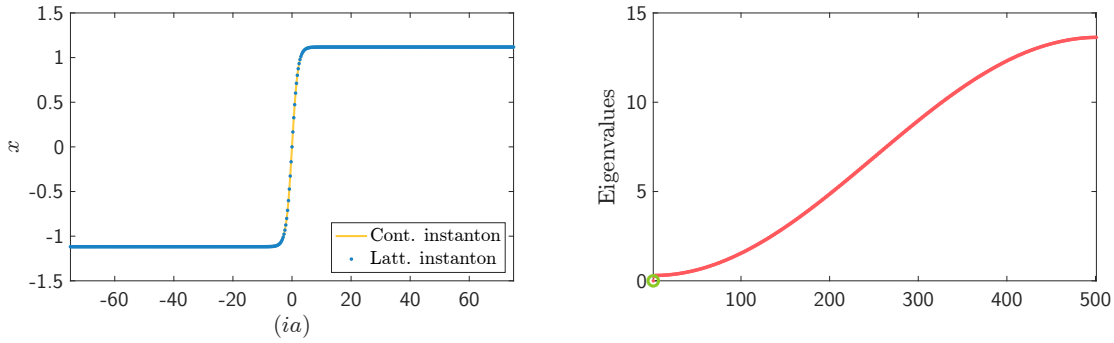

Figure 3: Left plot: Minimum action solution with antiperiodic boundary conditions. The instantonic lattice solution $\tilde{x}_i^*$ is represented with blue dots using $a = 0.3$, $L = 500$, $T = [-75, 75]$, $m = \omega = 1$, $\lambda = 0.1$. For the Gradient Descent equations, we used $\epsilon = 5 \cdot 10^{-5}$ and $N_{step} = 10^6$ configuration updates. The continuous yellow line represents the continuum solution given in Eq. (184) with the same parameters as before. Right plot: all the set of eigenvalues of the matrix K_{ij} in Eq. (227) with $a = 0.3$, $L = 500$, $m = \omega = 1$, $\lambda = 0.1$. In addition, the green circle shows the zero eigenvalue of the kernel.

where t_0^* lies in the integration domain. For a generic function $f(t_0)$ with only one zero located at t_0^*, the following property holds

$$\delta(t_0 - t_0^*) = \delta(f(t_0))|f'(t_0^*)|\,. \tag{229}$$

The key-point is to select fluctuations having zero component along the zero-mode, by making an appropriate choice of $f(t_0)$. This occurs by setting

$$f(\tau_0) = \sum_k (\tilde{x}_k - \tilde{x}_k^*(-t_0)\,)\,\tilde{x}_k^0(-t_0) \tag{230}$$

where $\tilde{x}_k^*(-t_0)$ is the minimum action solution with transition point at t_0 and $\tilde{x}_k^0(-t_0)$ is the normalized zero-mode. In other words, $\tilde{x}_k^0(-t_0)$ is the eigenvector of the matrix K_{ij} with zero eigenvalue. We show in Fig. 4 - left panel, the zero-mode shape $\tilde{x}_k^0$ and the continuum counterpart $\dot{\tilde{x}}_c^+/||\dot{\tilde{x}}_c^+||$. Let us note that the zero-mode dependence on the transition point t_0 is induced by the specific minimum $\tilde{x}^*(-t_0)$ around which we expand the action. The minus sign in the argument of the instanton and the zero-mode reflects the functional form of their continuum counterparts. Furthermore, this is the correct functional form that yields the proper discretization along the transition point (see below for a detailed explanation). The derivative of Eq. (230)

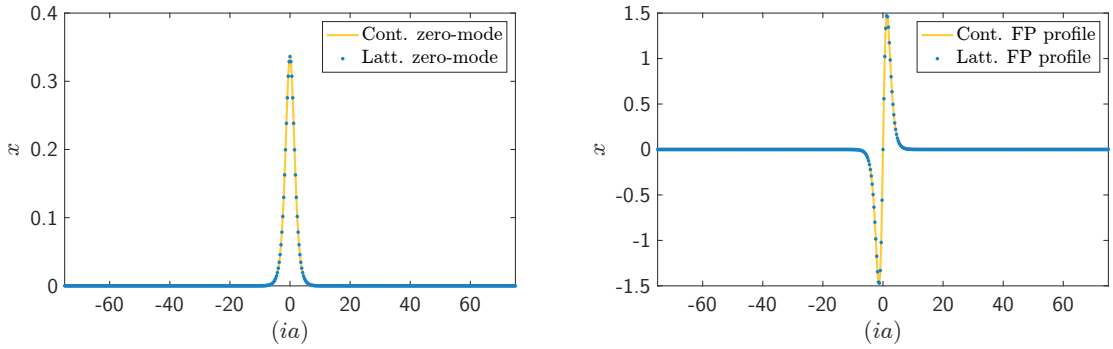

Figure 4: Left plot: zero-mode profile. The lattice zero-mode shape $\tilde{x}_i^0$ is represented with blue markers. We set $a = 0.3$, $L = 500$, $T = [-75, 75]$, $m = \omega = 1$, $\lambda = 0.1$. The continuous yellow line represents the continuum zero-mode shape, see Eq. (193). Right plot: Faddeev-Popov geometric shape v_i of Eq. (242). We display in blue the lattice shape for $a = 0.3$, $L = 500$, $m = \omega = 1$, $\lambda = 0.1$. With the solid yellow line the continuum counterpart $\ddot{x}_c(t)$ is shown. As before, the continuous functions were sampled at discrete steps of size a.

with respect to the transition time reads

$$f'(t_0) = \sum_k \dot{\tilde{x}}_k^*(-t_0)\tilde{x}_k^0(-t_0) - \sum_k (\tilde{x}_k - \tilde{x}_k^*(-t_0))\dot{\tilde{x}}_k^0(-t_0) \tag{231}$$

It can be shown that $f'(t_0)$, for small values of the coupling constant $\tilde{\lambda}$, is always positive. Therefore, it is not necessary to take the absolute value (see Eq. (229)). Moreover, since the derivative with respect to the transition time is positive, the function vanishes at only one point t_0^*, justifying the use of the Dirac delta property in Eq. (229).

The transition time t_0 can also be discretized. Although in principle the transition can occur at points not detected by the lattice discretization, we can always achieve an approximation whose error tends to zero in the limit of vanishing lattice spacing:

$$\tilde{x}_k^*(-t_0) = \tilde{x}_{k-j}^* + O(a) \qquad \text{for} \qquad t_0 = j \cdot a + O(a)\,. \tag{232}$$

The new minimum $\tilde{x}_{k-j}^*$ leads to a redefinition of the matrix K_{ij}. We indicate the new zero-mode as $\tilde{x}_{k-j}^0$. In addition, the regularized version of Eq. (231) reads

$$f'(t_0) \to f'_k = \sum_k \tilde{x}_k \Big(\frac{\tilde{x}_{k-j-1}^0 - \tilde{x}_{k-j}^0}{a} \Big)\,. \tag{233}$$

We use the FP procedure in the twisted partition function of the lattice theory, namely

$$
\begin{aligned}
Z_a &= \int_{ABC} \prod_i d\tilde{x}_i \; e^{-S[\tilde{x}]} \\
&= \int_{ABC} \prod_i d\tilde{x}_i \; \int d\tau_0 \; \delta(\tau_0 - \tau_0^*) \; e^{-S[\tilde{x}]} \\
&= \int_{ABC} \prod_i d\tilde{x}_i \; \sum_j a \; \delta\Big[\sum_k (\tilde{x}_k - \tilde{x}^*_{k-j})\tilde{x}^0_{k-j}\Big] \; \sum_l \tilde{x}_l \Big(\frac{\tilde{x}^0_{l-j-1} - \tilde{x}^0_{l-j}}{a}\Big) \; e^{-S[\tilde{x}]} \, .
\end{aligned}
\tag{234}
$$

As usual, the path of the particle can be decomposed to the classical path plus a fluctuation field, *i.e.* we write

$$
\tilde{x}_i = \tilde{x}^*_{i-j} + \tilde{\xi}_i = \tilde{x}_0 \bar{x}_{i-j} + \tilde{\xi}_i \, .
\tag{235}
$$

Expanding the action associated to the fluctuations as we did in the similar case of Sec. 2.3.1 we obtain

$$
Z_a = e^{-S[\tilde{x}^*]} \int_{ABC} \prod_i d\tilde{\xi}_i \; \sum_j a \; \delta\Big[\sum_k \tilde{\xi}_k \tilde{x}^0_{k-j}\Big] \; \sum_l (\tilde{x}^*_{l-j} + \tilde{\xi}_l) \Big(\frac{\tilde{x}^0_{l-j-1} - \tilde{x}^0_{l-j}}{a}\Big) \; e^{-S[\tilde{\xi}]} \, .
\tag{236}
$$

To remove the zero-mode we need to introduce the orthogonal component

$$
\tilde{\xi}_k = c_0 \tilde{x}^0_{k-j} + \tilde{\xi}^\perp_k
\tag{237}
$$

in the twisted partition function

$$
\begin{aligned}
Z_a &= e^{-S[\tilde{x}^*]} \int \frac{c_0}{\sqrt{2\pi}} \int_{ABC} \prod_i d\tilde{\xi}^\perp_i \; \sum_j a \; \delta(c_0) \; \sum_l (\tilde{x}^*_{l-j} + c_0 \tilde{x}^0_{l-j} + \tilde{\xi}^\perp_l) \Big(\frac{\tilde{x}^0_{l-j-1} - \tilde{x}^0_{l-j}}{a}\Big) \; e^{-S[\tilde{\xi}]} \\
&= \frac{e^{-S[\tilde{x}^*]}}{\sqrt{2\pi}} \sum_j a \int_{ABC} \prod_i d\tilde{\xi}^\perp_i \; \sum_l (\tilde{x}^*_{l-j} + \tilde{\xi}^\perp_l) \Big(\frac{\tilde{x}^0_{l-j-1} - \tilde{x}^0_{l-j}}{a}\Big) \; e^{-S[\tilde{\xi}^\perp]} \\
&= \frac{e^{-S[\tilde{x}^*]}}{\sqrt{2\pi}} \sum_j a \int_{ABC} \prod_i d\tilde{\xi}^\perp_i \; \sum_l (\tilde{x}^*_{l} + \tilde{\xi}^\perp_{l+j}) \Big(\frac{\tilde{x}^0_{l-1} - \tilde{x}^0_{l}}{a}\Big) \; e^{-S[\tilde{\xi}^\perp]} \\
&= \frac{e^{-S[\tilde{x}^*]}}{\sqrt{2\pi}} \sum_j a \int_{ABC} \prod_i d\tilde{\xi}^\perp_i \; \sum_l (\tilde{x}^*_{l} + \tilde{\xi}^\perp_{l}) \Big(\frac{\tilde{x}^0_{l-1} - \tilde{x}^0_{l}}{a}\Big) \; e^{-S[\tilde{\xi}^\perp]} \\
&= \frac{e^{-S[\tilde{x}^*]}\beta}{\sqrt{2\pi}} \int_{ABC} \prod_i d\tilde{\xi}^\perp_i \; \sum_l (\tilde{x}^*_{l} + \tilde{\xi}^\perp_{l}) \Big(\frac{\tilde{x}^0_{l-1} - \tilde{x}^0_{l}}{a}\Big) \; e^{-S[\tilde{\xi}^\perp]} \, ,
\end{aligned}
\tag{238}
$$

where in the first equality we have made explicit use of

$$
\int_{ABC} \prod_i d\tilde{\xi}_i = \int \frac{dc_0}{\sqrt{2\pi}} \int_{ABC} \prod_i d\tilde{\xi}^\perp_i
\tag{239}
$$

and the orthonormality property of the basis of eigenvectors. Notice that in the third equality we shift the index $l \to l + j$. Additionally, in the fourth equality we also shift $\tilde{\xi}_{l+j} \to \tilde{\xi}_l$ which is

legitimate because we are integrating over all possible fluctuations. Of the two Faddeev-Popov terms, one represents a purely geometric quantity that has nothing to do with the sum of the functional integral. In fact the scalar product

$$\gamma = \sum_l \tilde{x}_l^* \Big(\frac{\tilde{x}_{l-1}^0 - \tilde{x}_l^0}{a} \Big) = \tilde{x}_0 \sum_l \bar{x}_l \Big(\frac{\tilde{x}_{l-1}^0 - \tilde{x}_l^0}{a} \Big) = \tilde{x}_0 \bar{\gamma} = \sqrt{\frac{\tilde{m}\tilde{\omega}^2}{8\tilde{\lambda}}} \bar{\gamma} \tag{240}$$

appears only in the one-loop calculation and therefore can be factorized in front of the functional integral. It follows that

$$\begin{aligned} Z_a &= \frac{e^{-S[\tilde{x}^*]}\beta\gamma}{\sqrt{2\pi}} \int_{ABC} \prod_i d\tilde{\xi}_i^\perp \ \Big[1 + \sum_l \tilde{\xi}_l^\perp \frac{1}{\gamma} \Big(\frac{\tilde{x}_{l-1}^0 - \tilde{x}_l^0}{a} \Big) \Big] \ e^{-S[\tilde{\xi}^\perp]} \\ &= \frac{e^{-S[\tilde{x}^*]}\beta\gamma}{\sqrt{2\pi}} \int_{ABC} \prod_i d\tilde{\xi}_i^\perp \ \Big[1 + \sqrt{\tilde{\lambda}} \sum_l \tilde{\xi}_l^\perp \sqrt{\frac{8}{\tilde{m}\tilde{\omega}^2}} \frac{1}{a\bar{\gamma}} (\tilde{x}_{l-1}^0 - \tilde{x}_l^0) \Big] \ e^{-S[\tilde{\xi}^\perp]} \\ &= \frac{e^{-S[\tilde{x}^*]}\beta\gamma}{\sqrt{2\pi}} \int_{ABC} \prod_i d\tilde{\xi}_i^\perp \ \Big[1 + \sqrt{\tilde{\lambda}} \sum_l \tilde{\xi}_l^\perp v_l \Big] \ e^{-S[\tilde{\xi}^\perp]} \end{aligned} \tag{241}$$

where

$$\sqrt{\frac{8}{\tilde{m}\tilde{\omega}^2}} \frac{1}{a\bar{\gamma}} (\tilde{x}_{l-1}^0 - \tilde{x}_l^0) = v_l \, . \tag{242}$$

In Fig. 4 we depict an example of the profile v_l at lattice spacing $a = 0.3$. In Eq. (241), the zero-mode has been completely regularized and the functional integral includes only fluctuations orthogonal to the zero-mode. In the Faddeev-Popov approach, the price to pay is an additional term into the twisted partition function proportional to $\sqrt{\tilde{\lambda}}$. This term also has a series expansion in perturbation theory, coming from the formal expansion in power series of the fluctuation field, which is naturally interpreted in the NSPT framework.

2.3.3 Perturbative Free Energy

Let us notice that in Monte Carlo simulations the free energy, corresponding to the partition function of Eq. (241), is the observable to be computed. However, the additional FP interaction term is not yet an observable. We can rewrite the twisted partition function as

$$Z_a = \frac{e^{-S[\tilde{x}^*]}\beta\gamma}{\sqrt{2\pi}} Z_a^\perp \langle [1 + \sqrt{\tilde{\lambda}} \sum_l \tilde{\xi}_l^\perp v_l \Big] \rangle_a^\perp \, , \tag{243}$$

where $\langle \ldots \rangle_a^\perp$ denotes the average in the antiperiodic setting for the theory without zero-mode and

$$Z_a^\perp = \int_{ABC} \prod_i d\tilde{\xi}_i^\perp \ e^{-S[\tilde{\xi}^\perp]} \tag{244}$$

is the regularized twisted partition function. The FP term can now be calculated through NSPT simulations. On the other hand, the quantity in Eq. (244) can be computed considering the equation

$$\frac{d}{d\tilde{\lambda}} Z_a^{\perp} = \int_{ABC} \prod_i d\tilde{\xi}_i^{\perp} \; e^{-S[\tilde{\xi}^{\perp}]} \left[-\frac{1}{2\sqrt{\tilde{\lambda}}} S^{(1)} - S^{(2)} \right], \tag{245}$$

which by means of Eq. (226) and

$$S^{(1)} = \sqrt{2\tilde{m}\tilde{\omega}^2} \sum_i \bar{x}_i \tilde{\xi}_i^{\perp\, 3} \,, \tag{246}$$

$$S^{(2)} = \sum_i \tilde{\xi}_i^{\perp\, 4} \,, \tag{247}$$

we get

$$\frac{1}{Z_a^{\perp}} \frac{d}{d\tilde{\lambda}} Z_a^{\perp} = \frac{d}{d\tilde{\lambda}} \ln Z_a^{\perp} = \left\langle -\frac{1}{2\sqrt{\tilde{\lambda}}} S^{(1)} - S^{(2)} \right\rangle_a^{\perp} = \frac{1}{\tilde{\lambda}} \left\langle -\frac{1}{2} \sqrt{\tilde{\lambda}} S^{(1)} - \tilde{\lambda} S^{(2)} \right\rangle_a^{\perp}. \tag{248}$$

The quantity in Eq. (248) can be very efficiently calculated with NSPT, from which we get the coefficients in perturbation theory. By expanding the RHS of (248) in power of lambda, the series is given by

$$\frac{1}{\tilde{\lambda}} \left\langle -\frac{1}{2} \sqrt{\tilde{\lambda}} S^{(1)} - \tilde{\lambda} S^{(2)} \right\rangle_a^{\perp} = \frac{1}{\tilde{\lambda}} \left(\tilde{\lambda} a^{(1)} + \tilde{\lambda}^2 a^{(2)} + ... \right). \tag{249}$$

The coefficients $a^{(i)}$ are related to the perturbative series of the partition function and the free energy. In fact, integrating Eq. (249) from $\tilde{\lambda}' = 0$ to $\tilde{\lambda}' = \tilde{\lambda}$ we obtain

$$\ln Z_a^{\perp} = \ln Z_a^{\perp}(\tilde{\lambda} = 0) + \sum_{n=1}^{\infty} \frac{\tilde{\lambda}^n}{n} a_n \qquad \rightarrow \qquad Z_a^{\perp} = Z_{a,0}^{\perp} \cdot \exp\left[\sum_{n=1}^{\infty} \frac{\tilde{\lambda}^n}{n} a_n \right], \tag{250}$$

where $Z_{a,0}^{\perp}$ is the twisted partition function for the free-theory having no zero-mode contribution. Inserting the last expression in Eq. (243) we finally get

$$Z_a = \frac{e^{-S[\tilde{x}^*]} \beta\gamma}{\sqrt{2\pi}} Z_{a,0}^{\perp} \cdot \exp\left[\sum_{n=1}^{\infty} \frac{\tilde{\lambda}^n}{n} a_n \right] \cdot \left\langle 1 + \sqrt{\tilde{\lambda}} \sum_l \tilde{\xi}_l^{\perp} v_l \right\rangle_a^{\perp}. \tag{251}$$

Given the functional form of Eq. (250), we will refer to the series in Eq. (249) as the (perturbative) free energy.

Referring back to Eq. (178), we notice that for the calculation of the energy splitting the computation of the partition function is also necessary. This too can be expressed in terms of

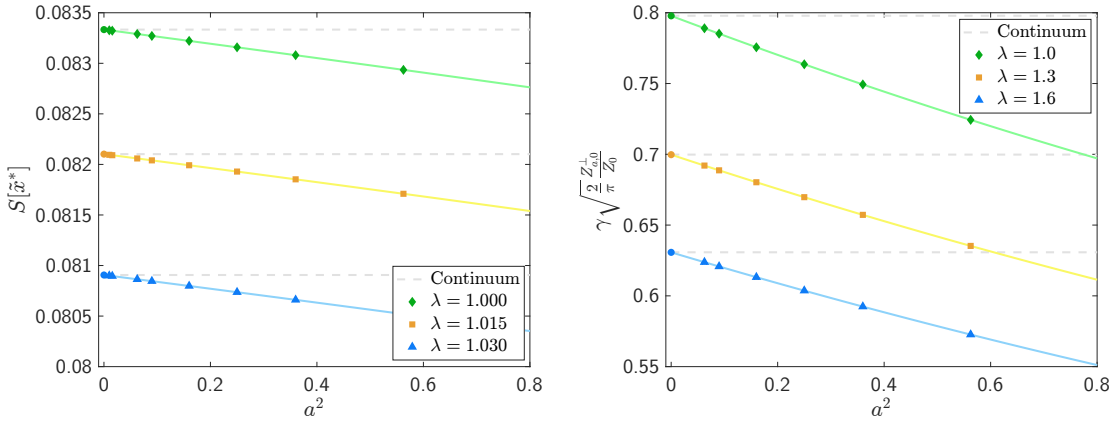

Figure 5: Left plot: continuum limit for the action evaluated on the lattice minimum solution $S[\tilde{x}^*]$. Right plot: one-loop prefactor for the lattice theory, see Eq. (253). We use the symmetric derivative in the definition of γ (see Eq. (240)) to improve convergence. Green diamonds, orange squares and blue triangles represent the values at finite lattice spacing, while circles of the respective color show the extrapolation to the continuum limit by employing second-order fits in a^2. The three colors refer to three different values of the coupling λ reported in the labels, while the other parameters have been set to $m = \omega = 1$. The dashed gray lines represent the values of the continuum theory given by Eq. (206) at the same value of λ.

the free energy. For $\beta \gg 1$ and small coupling constant the form of the partition function reads

$$\begin{aligned} Z &= \int_{PBC} \prod_i d\tilde{\xi}_i e^{-S[\tilde{\xi}]} \\ &= e^{-\beta E_0} = e^{-\beta(E_0^{(0)} + \tilde{\lambda} E_0^{(0)} + \tilde{\lambda}^2 E_0^{(1)} + \ldots)} \\ &= Z_0 \exp\left[\sum_{n=1}^{\infty} \frac{\tilde{\lambda}^n}{n} b_n\right], \end{aligned} \tag{252}$$

where the coefficients b_n are known since they are simply the coefficients of the perturbative expansion of the energy in standard perturbation theory. By means of Eq. (178), the energy splitting for the lattice theory will be given by

$$\Delta E = \frac{2}{\beta}\frac{Z_a}{Z} = e^{-S[\tilde{x}^*]}\gamma\sqrt{\frac{2}{\pi}}\left(\frac{Z^{\perp}_{a,0}}{Z_0}\right) \cdot \exp\left[\sum_{n=1}^{\infty} \frac{\tilde{\lambda}^n}{n}(a_n - b_n)\right] \cdot \left\langle 1 + \sqrt{\tilde{\lambda}} \sum_l \tilde{\xi}^{\perp}_l v_l \right\rangle^{\perp}_a . \tag{253}$$

The above equation needs to be studied in perturbation theory by means of an expansion of the exponential in Taylor series of the coupling, multiplied order-by-order by the FP term. This procedure generates the perturbative corrections as the one introduced in Eq (206).

2.3.4 Numerical Results

Before presenting the analysis of the results, we discuss the one-loop scaling to the continuum limit. By comparing Eqs. (253) and (205), it becomes clear that in the continuum limit $a \to 0$ we must have

$$\begin{aligned} S[\tilde{x}_c] \quad &\to \quad \frac{1}{12\lambda}\,, \\ \gamma\sqrt{\frac{2}{\pi}}\left(\frac{Z^{\perp}_{a,0}}{Z_0}\right) \quad &\to \quad \sqrt{\frac{2}{\pi\lambda}}\,, \end{aligned} \tag{254}$$

where the quantities on the LHS can be deterministically calculated on the lattice. In Fig. 5, the approach to the continuum limit for different values of λ is shown. Notice that no error bars are associated with points since there are no statistics involved. One-loop lattice extrapolations and continuum limit coefficients are always in agreement.

We used the NSPT algorithm to estimate the perturbative coefficients in Eq. (253). In this work, the Langevin equation was integrated using the Euler scheme, see Eq. (78). The numerical integration was implemented with six different time steps, namely $\Delta\tau = 0.0025$, 0.005, 0.01, 0.015, 0.02, 0.025. Moreover, the evolution was considered in terms of the dimensionless fluctuation field $\tilde{\xi}_i$ expanded as

$$\tilde{\xi}_i = \tilde{\xi}_i^{(0)} + \sqrt{\tilde{\lambda}}\tilde{\xi}_i^{(1)} + \tilde{\lambda}\tilde{\xi}_i^{(2)} + \tilde{\lambda}^{\frac{3}{2}}\tilde{\xi}_i^{(3)} + \tilde{\lambda}^2\tilde{\xi}_i^{(4)} + \ldots = \tilde{\xi}_i^{(0)} + \sum_{n>0}\tilde{\lambda}^{\frac{n}{2}}\tilde{\xi}_i^{(n)}\,. \tag{255}$$

The evolution occurs by means of the Langevin equation containing the gradient of the action in Eq. (226). Since the twisted partition function regularized with the Faddeev-Popov method requires only orthogonal fluctuations, we subtracted the zero-mode component from the fluctuation field at each Monte Carlo step [7]. During the stochastic evolution two observables were measured, namely

$$\sqrt{\tilde{\lambda}}\sum_i \tilde{\xi}_i^{\perp} v_i = \tilde{\lambda}c^{(1)} + \tilde{\lambda}^2 c^{(2)} + \ldots\,, \tag{256}$$

$$-\frac{1}{2}\sqrt{\tilde{\lambda}}\sqrt{\tilde{m}\tilde{\omega}^2}\sum_i \bar{x}_i(\tilde{\xi}_i^{\perp})^3 - \tilde{\lambda}\sum_i(\tilde{\xi}_i^{\perp})^4 = \tilde{\lambda}a^{(1)} + \tilde{\lambda}^2 a^{(2)} + \ldots\,. \tag{257}$$

We emphasize that even though interactions proportional to $\sqrt{\tilde{\lambda}}$ appear in the action, terms with non-integer powers are null in the perturbative expansion. This is exactly what also

[7] Since in NSPT simulations the fields are expanded in formal series, the zero-mode subtraction should be understood as an order-by-order operation.

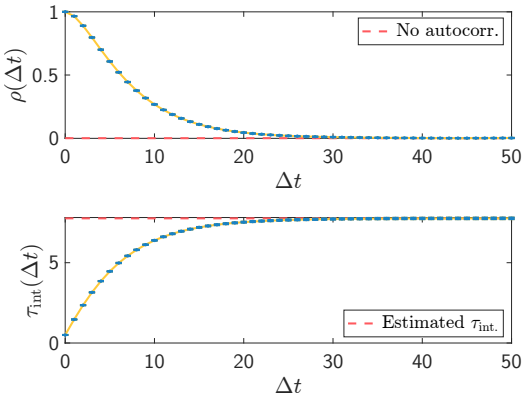

(a) *Estimation of the normalized autocorrelation function and of the integrated autocorrelation time for the first-order Faddeev-Popov term. The functional dependence on Δt indicates the summation region.*

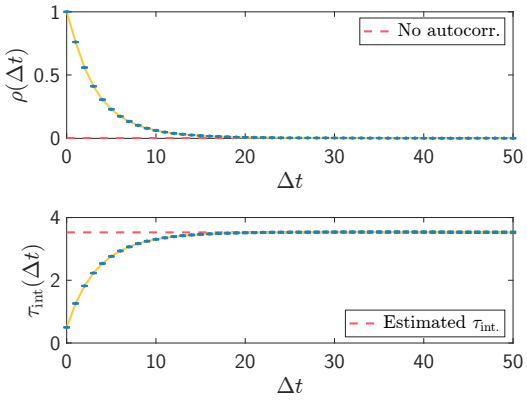

(b) *Estimation of the normalized autocorrelation function and of the integrated autocorrelazion time for the first-order perturbative free energy. The functional dependence on Δt indicates the summation region.*

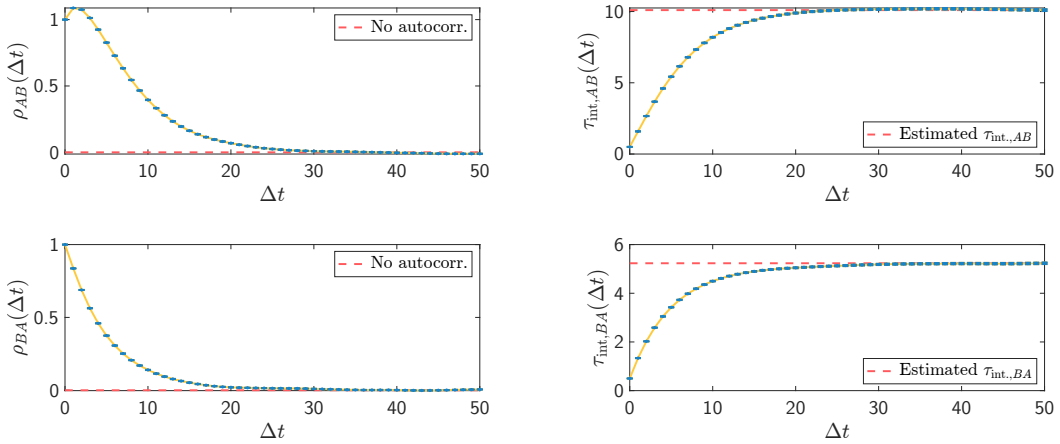

(c) *Estimation of the normalized cross-correlation function and of the integrated cross-correlation time between the first-order Faddeev-Popov term and the first-order perturbative free energy. As before, the functional dependence on Δt indicates the summation region.*

Figure 6: We show the estimation of the autocorrelation (Fig. a-b) and cross-correlation times (Fig. c) necessary for the definition of the covariance matrix $\Sigma(n,m)_{\Delta\tau}$ in Eq. (115). The estimates are for $a = 0.4$, $m = \omega = 1$, $\Delta\tau = 0.025$. The blue markers indicate the values of ρ and $\tau_{\text{int.}}$ as the summation window varies, see Eq. (127) and Eq. (133).

happens in the calculation with Feynman diagrams in the continuum theory. We call the perturbative coefficients of the free energy and FP terms as $a^{(i)}$ and $c^{(i)}$, respectively. Although the coefficients are related to different observables, since they are calculated on the same configurations, they turn out to be correlated. Because of this fact, we need to take into account also cross-correlations between the FP term and the free energy. We used the Gamma Function Method introduced in Sec. 1.6.1. In Fig. 6 we show an example for a particular choice of the lattice spacing, $a = 0.4$. In this study, the hard cut at $\Delta t = 50$ works well for all the different perturbative orders. In particular, we simulate perturbative order up to $n_{\max} = 3$ [8].

Notice that while in Eqs. (256) and (257) the perturbative expansions are in $\tilde{\lambda}$, in the continuum theory typically we consider the expansion parameter to be $S_0^{-1} = 12\lambda$. This requires the following rescaling

$$k^{(n)} \qquad \to \qquad \frac{a^{5n}}{12^n} k^{(n)} \,. \tag{258}$$

From now on, we will use the rescaled coefficients in the expansion of Eq. (253), without changing the notation.

The coefficients related to the expansions of Faddeev-Popov term and free energy, simulated at fixed a, require an extrapolation to vanishing stochastic time step. Once the covariance matrix is defined by means of the Gamma Function Method, the χ^2 function is minimized as discussed in Sec. 1.5. To check the extrapolations, both linear fits (considering the three smallest time step values) and quadratic fits (considering all the time step values) were considered, following Eq. (117) and Eq. (119). In Fig. 7, we show the extrapolations for $a = 0.6$ with $m = \omega = 1$. The two extrapolations agree well. For getting the values in the continuum limit, only the quadratic extrapolations were considered.

Considering Eq. (253), it is easy to derive the first perturbative correction, namely the two-loop correction:

$$\begin{aligned} \Delta E =& e^{-S[\tilde{x}^*]} \gamma \sqrt{\frac{2}{\pi}} \left(\frac{Z^{\perp}_{a,0}}{Z_0} \right) \cdot \left(1 + (12\lambda) c^{(1)} + \ldots \right) \cdot \left(1 + (12\lambda)(a^{(1)} - b^{(1)}) + \ldots \right) \\ =& e^{-S[\tilde{x}^*]} \gamma \sqrt{\frac{2}{\pi}} \left(\frac{Z^{\perp}_{a,0}}{Z_0} \right) \cdot \left[1 + (12\lambda)(c^{(1)} + a^{(1)} - b^{(1)}) + \ldots \right] . \end{aligned} \tag{259}$$

In light of Eq. (206), we can identify

$$z^{(1)} = c^{(1)} + a^{(1)} - b^{(1)} \,, \tag{260}$$

[8] Reaching the third order in $\tilde{\lambda}$ requires simulating the system up to the sixth order in $\sqrt{\tilde{\lambda}}$, significantly increasing the computational effort.

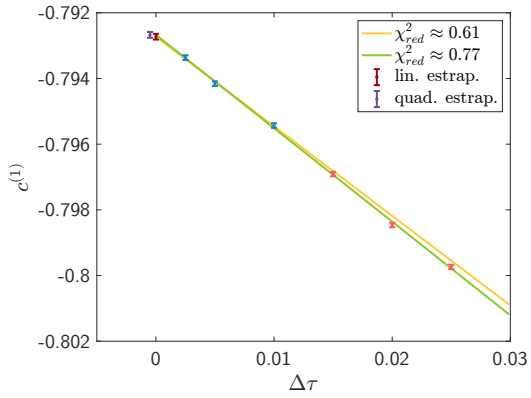

(a) *First-order Faddeev-Popov term* $c^{(1)}$.

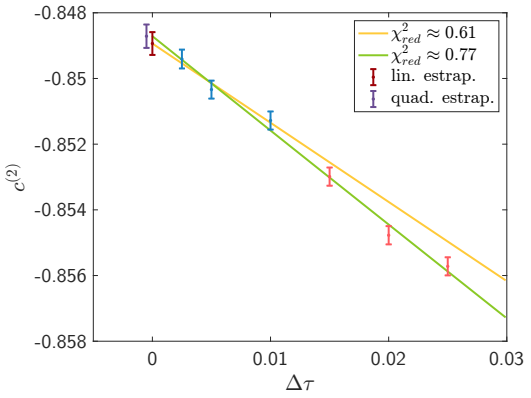

(b) *Second-order Faddeev-Popov term* $c^{(2)}$.

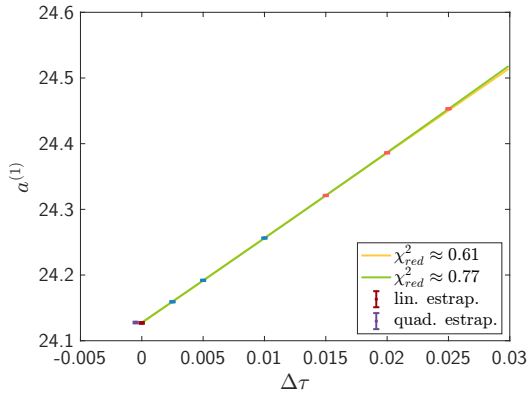

(c) *First-order perturbative free energy term* $a^{(1)}$.

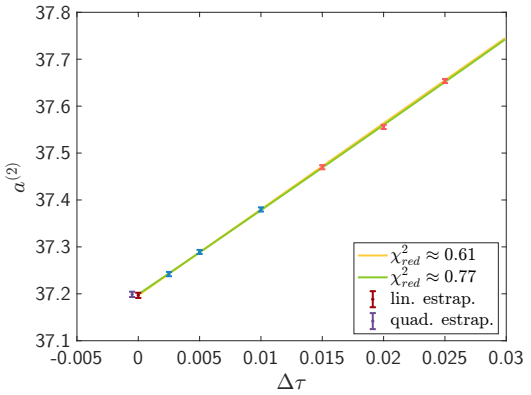

(d) *Second-order perturbative free energy term* $a^{(2)}$.

Figure 7: Continuum stochastic time extrapolations for the first- and second-order Faddeev-Popov term (Fig. a-b) and first- and second-order free energy (Fig. c-d). The NSPT computations at fixed $\Delta\tau$ are represented with blue and red markers with error bars. Blue points are included in the linear fit, see Eq. (117), represented by the yellow solid lines. Blue and red points are included in the quadratic fit, see Eq. (119), which are shown with green solid lines. The extrapolated quantities are shown in dark red and purple for the linear and quadratic minimization respectively, with a little shift along the $\Delta\tau$ axis for convenience. The $\chi^2_{red.}$ are reported in the labels.

where the coefficients on the RHS are always calculated at fixed and finite lattice spacing. Notice that the lattice spacing has a significant impact on the stochastic evolution. In fact, the integrated autocorrelation time is observed to grow like

$$\tau_{\text{int.}} \approx \frac{1}{\Delta\tau \cdot a^3} \,. \tag{261}$$

The simulations thus experience a slowdown as the continuum limit is approached (mimicking the critical slowing down of lattice gauge theories). For this reason, it was not possible to simulate lattice spacings smaller than $a = 0.15$. In practice, we have done simulations for values of $a = 0.15$, 0.2, 0.25, 0.3, 0.4, 0.5, 0.6, 0.75 with $L = 1001$, 751, 601, 501, 376, 301, 251, 201 so that $\beta = L \cdot a \approx 150$.

In Fig. 8 we report the continuum limit extrapolation for the one-loop coefficient $z^{(1)}$ defined in Eq. (260). The extrapolation $a \to 0$ has been performed considering linear and quadratic fits in a^2. The two fits show complete agreement with each other. For the following, only quadratic fits were considered. In this case, we get

$$c^{(1)} = -0.81660(50) \,, \tag{262}$$

$$a^{(1)} - b^{(1)} = -0.1657(71) \,, \tag{263}$$

and we finally obtain

$$z^{(1)}_{\text{NSPT}} = -0.9823(71) \,, \tag{264}$$

which is consistent with the continuum value given in Eq. (206). The two-loop correction error is dominated by 99.5% from the extrapolation of the free energy, while the contribution of the Faddeev-Popov term represents only 0.5% of the total error. Indeed, it is worth noting that the free energy in the antiperiodic theory is of order ≈ 10 with a relative error below one-tenth of a percent (refer to Fig. 7). The result of Eq. (263) has a rather large error since it turns out to be a subtraction of coefficients taking similar values.

2.4 Higher-order corrections and discussions

We presented the calculation of the first perturbative correction on the one-instanton sector with NSPT. Although it is a simple model of quantum mechanics, we have emphasized that even in this case the calculations with Feynman diagrams are not simple. NSPT only partially solves these issues. We have shown that we end up with a subtraction of contributions coming from

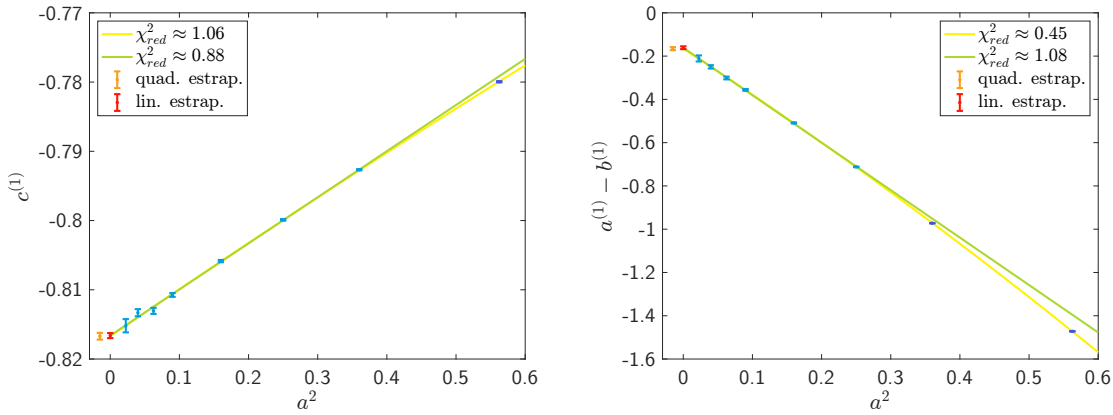

Figure 8: Continuum limit extrapolations of the Faddeev-Popov term (plot on the left) and free energy (plot on the right). The extrapolated values, shown by orange and red points, have been obtained using quadratic and linear fits, respectively. We used the first 7 (6) points for the linear fits of the FP term (free energy). For the quadratic fits, all points have been employed. The expected $\chi^2_{\rm red}$ are given in the labels.

calculations on two different vacua. Incidentally, the values involved are very similar, thus requiring high precision. Furthermore, reaching the continuum limit for not-so-high perturbative orders is a challenging task and must be performed with care. In this regard, simulations at higher orders are still ongoing, and results at the level of precision we are aiming at are not yet available. Some of these issues could be sort of a pathology of the problem at hand, and they are not going to stop us from exploring NSPT expansions around non-trivial vacua in other theories.

There is nevertheless something more to point out: not surprisingly, at not-so-high orders, we found that the NSPT signal exhibits large oscillations. This last observation is of a much more general nature, it is not that new and it is expected to involve all low-dimensional models. For this reason, the remaining part of this thesis is mostly dedicated to confronting the large fluctuations problem in NSPT.

3 | High-order NSPT computations for $O(N)$ in the large N limit

3.1 Introduction to the large fluctuations problem

From the first formulation of NSPT, it has been clear that the estimation of perturbative coefficients via stochastic process leads to results that are affected by statistical and systematic errors. Moreover, since we are obliged to work on finite volume, it is important to study the finite volume effects on our results. Considerable progress has been achieved regarding both issues [8, 13, 19, 20]. However, also the distributions of NSPT coefficients display features and aspects that require attention. This remark was prompted by inconsistencies between NSPT predictions and established results for the $O(3)$ non-linear sigma model[9]. Furthermore discrepancies were detected and analyzed in different zero-dimensional models: the zero-dimensional $\lambda\phi^4$ model, the dipole random variable model, and the Weingarten's "pathological model" [15].

In short, NSPT simulations in low-dimensional systems display statistical properties that are very different from those of a normal process. Normal processes show exponential suppressed tails, while NSPT stochastic processes display long tails and rare events that introduce *spikes* that challenge the traditional statistical analysis methods. Although the calculation of statistical errors can be reliably performed using non-parametric approaches (using the bootstrap method [15]), there still remains the practical challenge of determining whether accurate estimates can be obtained at high perturbative orders for low-dimensional systems.

Indeed, the presence of huge deviations at high perturbative orders is not unexpected. This can be verified even in the case of simple models as the following one. Let's consider the case of the zero-dimensional action

$$S[\varphi] = \frac{1}{2}\varphi^2 + \frac{g}{3}\varphi^3 \tag{265}$$

[9] These discrepancies were observed by M. Pepe [74], known as the *Pepe effect*.

for which the non-perturbative Langevin equation reads

$$\dot{\varphi} = -(\varphi + g\varphi^2) + \eta \tag{266}$$

Considering the formal series expansion shown in Eq. (68), the above equation leads to the following order-by-order set of equations

$$\begin{aligned}
\dot{\varphi}^{(0)} &= -\varphi^{(0)} + \eta \\
\dot{\varphi}^{(1)} &= -\varphi^{(1)} - \varphi^{(0)}\varphi^{(0)} \\
\dot{\varphi}^{(2)} &= -\varphi^{(2)} - 2\varphi^{(0)}\varphi^{(1)} \\
\dot{\varphi}^{(3)} &= -\varphi^{(3)} - (2\varphi^{(0)}\varphi^{(2)} + \varphi^{(1)}\varphi^{(1)}) \\
&\dots
\end{aligned} \tag{267}$$

It is evident that any fluctuation driven by the Gaussian noise at the leading order is amplified as squared at the first order, resulting in a cubic effect at the second order, and so on. In summary, a potentially large fluctuation becomes increasingly amplified at higher perturbative orders, leading eventually to a situation in which the signal is lost. We naturally inquire about the effectiveness of the restoring mechanism built into the Langevin equation in reabsorbing large fluctuations (and up to which order), its impact on the autocorrelation time and on the emerging standard deviation. A logical assumption is the problem will become progressively less intense as more degrees of freedom are involved (coherent large fluctuations will be improbable, and overall, the interaction among the numerous degrees of freedom is expected to lead to a kind of self-averaging towards gaussianity). However, this leads to the question of the required size that a system should have in order to ensure stability.

3.2 $O(N)$ Non-Linear Sigma Model

The process outlined in Eq. (267) is quite broad. The conjecture that increasing the number of degrees of freedom would lead to less problematic signal appears to be confirmed by Lattice QCD simulations, where fluctuations do occur only at extremely high orders. In large systems, the equations for different degrees of freedom are coupled so that we expect that rare deviations with an independent impact on single degree of freedom will have less and less contribution. All in all, it makes sense to explore the connections between NSPT stochastic distributions and the number of degrees of freedom. From this point of view, the $O(N)$ non-linear sigma model becomes an ideal laboratory, as it allows for simulations of the same model with varying values

of the parameter N, thus modifying the number of degrees of freedom. Naturally, increasing the number of degrees of freedom leads to higher computational costs.

Two-dimensional $O(N)$ non-linear sigma models are very important in quantum field theory. Theoretically, these models exhibit interesting properties, such as asymptotic freedom. Phenomenologically, they have successfully modeled various features across different contexts (for an introduction to this subject, we refer the reader to [75]). From our perspective, our interest in that model consists in the possibility of changing the number of degrees of freedom through the choice of the value of N. In the continuum the action of the model reads

$$S[\boldsymbol{s}] = \frac{1}{2g} \int d^2x \, \Big(\partial_\mu \boldsymbol{s}(x)\Big)^2 , \tag{268}$$

where $\boldsymbol{s}(x)$ is a N-component real scalar field with the local constrain $\boldsymbol{s}(x) \cdot \boldsymbol{s}(x) = 1$ for all x. Various lattice regularizations of this model are known. For our purposes, we use the simplest $2D$ version, namely

$$S[\boldsymbol{s}] = -\frac{1}{g} \sum_{x,\mu} \boldsymbol{s}_x \cdot \boldsymbol{s}_{x+\mu} \, , \tag{269}$$

where $\boldsymbol{s}_x$ is a N-component lattice real scalar field obeying the constraint $\boldsymbol{s}_x \cdot \boldsymbol{s}_x = 1$ on all lattice sites. Here, g is the coupling constant and μ runs over the two lattice directions. The partition function can be expressed by incorporating the constraint into a local Dirac delta function

$$Z = \int \prod_x \, d\boldsymbol{s}_x \; \delta(\boldsymbol{s}_x^2 - 1) \; e^{\frac{1}{g} \sum_{x,\mu} \boldsymbol{s}_x \cdot \boldsymbol{s}_{x+\mu}} \, . \tag{270}$$

3.3 Perturbation theory setup

In the $O(N)$ non-linear sigma models, the interaction is encoded in the local constraint. Perturbation theory requires the identification of the correct degrees of freedom. Here we follow the approach discussed in [76]. By using the decomposition

$$\boldsymbol{s}_x = (\boldsymbol{\pi}_x, \sigma_x) \tag{271}$$

the partition function becomes

$$Z = \int \prod_x \, d\boldsymbol{\pi}_x \; d\sigma_x \; \delta(\boldsymbol{\pi}^2 + \sigma_x^2 - 1) \; e^{\frac{1}{g} \sum_{x,\mu} \left(\boldsymbol{\pi}_x \cdot \boldsymbol{\pi}_{x+\mu} + \sigma_x \sigma_{x+\mu}\right)} \, . \tag{272}$$

The σ_x component can be integrated-out by means of the Dirac delta function

$$\sigma_x = \epsilon(x) \sqrt{1 - \boldsymbol{\pi}_x^2} \, , \tag{273}$$

with $\epsilon(x) = \pm 1$, and we get

$$\delta(f(\sigma_x)) = \frac{\delta(\sigma_x - x_0)}{|f'(x_0)|} = \frac{\delta(\sigma_x - \epsilon(x)\sqrt{1-\boldsymbol{\pi}_x^2})}{2\epsilon(x)\sqrt{1-\boldsymbol{\pi}_x^2}}\,, \qquad f(\sigma_x) = \boldsymbol{\pi}^2 + \sigma_x^2 - 1\,. \tag{274}$$

The partition function now reads

$$\begin{aligned} Z &= \sum_{\epsilon(x)=\pm 1} \int \prod_x d\boldsymbol{\pi}_x \; d\sigma_x \frac{\delta(\sigma_x - \sqrt{1-\boldsymbol{\pi}_x^2})}{2\epsilon(x)\sqrt{1-\boldsymbol{\pi}_x^2}} \; e^{\frac{1}{g}\sum_{x,\mu}\left(\boldsymbol{\pi}_x\cdot\boldsymbol{\pi}_{x+\mu} + \sigma_x\sigma_{x+\mu}\right)} \\ &= \sum_{\epsilon(x)=\pm 1} \int \prod_x \frac{d\boldsymbol{\pi}_x}{\epsilon(x)\sqrt{1-\boldsymbol{\pi}_x^2}} \; e^{\frac{1}{g}\sum_{x,\mu}\left(\boldsymbol{\pi}_x\cdot\boldsymbol{\pi}_{x+\mu} + \epsilon(x)\epsilon(x+\mu)\sqrt{1-\boldsymbol{\pi}_x^2}\sqrt{1-\boldsymbol{\pi}_{x+\mu}^2}\right)}\,. \end{aligned} \tag{275}$$

By defining

$$\Delta_\mu \boldsymbol{\pi}_x = \boldsymbol{\pi}_{x+\mu} - \boldsymbol{\pi}_x\,, \tag{276}$$

$$(\Delta_\mu \sqrt{1-\boldsymbol{\pi}_x^2})_\epsilon = \epsilon(x+\mu)\sqrt{1-\boldsymbol{\pi}_{x+\mu}^2} - \epsilon(x)\sqrt{1-\boldsymbol{\pi}_x^2}\,, \tag{277}$$

we can write the action terms as follows

$$(\Delta_\mu \boldsymbol{\pi}_x)\cdot(\Delta_\mu \boldsymbol{\pi}_x) = (\Delta_\mu \boldsymbol{\pi}_x)^2 = \boldsymbol{\pi}_{x+\mu}^2 - 2\boldsymbol{\pi}_{x+\mu}\boldsymbol{\pi}_x + \boldsymbol{\pi}_x^2\,, \tag{278}$$

$$(\Delta_\mu \sqrt{1-\boldsymbol{\pi}_x^2})_\epsilon (\Delta_\mu \sqrt{1-\boldsymbol{\pi}_x^2})_\epsilon = (\Delta_\mu \sqrt{1-\boldsymbol{\pi}_x^2})_\epsilon^2 \tag{279}$$

$$= 1 - \boldsymbol{\pi}_{x+\mu}^2 - 2\epsilon(x+\mu)\epsilon(x)\sqrt{1-\boldsymbol{\pi}_{x+\mu}^2}\sqrt{1-\boldsymbol{\pi}_x^2} + 1 - \boldsymbol{\pi}_x^2\,. \tag{280}$$

Adding the previous two equations we get

$$(\Delta_\mu \boldsymbol{\pi}_x)^2 + (\Delta_\mu \sqrt{1-\boldsymbol{\pi}_x^2})_\epsilon^2 = -2\boldsymbol{\pi}_x\boldsymbol{\pi}_{x+\mu} - 2\epsilon(x)\epsilon(x+\mu)\sqrt{1-\boldsymbol{\pi}_{x+\mu}^2}\sqrt{1-\boldsymbol{\pi}_x^2} + 2\,, \tag{281}$$

so the partition function is written as

$$Z = \sum_{\epsilon(x)=\pm 1} \int \prod_x \frac{d\boldsymbol{\pi}_x}{\sqrt{1-\boldsymbol{\pi}_x^2}} \; e^{-\frac{1}{2g}\sum_{x,\mu}\left[(\Delta_\mu \boldsymbol{\pi}_x)^2 + (\Delta_\mu \sqrt{1-\boldsymbol{\pi}_x^2})_\epsilon^2 + 1\right]}\,. \tag{282}$$

The last term in the action can be neglected since it is a constant contribution to the partition function that can be reabsorbed into the definition of the lattice functional integral. To obtain the usual perturbation theory, it is customary to use the rescaling

$$\boldsymbol{\pi}_x^2 \qquad \to \qquad g\boldsymbol{\pi}_x^2\,. \tag{283}$$

In fact, using Eq. (283), the partition function reads

$$Z = \sum_{\epsilon(x)=\pm 1} \int \prod_x \frac{d\boldsymbol{\pi}_x}{\sqrt{1-g\boldsymbol{\pi}_x^2}} \; e^{-\frac{1}{2}\sum_{x,\mu}\left[(\Delta_\mu \boldsymbol{\pi}_x)^2 + \frac{1}{g}(\Delta_\mu \sqrt{1-g\boldsymbol{\pi}_x^2})_\epsilon^2\right]}\,. \tag{284}$$

We note that every time we choose a non-constant sign field $\epsilon(x)$, in Eq. (282) the constant terms in the action no longer vanish. As a result, we obtain a contribution that scales as $e^{-\frac{A}{g}}$ and thus does not contribute to the perturbation theory. From now on we will therefore consider only constant fields, namely $\epsilon(x) = 1$. It is easy to see that $\epsilon(x) = -1$ leads to the same perturbation theory. The two perturbation theories can be summed, giving an additional constant in front of the partition function that still can be reabsorbed into the definition of the functional integral. We introduce the infrared regulator λ to set a temporary mass term to be removed at the end of the calculations. The partition function has the form

$$Z = \lim_{\lambda \to 0} \int \prod_x d\boldsymbol{\pi}_x \; e^{-\frac{1}{2}\sum_{x,\mu}\left[(\Delta_\mu \boldsymbol{\pi}_x)^2 + \lambda^2 \boldsymbol{\pi}_x^2 - \frac{1}{g}(\Delta_\mu \sqrt{1 - g\boldsymbol{\pi}_x^2})^2\right] - \frac{1}{2}\sum_x \log(1 - g\boldsymbol{\pi}_x^2)}, \tag{285}$$

where the logarithmic term arises from the additional integral measure term. As for the propagator, this is given by

$$\langle \pi_x^i \pi_y^j \rangle = \delta^{ij} G(x - y) = \delta^{ij} \int_{-\pi}^{+\pi} \frac{d^2k}{(2\pi)^2} \frac{e^{ik\cdot(x-y)}}{4\sum_\mu \sin^2\left(\frac{k\cdot\mu}{2}\right) + \lambda^2} \tag{286}$$

We note that the propagator diverges like $\log(\lambda)$ as $\lambda \to 0$. This issue is related to the fact that in perturbation theory, expansion occurs around a free vacuum with broken symmetry, while a theorem prohibits this kind of symmetry breaking in 2-dimensional systems [77]. As a result, the fundamental building block of perturbation theory, the free propagator, is ill-defined. However, it has been noted in the context of the $O(N)$ sigma models that any $O(N)$ invariant quantity can be expanded perturbatively [76, 78], with the infrared divergences precisely canceling out order-by-order.

3.3.1 One-loop computation

In this work we consider a well-defined $O(N)$ invariant quantity [76], which is the energy (that is given from the propagator in terms of the original fields)

$$\begin{aligned} E &= -\frac{1}{2V}\frac{\partial \log Z}{\partial\left(\frac{1}{g}\right)} = -\frac{1}{2VZ}\frac{\partial Z}{\partial\left(\frac{1}{g}\right)} \\ &= \frac{1}{2V}\sum_{x,\mu}\langle \boldsymbol{s}_x \cdot \boldsymbol{s}_{x+\mu}\rangle = \langle \boldsymbol{s}_0 \cdot \boldsymbol{s}_1\rangle\,. \end{aligned} \tag{287}$$

Working in perturbation theory, up to second-order terms, we get

$$\begin{aligned}\langle \boldsymbol{s}_0 \cdot \boldsymbol{s}_1 \rangle &= g\langle \boldsymbol{\pi}_0 \cdot \boldsymbol{\pi}_1 \rangle + \langle \sqrt{1+g\boldsymbol{\pi}_0^2}\sqrt{1+g\boldsymbol{\pi}_1^2} \rangle \\ &= 1 + g\Big(\langle \boldsymbol{\pi}_0 \cdot \boldsymbol{\pi}_1 \rangle^{(0)} - \langle \boldsymbol{\pi}_0^2 \rangle^{(0)} \Big) \\ &+ g^2 \Big(\langle \boldsymbol{\pi}_0 \cdot \boldsymbol{\pi}_1 \rangle^{(1)} - \langle \boldsymbol{\pi}_0^2 \rangle^{(1)} + \frac{1}{4}\langle \boldsymbol{\pi}_0^2 \boldsymbol{\pi}_1^2 \rangle^{(0)} - \frac{1}{4}\langle \boldsymbol{\pi}_0^4 \rangle^{(0)} \Big) + O(g^3)\,,\end{aligned} \tag{288}$$

where in the last line we use the Taylor expansion and $\langle \boldsymbol{\pi}_x \boldsymbol{\pi}_y \rangle^{(n)}$ is the n-loop correction to the free propagator. The leading-order energy thus is

$$E^{(0)} = 1\,. \tag{289}$$

Given the Eq. (288), the first-order correction to the energy is given by the expression

$$\begin{aligned}E^{(1)} &= \langle \boldsymbol{\pi}_0 \cdot \boldsymbol{\pi}_1 \rangle^{(0)} - \langle \boldsymbol{\pi}_0^2 \rangle^{(0)} \\ &= \lim_{\lambda \to 0} (N-1)[G(1) - G(0)] \\ &= \lim_{\lambda \to 0} (N-1) D(x=1) = -\frac{(N-1)}{4}\,,\end{aligned} \tag{290}$$

where we define

$$D(x) = G(x) - G(0) = \int_{-\pi}^{+\pi} \frac{d^2k}{(2k)^2} \frac{e^{ikx} - 1}{4\sum_\mu \sin^2(k_\mu/2) + \lambda^2}\,. \tag{291}$$

Notice that in the final result of Eq. (290) we have used

$$D(1) = -\frac{1}{4}\,. \tag{292}$$

In this case infrared divergences in $\langle \boldsymbol{\pi}_0 \cdot \boldsymbol{\pi}_1 \rangle^{(0)}$ are exactly canceled out by the additional term $\langle \boldsymbol{\pi}_0^2 \rangle^{(0)}$.

3.3.2 Two-loop computation

The same cancellation takes place at the second perturbative order. The form for the second-loop correction to the energy follows

$$E^{(2)} = \langle \boldsymbol{\pi}_0 \cdot \boldsymbol{\pi}_1 \rangle^{(1)} - \langle \boldsymbol{\pi}_0^2 \rangle^{(1)} + \frac{1}{4}\langle \boldsymbol{\pi}_0^2 \boldsymbol{\pi}_1^2 \rangle^{(0)} - \frac{1}{4}\langle \boldsymbol{\pi}_0^4 \rangle^{(0)}\,. \tag{293}$$

The above equation can be rewritten using the Wick contractions

$$\begin{aligned}\langle \boldsymbol{\pi}_0^2 \boldsymbol{\pi}_1^2 \rangle^{(0)} &= (N-1)^2 G^2(0) + 2(N-1)G^2(1)\,, \\ \langle \boldsymbol{\pi}_0^2 \boldsymbol{\pi}_1^2 \rangle^{(0)} &= (N-1)^2 G^2(0) + 2(N-1)G^2(0)\,,\end{aligned} \tag{294}$$

through the use of which we get

$$\begin{aligned} E^{(2)} &= -(N-1)G(1)G(1) + (N-1)G(1)G(0) + \frac{1}{4}[(N-1)^2G^2(0) + 2(N-1)G^2(1)] \\ &\quad - \frac{1}{4}[(N-1)^2G^2(0) + 2(N-1)G^2(0)] + O(\lambda^2) \\ &= -(N-1)G(1)(G(1)-G(0)) + \frac{1}{2}(N-1)[G^2(x) - G^2(0)] + O(\lambda^2) \\ &= \frac{1}{2}[G(1) - G(0) - 2(G(1)-G(0))][G(1)-G(0)] + O(\lambda^2) \\ &= \frac{1}{2}(N-1)[D^2(1) - \frac{1}{2}D(1)] + O(\lambda^2) \\ &= -\frac{N-1}{32} + O(\lambda^2)\,. \end{aligned} \tag{295}$$

In Eq. (295) we use the expression for the first-order correction of the propagator. We report on this computation in App. C. The second-loop correction yields still a finite result where all the logarithmic divergences are canceled.

Higher-order computations are not simple because we have to face an intricate perturbation theory, where not only new Feynman diagrams are generated but also new vertices appear at each order. Until now, only the first four corrections are known analytically [76, 79] and read

$$\begin{aligned} E^{(0)} &= 1\,, \\ E^{(1)} &= -(N-1)/4\,, \\ E^{(2)} &= -(N-1)/32\,, \\ E^{(3)} &= -0.00726994(N-1) - 0.00599298(N-1)^2\,, \\ E^{(4)} &= -0.00291780(N-1) - 0.00332878(N-1)^2 - 0.00156728(N-1)^3\,. \end{aligned} \tag{296}$$

3.4 Perturbative computations with NSPT

We rewrite Eq. (285) for the partition function in the form

$$\begin{aligned} Z = \int \prod_x d\boldsymbol{\pi}_x \;\; &\exp\Big\{\sum_{x,\mu}\Big(\boldsymbol{\pi}_x\cdot\boldsymbol{\pi}_{x+\mu} + \frac{1}{g}\sqrt{1-g\boldsymbol{\pi}_x^2}\sqrt{1-g\boldsymbol{\pi}_{x+\mu}^2}\Big)\Big\} \\ &\times \exp\Big\{-\frac{1}{2}\sum_x \log(1-g\boldsymbol{\pi}_x^2)\Big\}\,, \end{aligned} \tag{297}$$

from which we define the action as

$$S = -\sum_{x,\mu}\Big(\boldsymbol{\pi}_x\cdot\boldsymbol{\pi}_{x+\mu} + \frac{1}{g}\sqrt{1-g\boldsymbol{\pi}_x^2}\sqrt{1-g\boldsymbol{\pi}_{x+\mu}^2}\Big) + \frac{1}{2}\sum_x \log(1-g\boldsymbol{\pi}_x^2)\,. \tag{298}$$

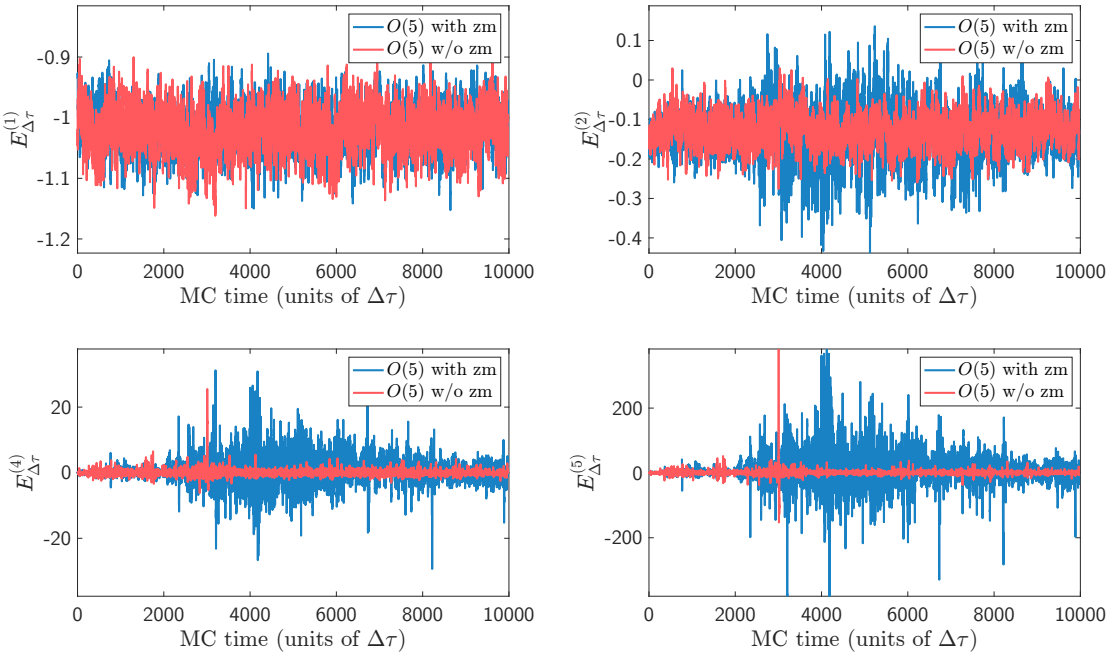

Figure 9: NSPT simulations of the $O(5)$ NLSM model in a 20×20 lattice. The figures represent the energy at increasing loop orders, computed using configurations with zero-mode (blue solid line) and without zero-mode (red solid line). The signals with zero-mode are much noisier.

The associated non-perturbative Langevin equation is straightforward

$$\dot{\pi}^j_y(\tau) = \sum_\mu \left\{ \pi^j_{y+\mu} + \pi^j_{y-\mu} - \pi^j_y \left(\sqrt{\frac{1 - g\boldsymbol{\pi}^2_{y+\mu}}{1 - g\boldsymbol{\pi}^2_y}} + \sqrt{\frac{1 - g\boldsymbol{\pi}^2_{y-\mu}}{1 - g\boldsymbol{\pi}^2_y}} \right) \right\} \Bigg|_{\boldsymbol{\pi}(\tau)} + \frac{g\pi^j_y}{1 - g\boldsymbol{\pi}^2_y} \Bigg|_{\boldsymbol{\pi}(\tau)} + \eta^j_y(\tau) \tag{299}$$

with

$$\langle \eta^j_y(\tau) \rangle = 0\,, \qquad \langle \eta^j_y(\tau) \eta^\sigma_k(\tau') \rangle = \delta_{j\sigma}\delta_{yk}\delta(\tau - \tau')\,. \tag{300}$$

Notice that $\pi^j_y(\tau)$ represents the j-component of the $\boldsymbol{\pi}$ field at the lattice site y, evaluated at the stochastic time τ. With NSPT we can proceed straight ahead and go beyond the fourth order, especially (as already stated and as we will see below) in the large N regime. In fact, NSPT simulations are completely insensitive to the increasing number of terms of the diagrammatic perturbation theory: the order-by-order encoding of the Eq. (299) is automatically generated.

In Eqs. (297)-(299) we consider directly the limit $\lambda \to 0$. In this setting the stochastic evolution displays the zero-mode which needs to be regularized. In Eq. (288) the additional term to the fundamental $\pi\pi$ propagator cancels the zero-mode contribution. In the context of

N	n_{max}	V	Statistics $\times N$	$\Delta\tau$
$5:1:15$	15	20×20	$\approx 1.6\cdot 10^9$	$[18,\ 25,\ 35,\ 50,\ 75,\ 100]\cdot 10^{-4}$
$18:3:45$	15	20×20	$\approx 2.1\cdot 10^9$	$[18,\ 25,\ 35,\ 50,\ 75,\ 100]\cdot 10^{-4}$
$15:3:43$	23	20×20	$\approx 1.2\cdot 10^9$	$[18,\ 25,\ 35,\ 50,\ 75,\ 100]\cdot 10^{-4}$
45	23	20×20	$\approx 2.7\cdot 10^9$	$[18,\ 25,\ 35,\ 50,\ 75,\ 100]\cdot 10^{-4}$
5	23	66×66	$\approx 9\cdot 10^7$	$[18,\ 25,\ 35,\ 50,\ 75,\ 100]\cdot 10^{-4}$

Table 1: Details of the simulations: the notation $N:\Delta:M$ represents the set of values N, $N+\Delta$, $N+2\Delta$, ..., M. Six different time steps $\Delta\tau$ were considered. The term n_{max} denotes the highest perturbative order achieved for the respective set of simulations; it is important to note that streams with varying n_{max} must be treated individually due to correlations among different orders within a single stream. The statistics are normalized by N, thus different rows carry roughly equivalent computational weight.

NSPT, this cancellation is expected to happen in a statistical sense and thus does not find an equivalent in real-world Monte Carlo simulations.

One approach is to implement an infrared regulator λ in the same spirit as in Eq. (357) and to remove it at the end of the simulations. This requires additional simulations and extra extrapolations. Furthermore, based on our experience, we cannot achieve good regularizations without considering large values of λ, which however make systematic effects increase. A more efficient choice is to eliminate the zero-mode component by subtracting this contribution directly from the configurations [9]. This method is convenient because it does not introduce additional steps, while reproducing the perturbative expansion of the lattice theory in the limit of infinite volume. It is worth noting that the subtraction of the zero-mode at each step of the Monte Carlo process is an exact procedure at the leading order for the energy (we present in detail this calculation in App. D). The effects of this regularization on the $O(5)$ model are reported in Fig. 9: at one-loop no difference can be seen, while at higher loops the signals without zero-mode are manifestly better under control.

Most of our simulations have been performed on 20×20 lattices for several values of N (see Tab. 1 for the simulation details). We should stress that even in the case of these small lattices, we observed tiny finite size effects: by comparing our results with the respective results known analytically, which are given by Eq. (296), we found discrepancies of the order of a few per mille. This is shown in Fig. 10 where our numerical NSPT results have been plotted together with the

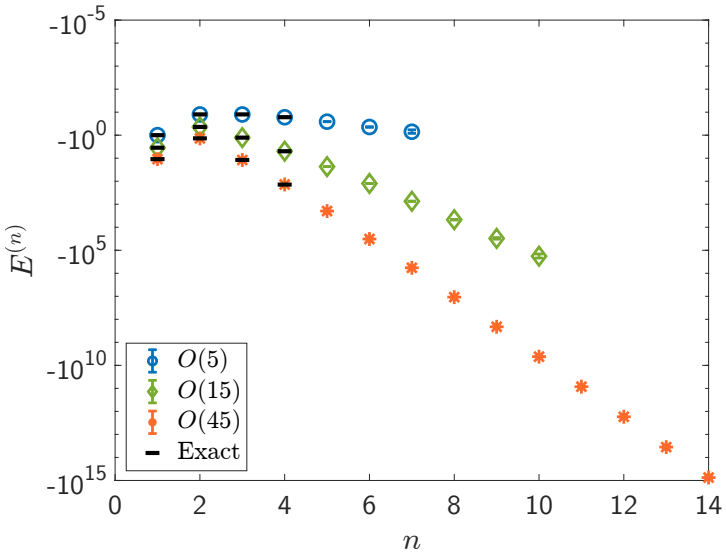

Figure 10: NSPT perturbative computations in $O(N)$ sigma models: the energy of the model is computed at increasing perturbative order n; blue, green and orange points refer to the $O(5)$, $O(15)$ and $O(45)$ models, respectively. Analytical results are shown in black. The larger is N, the higher loop corrections can be safely computed.

exact analytical results. Note that in Fig. 10, the influence of N on the highest perturbative order achievable becomes evident. The distinction between the regions of low and high perturbative orders is clear: for all $O(N)$ models considered here, we managed to compute three additional perturbative orders beyond the known ones. However, as the perturbative order n increases, reliable results were achieved only with progressively higher values of N. To be more specific, in the case of the $O(5)$ NLSM we extended the calculations from the fourth to the seventh order. For the $O(15)$ model, we successfully reached the tenth order, and remarkably, for the $O(45)$ model, we were able to compute up to the 14th order. This is due to the fluctuations in the stochastic process and we will investigate this connection in depth in the following sections. Determining the perturbative order at which one should stop stochastic calculations for a specific $O(N)$ model is a non-trivial task. We have contextually performed several sanity checks to assess the reliability of our findings, including analyses of time series, cumulative moving averages, cumulative moving standard deviations and scaling of relative errors.

In Fig. 10 systematic errors coming from the numerical integration scheme have been removed (in Fig. 11 we show an example for the $O(15)$ model). For the extrapolations we take into account autocorrelations and cross-correlations by means of the Blocking Method (see Fig. 12)

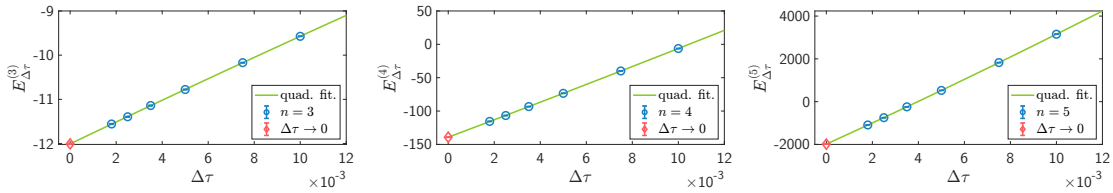

Figure 11: Extrapolation to the continuum stochastic process in the $O(15)$ model for perturbative orders $n = 3, 4, 5$. Simulations were performed using 20×20 lattices and the Euler integration scheme. We consider first- and second-order corrections in $\Delta\tau$, with $\chi^2_{\text{red}} \approx 1.33$. NSPT results are shown with the blue points, while green lines represent quadratic fits. Red diamonds show the extrapolated results.

as described in Sec. 1.6.2. In this work we mainly used the Euler integration scheme. In Sec. 1.3.2 we have mentioned that continuum stochastic process extrapolations are still under debate. We note that our focus here lies in higher-order computations. Therefore, we aim to ensure the safety of extrapolations while incorporating all perturbative orders. Using high-order schemes (see Sec. 1.8.1 and 1.8.2) one can be tempted to avoid extrapolations by considering simulations for a single tiny time step. However, there is no way to find a time step value that is small enough to guarantee that we cannot distinguish systematic from statistical errors. Higher orders can always introduce new surprises, for example because different orders can be of different orders of magnitude. In fact, this actually happens in $O(N)$ NLSMs (see the increasing systematic effects as the order n increases in Fig. 11). Additionally, it is worth noting that the feasibility of stochastic time extrapolation provides further confidence that results at a specific order are reliable and not affected by significant fluctuations. In essence, while stochastic time extrapolation requires additional computational effort, nevertheless, we are more confident that mean values and errors become more accurate.

As discussed in Sec. 1.4 other integration schemes are viable: we can take advantage of this by making combined extrapolation fits using results from different integration schemes. In Fig 13 we show combined fit results using at the same time data from the Euler and the Runge-Kutta schemes. In this case simulations were performed for the $O(80)$ NLSM on a 32×32 lattice.

A preliminary insight into the emergence of fluctuations can be obtained by examining the stochastic time series. In Fig. 14, signals for $O(5)$, $O(15)$, and $O(45)$ are displayed at different perturbative orders using the same time step, namely $\Delta\tau = 0.0035$. In particular, in the first row, we display the evolution in the stochastic time for perturbative order $n = 3$. Here, no huge spikes are detected. Furthermore, the distribution of fluctuations in each case turns out to look

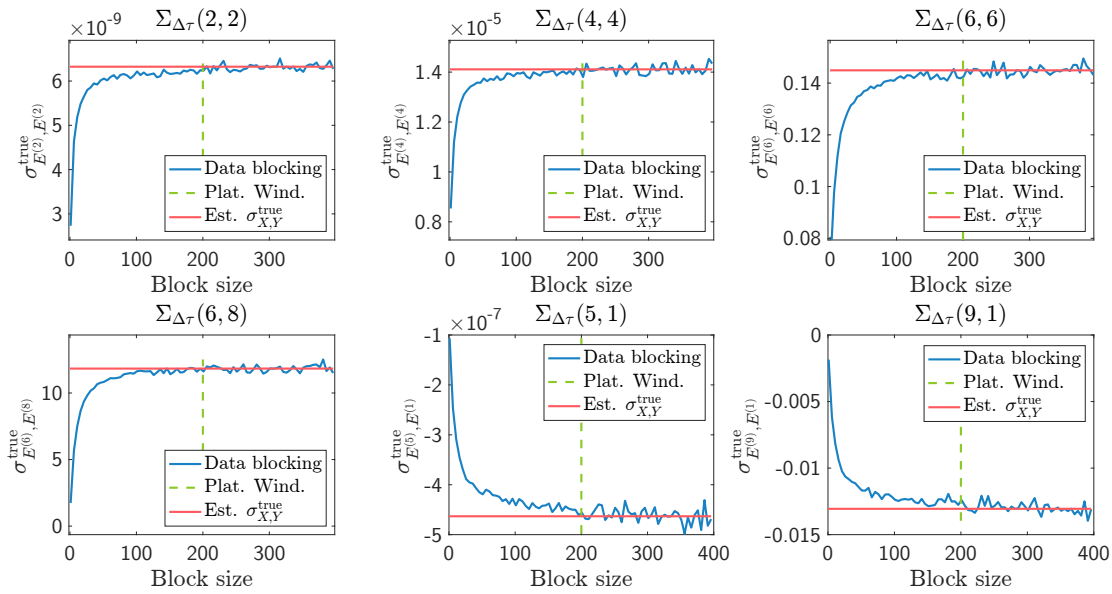

Figure 12: Estimation of the matrix elements $\Sigma_{\Delta\tau}(n,m)$ using the Blocking Method for the $O(15)$ sigma model. Block sizes are multiples of 100. The value of variances and covariances for different perturbative orders (n,m) as the block sizes increase are shown with blue lines. The estimated matrix elements $\Sigma_{\Delta\tau}(n,m)$ are displayed with horizontal red lines, computed as the mean in the plateau (region to the right of the green dashed line). All the data refer to a value of $\Delta\tau = 0.005$.

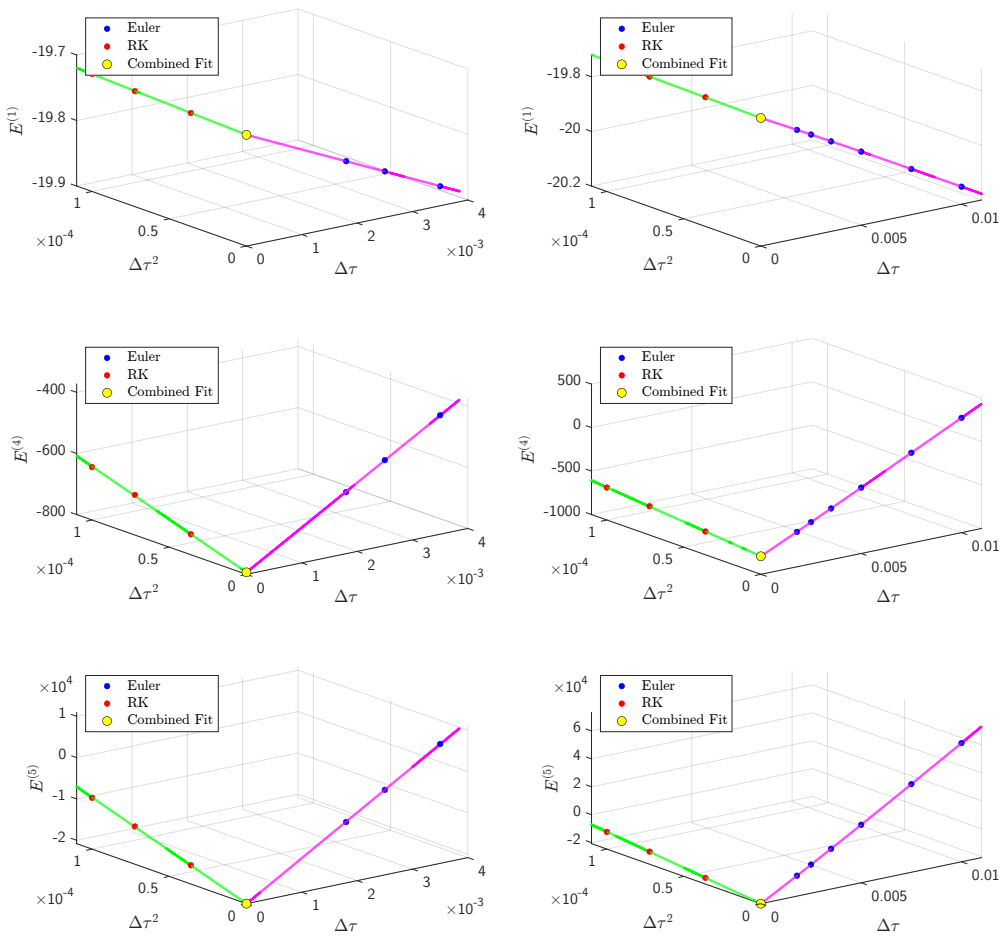

Figure 13: Combined fit extrapolations for the $O(80)$ NLSM using two integration schemes. We display fits for different perturbative orders, namely $n = 3, 4, 5$. Simulations with Euler and Runge-Kutta schemes are depicted with blue and red symbols, respectively. For the plots on the left, the fitting procedure includes linear extrapolations in $\Delta\tau$ for Euler (magenta solid line) and linear extrapolations in $\Delta\tau^2$ for Runge-Kutta (green solid line). The three plots on the right (using the same color code) show cubic extrapolations in $\Delta\tau$ for the Euler integrator, over a larger set of points. Yellow points on all plots show the extrapolated values.

similar to a Gaussian process, where events in the tails are suppressed exponentially.

At perturbative order $n = 8$ (see the second row of Fig. 14), pronounced fluctuations appear in the $O(5)$ evolution. They give a substantial contribution to the mean and the standard deviation (we will discuss this point in more detail in Sec. 3.4.1). On the contrary, the stochastic evolution for the $O(15)$ model still looks under control, and that for $O(45)$ is excellent. Note that most of the signals tend to display a *band*, which naturally characterizes the amplitude of the oscillations: if we want to inspect the presence of large fluctuations by eye, we have to compare them to the width of this band.

By inspecting higher perturbative orders, namely $n = 11, 14$ (third and fourth rows of Fig. 14), large fluctuations become predominant in the $O(5)$ model: here the evolution is completely dominated by large spikes. In addition, fluctuations emerge also in the $O(15)$ model. It turns out that for such a perturbative order the NSPT distributions significantly deviate from a Gaussian distribution. The signal-to-noise ratio is very poor. In contrast, the NSPT evolution for the $O(45)$ model (reported in the last column of Fig. 14) still appears well-behaved. In this case, the signal-to-noise ratio is good, and the distributions are reliable.

3.4.1 Cumulative moving averages and standard deviations

Cumulative moving average and standard deviation are statistical tools that can be helpful in analyzing our data. Following the approach outlined in [15], here we will analyze NSPT evolutions using these tools. Broadly speaking, as more data points are considered, the cumulative moving average and standard deviation evolve, tracking the data's spread with each new observation. By examining the evolution of the cumulative average and standard deviation, we can naturally assess data stability in relation to the emergence of large fluctuations.

We define the cumulative moving average (in short, cumulative mean) as

$$\langle E^{(n)} \rangle_\tau = \frac{1}{\tau} \sum_{i=1}^{\tau} E_i^{(n)} \,, \tag{301}$$

where $E_i^{(n)}$ indicates the n-th perturbative order of the energy measured on the i-th Monte Carlo configuration. The subscript $\langle ... \rangle_\tau$ indicates that the summation window extends from the first configuration to the τ-th. Note that here we are using the same terminology as in the non-perturbative Monte Carlo simulations. In this context, however, a field configuration refers to a set of different field values, each field identifying a different perturbative order.

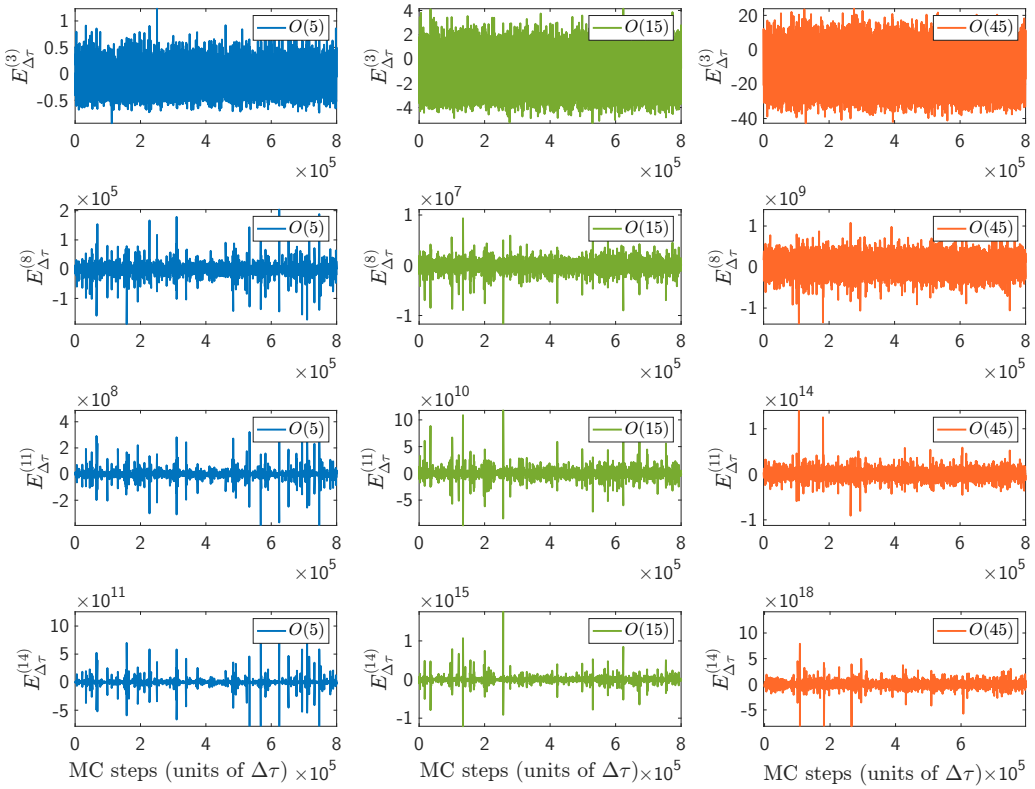

Figure 14: Signals from NSPT simulations. We display the evolution for the $O(5)$, $O(15)$ and $O(45)$ models with blue, green and orange solid lines. The different rows refer to different perturbative corrections, namely $n = 3$, 8, 11, 14, at $\Delta\tau = 0.0035$. We considered for all models 8×10^5 steps, after having previously subtracted 4000 thermalization steps (this number has been decided based on the behaviour of the evolution at the highest order available).

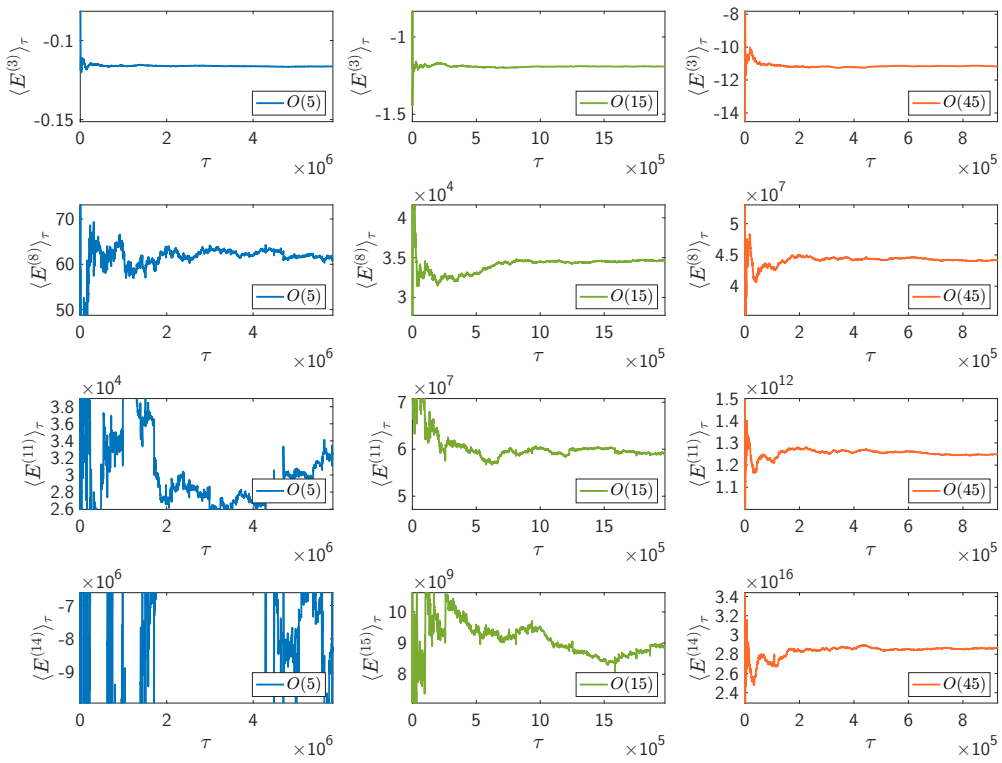

Figure 15: Cumulative moving averages of NSPT evolutions. We display cumulative means for the $O(5)$, $O(15)$ and $O(45)$ models with blue, green and orange solid lines. The different rows refer to different perturbative orders, namely $n = 3$, 8, 11, 14 (same convention of Fig. 14) and $\Delta\tau = 0.01$. The y-axis is centered around the mean values, with a fixed relative window for each perturbative order. Furthermore, comparisons are made by considering approximately the same amount of statistics.

In the same way we can define the cumulative standard deviation as

$$\sigma(E^{(n)})_\tau = \sqrt{\langle E^{(n)2}\rangle_\tau - \langle E^{(n)}\rangle_\tau^2}\,. \tag{302}$$

It is expected that in a good Monte Carlo simulation, the evolution of the quantities in Eqs. (301)-(302) will converge towards an asymptotic constant value, effectively exploring a well-defined distribution. Notice that to achieve a fair comparison of the cumulative evolutions at different values of N, given that loop corrections vary significantly by orders of magnitude (see the analytical results in Eq. (296) and also the plot in Fig. 10), we need to focus exclusively on relative fluctuations with respect to the estimates of the mean and the standard deviation. Furthermore, a reasonable comparison should consider the fact that different $O(N)$ models require different

computational costs. With this in mind, we will show in the following cumulative evolutions at the same computational time rather than at the same statistics.

In Fig. 15, we show the cumulative means for the $O(5)$, $O(15)$ and $O(45)$ models at perturbative orders $n = 3$, 8, 11, 14 and $\Delta\tau = 0.01$. The color code is the same as in Fig. 14. The overall scenario is consistent with what we have broadly seen before: at low perturbative order $n = 3$ (see the plots on the first row of Fig. 15), the cumulative means tend to flatten across all values of N, consistently with expectations. On the contrary, as the loop order rises from $n = 3$ to $n = 8$ (second row plots in Fig. 15), the cumulative mean for $O(5)$ is prone to considerable fluctuations, despite a substantial amount of statistics. In the plots of the third row of the same figure, we display results concerning the perturbative order $n = 11$: here, fluctuations also affect the $O(15)$ model, while the cumulative average for the $O(5)$ model flattens even less than at $n = 8$. On the other hand, the $O(45)$ model can still be considered unaffected by any pathologies at the order $n = 11$ up to perturbative order $n = 14$ (see and compare plots in the last column of Fig. 15); in this cases, we obtain a well-behaved determination of the mean. This last observation turns out to be independent of the time step $\Delta\tau$ considered, and the respective extrapolation to the continuum process turns out to be under control.

In the case of smaller N values, the analysis of the cumulative standard deviation presents even more challenging issues. We display in Fig. 16 the cumulative standard deviation (with the same conventions as in Fig. 15). As a matter of fact, due to the definition itself (Eq. (302)), any fluctuations result in an increased estimation. Specifically, for cases where $[N = 5, n \geq 8]$ and $[N = 15, n \geq 11]$, we cannot be sure that our estimations of the variance are reliable (see plots on the third and fourth rows of Fig. 16). Nonetheless, for sufficiently large N values, evidence of finite and well-determined standard deviation can be noticed. Notably, for the $O(45)$ model, no pathological effects were detected up to $n = 14$ (see the plot in the last column of Fig. 16). The reliability of NSPT evolutions at $N = 45$ is additionally validated by the observation that statistical errors scale properly as $\sim 1/\sqrt{N_{\text{samples}}}$. This last empirical finding will be further discussed in Sec. 3.4.3.

All in all, we ended up with the conclusion that our best estimations of means and standard deviations can be unreliable: we will later look for criteria to finally discard some and retain only those that we can trust. This will finally make us decide at which perturbative order n we can push our computations at a given value of N.

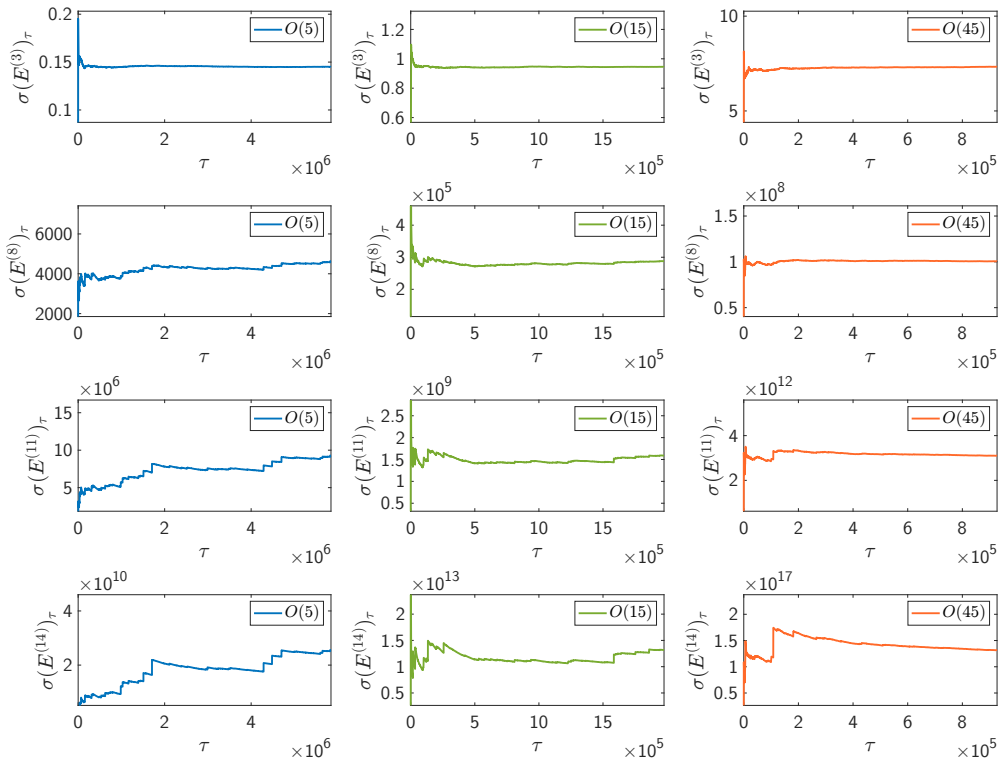

Figure 16: Cumulative moving standard deviation for NSPT evolutions. We display cumulative standard deviations for the $O(5)$, $O(15)$ and $O(45)$ models with blue, green and orange lines. The different rows refer to different perturbative orders, namely $n = 3$, 8, 11, 14 (same convention as in Figs. 14 and 15) and $\Delta\tau = 0.01$. The y-axis is centered around the mean values, with a fixed relative window for each perturbative order. Furthermore, comparisons are made by considering approximately the same amount of statistics.

3.4.2 Large N and Large L

A crucial aspect of Monte Carlo simulations on the lattice is the self-averaging property: in a given theory, increasing the lattice size should yield more stable statistical averages. In principle, employing progressively larger lattices for the computation of local quantities (this is the case of the energy in NLSMs, see Eq. (287)) will lead to a reduced standard deviation. Conversely, we have observed that, at a specific NSPT perturbative order, fluctuations are tamed at large N (where we are considering an increasing number of local degrees of freedom). At first glance, one might wonder about the relation between these two effects: it turns out, perhaps unsurprisingly, that these effects are fundamentally different. In this context, it might seem reasonable to

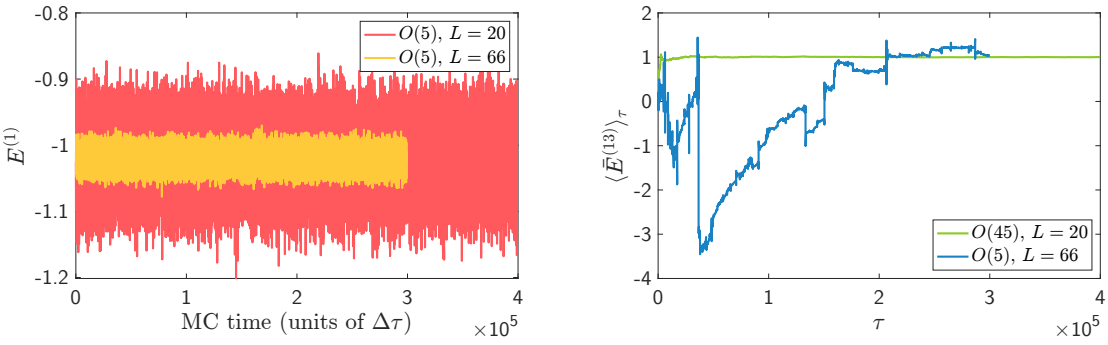

Figure 17: Large L limit for the $O(5)$ non-linear sigma model. Left plot: first-order correction for the energy. We show results for lattice sizes 20×20 and 66×66 with solid red and yellow lines, respectively. Lattice self-averaging effects are evident. Right plot: comparison between the $O(5)$ model on a 66×66 lattice (solid blue line) and the $O(45)$ model on a 20×20 lattice (solid green line). The large N limit behaves much better than the large L limit.

compare simulations with the same *total* number of degrees of freedom (specifically, comparing the large N - small L scenario with the small N - large L scenario). Roughly speaking, we may wonder about the *true* size of the system from the NSPT point of view.

In Fig. 17, left panel, we display the effect of large L simulations for $N = 5$ and $n = 1$. We show NSPT evolutions for two lattices, namely $L^2 = 20 \times 20$ and $L^2 = 66 \times 66$. In this case, simulations on larger lattices result in a reduced standard deviation of the signals, as anticipated. On the contrary, in the right panel of Fig. 17, we consider high-order corrections, namely $n = 13$. Here we compare cumulative means of the $O(5)$ model on a 66×66 lattice with the $O(45)$ model on a 20×20 lattice. Notice that the two simulations involve roughly the same amount of total degrees of freedom. In order to compare the evolution of the cumulative mean, we need to consider that different $O(N)$ models display various orders of magnitude of perturbative corrections. We normalize the evolution of the cumulative mean using the best estimate of the mean, namely we study the quantity

$$\langle \bar{E}^{(n)} \rangle_\tau = \langle E^{(n)} \rangle_\tau / \langle E^{(n)} \rangle_{\tau = T_{\text{end}}} , \tag{303}$$

where $\langle E^{(n)} \rangle_{\tau = T_{\text{end}}}$ indicates the mean over the complete dataset. In other words, the evolution of the cumulative mean has been normalized to have 1 as its final value of the series. It is noteworthy that the cumulative mean yields the wrong sign for almost half of the evolution for the $O(5)$ model. In contrast, the evolution for $N = 45$ displays a not-so-long thermalisation phase toward a stable value. In short, taming large deviations appears to be a genuine large N

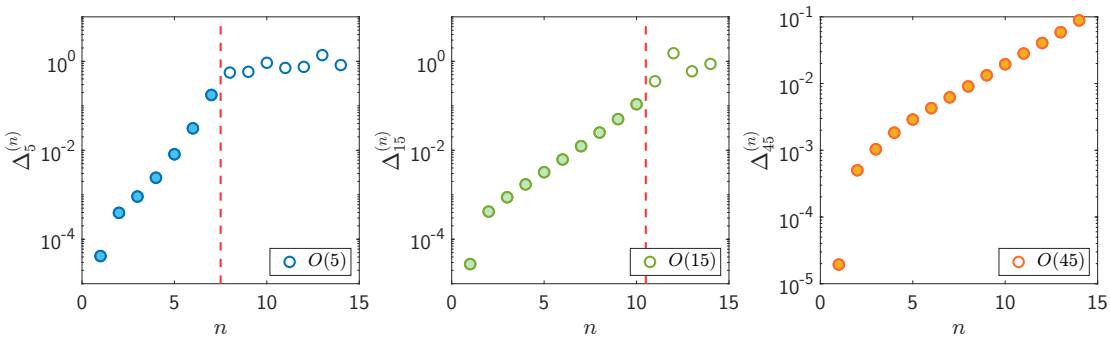

Figure 18: Scaling of relative errors at increasing loop order. The points reported in Fig. 10 are shown here with full circles, while the points in the region of scaling violation are indicated with empty circles. Notice that the two different regions are separated by a dashed red line. The color code is the same as in Fig. 10.

effect.

3.4.3 Relative error scaling

In Sec. 3.4.1 and 3.4.2 we provided evidence that fluctuations are naturally tamed by the stochastic process in the large N limit. This raises an important question: up to what perturbative order do NSPT computations maintain stability for a given $O(N)$ model? Alternatively, for a specific target loop order, how large must N be to compute corrections reliably up to that order? Although a comprehensive and rigorous explanation for the origins of fluctuations is not yet established, a *sanity check* would be advantageous. We present numerical evidence suggesting that the emergence of fluctuations can be identified by the breakdown of two simple yet reliable hypotheses concerning the scaling of relative errors.

In Monte Carlo simulations, analyzing the scaling of relative errors plays a key role in determining the robustness of the computations; unsurprisingly, NSPT also benefits from this kind of statistical analysis. Using relative error analysis, we illustrate how to determine *a posteriori* N regions where large fluctuations have not yet affected the precision of high-order NSPT computations, and areas where fluctuations are predominant. Our primary goal is to empirically establish a first meaning of large N in NSPT computations at any specified perturbative order n.

n-scaling

For a given $O(N)$ model let us call the relative errors of the energy as

$$\Delta_N^{(n)} = \left.\frac{\delta E^{(n)}}{E^{(n)}}\right|_N , \tag{304}$$

which are explicitly dependent on the order n; $E^{(n)}|_N$ and $\delta E^{(n)}|_N$ stand, respectively, for the values of the energy and its error for a given value of N. Notice that these values are the results of the extrapolation procedure in the continuum stochastic process limit and for this reason relative errors are supposed to contain all the information about autocorrelations and cross-correlations. It is worth noticing that we compute relative errors from our *best* estimation of $E^{(n)}$ and $\delta E^{(n)}$. Given that at high-orders large uncertainties in the estimation of the mean and the standard deviation show up, we will find that some of these estimations may prove to be unreliable.

A quite natural hypothesis is that relative errors are expected to exhibit monotonic growth with respect to n; this assertion is suggested (also) by the observation of increasing values for the standard deviations as n increases. Furthermore, we also expect to observe increasing cross-correlations for increasing values of n, since at a given perturbative order the values of the fields depend on all the fields of lower orders.

In Fig. 18 we display the scaling of relative errors for the $O(5)$, $O(15)$, and $O(45)$ models (color code as in Fig. 10). Our hypothesis is confirmed in the case of the $O(45)$ model up to loop order $n = 14$. Moreover, for the $O(5)$ and $O(15)$ models the relative errors exhibit a smooth exponential trend up to $n = 7$ and $n = 10$, respectively (a behaviour which is similar to the $O(45)$ case). However, for loop corrections greater than $n = 7$ for the $O(5)$ model and $n = 10$ for the $O(15)$ model, the scaling behaviour violates our hypothesis. In the second and third plots of Fig. 18 the value of n at which this occurs (*i.e.* the breakdown of our hypothesis) for the $O(5)$ and $O(15)$ models, respectively, is indicated with a dashed red line. It is worth noting that as the parameter N increases, the region of breakdown shifts towards higher perturbative orders. Fig. 18 motivates our plot in Fig. 10: in any $O(N)$ model the maximum order of the loop corrections that can produce reliable results is strictly determined by the value of N.

N-scaling

In this paragraph we investigate how relative errors scale for different values of N. We now define the relative error as a function of the parameter N through

$$\bar{\Delta}_N^{(n)} = \left.\frac{\delta E^{(n)}}{E^{(n)}}\right|_N \cdot \Gamma(N) . \tag{305}$$

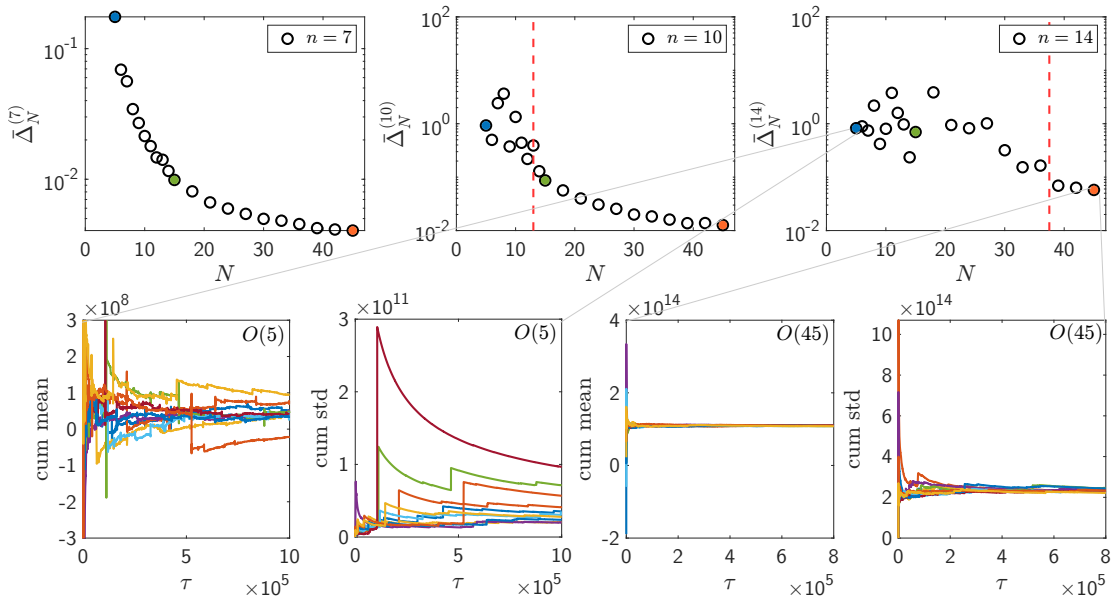

Figure 19: First row: scaling of relative errors per unit of statistics for increasing values of N. The empty black circles indicate the value of $\bar{\Delta}_N^{(n)}$ for $N = [5 : 45]$ at different loop orders $n =$ 7, 10, 14 (see labels). The solid colored circles represent the respective values for the $O(5)$, $O(15)$, and $O(45)$ models, also shown in Fig. 10 (color code as before). Second row: we display zoomed figures related to the determination of mean and cumulative standard deviation for the $O(5)$ and $O(45)$ models at loop order $n = 14$ for 10 different runs. In the large N limit, precise estimates are undoubtedly obtained. For the $O(5)$ model different runs yield completely different determinations for both quantities.

In the above definition, relative errors include an additional factor $\Gamma(N)$. This acts as a correction factor: we took into account all the data that are available for each value of N and then computed a factor $\Gamma(N)$ such that comparisons are made for the same number of independent measurements. In other words, we have one single effect left: different relative errors can only be due to different values of N.

Actually a quite natural hypothesis can be formulated regarding the scaling of relative errors defined in Eq. (305): as N increases, it is expected, on very general grounds, that $\bar{\Delta}_N^{(n)}$ should exhibit a monotonically decreasing trend. In fact, through the use of the factor $\Gamma(N)$, we are considering systems with an increasing number of degrees of freedom as N gets larger, while maintaining the same amount of statistics. In Fig. 19 we display the properties of the scaling for all the $O(N)$ models employed in our analysis (see Tab. 1) at perturbative orders $n = 7, 10, 14$.

At small perturbative order, namely $n \leq 7$, the expected scaling is perfectly observed. This is no longer true at perturbative orders $n = 10$ and $n = 14$ (see first row, central and right plots): in these cases, we identified regions that deviate from this hypothesis (see the regions on the left of the red dashed lines). All in all, we need to look at largest values of N to inspect the expected behavior at high order n. Notice that in Fig. 19 we depict with filled circles the estimates of the relative error, defined in Eq. (305), for the $O(5)$, $O(15)$ and $O(45)$ models (color code as in Fig. 10): the emerging scenario is perfectly consistent with those presented in Sec. 3.4.1 and Fig. 18. As a matter of fact, the threshold loop orders are in agreement with each other, as summarized in Fig. 10.

The four plots in the second row of Fig. 19 show the time evolution of the cumulative mean value of energy and the respective cumulative standard deviation concerning the models $O(5)$ and $O(45)$, computed at fixed perturbative order, namely $n = 14$. In all plots we show data produced in 10 independent runs; it is quite clear that while in the case of the $O(45)$ model the cumulative mean and standard deviation estimates from the different runs are consistent with each other, the different runs in the case of the $O(5)$ model however lead without any doubt to opposite conclusions: different runs yield much different values for the cumulative energy mean and standard deviation.

We have thus motivated what is depicted in Fig. 10: for lower values of N we could not compute to very large perturbative orders n, since large fluctuations affect high-orders. On the other side, we provided quite clear numerical evidence that large fluctuations are tamed in the large N limit.

4 | $O(N)$ NLSM renormalons in the Large N limit

An intriguing property of asymptotically free theories is the emergence of renormalons (we refer the reader to [17] for a complete introduction to the topic). Renormalons are related to a certain pattern of divergence in perturbative expansions and are crucial in understanding non-perturbative aspects of quantum field theories.

Renormalons have been probed in Lattice QCD using NSPT, by simulating the theory at incredibly high perturbative orders. By assessing the asymptotic factorial growth of loop corrections, renormalons have been observed in SU(3) gluodynamics [18–20] and in QCD with fermions [21]. Additionally, in recent years, NSPT has been used to study renormalons in the Principal Chiral Model [22].

In Sec. 3 we have shown that reliable NSPT predictions can be obtained in large N limit at high orders. In this section we want to explore the asymptotic perturbative regime of $O(N)$ sigma models. By studying a *large enough* N, namely the $O(80)$ sigma model, we will provide insights on renormalons in these low-dimensional models. Finite size effects will turn out to be extremely important, so we will try to carefully describe them.

4.1 Infrared renormalons

We revisit the standard infrared renormalon analysis as discussed in [80]. On very general grounds, the perturbative contribution to the expectation of a composite operator reads

$$W = \int_0^{Q^2} \frac{dk^2}{k^2} \left(\frac{k}{Q}\right)^{2\sigma} f(k)\,, \tag{306}$$

where 2σ is the dimension of the operator and Q is a UV cutoff. In lattice simulations, $Q \sim 1/a$. Furthermore $f(k)$ is a dimensionless and renormalization group invariant function. From now

on we consider the case where $f(k) = g(k)$, where $g(k)$ is the running coupling constant (this choice can be shown not to be restrictive). In the following, we will obtain a power series from the integral in Eq. (306).

We consider the one-loop definition of the β-function, namely [10]

$$\beta(g) = k\frac{dg}{dk} = \frac{dg}{d\ln k} = -\beta_0 g^2 \,. \tag{307}$$

By integrating the above equation, we get

$$\frac{1}{g(k)} = \frac{1}{g(k_0)} + \beta_0 \ln\frac{k}{k_0} = \frac{1}{g(k_0)}\left(1 + g(k_0)\beta_0 \ln\frac{k}{k_0}\right), \tag{308}$$

At first-order we can write

$$g(k) = \frac{g(k_0)}{1 + g(k_0)\beta_0 \ln\frac{k}{k_0}} \approx g(k_0)\left(1 - g(k_0)\beta_0 \ln\frac{k}{k_0} + \dots\right), \tag{309}$$

The ratio of scale which we need in the integral of Eq. (306) reads

$$\left(\frac{k}{Q}\right)^{2\sigma} = e^{-\frac{1}{g(Q)}\frac{2\sigma}{\beta_0}\left(1-\frac{g(Q)}{g(k)}\right)} \,. \tag{310}$$

We now change the integration variable according to [80]

$$z = \frac{2\sigma}{\beta_0}\left(1 - \frac{g(Q)}{g(k)}\right) = z_0\left(1 - \frac{g(Q)}{g(k)}\right), \qquad z_0 = \frac{2\sigma}{\beta_0} \,. \tag{311}$$

and obtain

$$\begin{aligned} \left(\frac{k}{Q}\right)^{2\sigma} &= e^{-\frac{z}{g(Q)}} \\ \frac{dk^2}{k^2} g(k) &= -\frac{2}{z_0\beta_0}\frac{dz}{1-\frac{z}{z_0}} \end{aligned} \tag{312}$$

The integral in Eq. (306) now has the structure of a Borel integral

$$W = \int_0^{Q^2} \frac{dk^2}{k^2}\left(\frac{k}{Q}\right)^{2\sigma} g(k) = \frac{2}{z_0\beta_0}\int_0^\infty dz \frac{e^{-\frac{z}{g}}}{1-\frac{z}{z_0}} \tag{313}$$

where g is the coupling defined at the hard scale $g = g(Q)$. In the lattice case, $Q = a^{-1}$ and g is the bare lattice coupling. The integral in Eq. (313) is divergent due to the presence of the pole and one needs a prescription to compute it. Typically this asks for a detour in the complex plane and as a result one picks up an imaginary part proportional to $e^{-\frac{z_0}{g}}$. This is the

[10] It is also feasible to consider the two-loop definition. In this scenario, we would obtain $1/n$ corrections in the scaling of the renormalon, where n is the perturbative order (see Eq. (316) for more details).

same ambiguity that will plague the resummation of the asymptotic series which we are now going to obtain from the Borel integral. The series will display a factorial divergence: this is the signature of the renormalon. Basically, we ignore the pole and expand the geometric series in Eq. (313), namely

$$\begin{aligned} W &= \frac{2}{\beta_0 z_0}\int_0^{+\infty} dz e^{-\frac{z}{g}} \sum_{n=0}^{\infty}\left(\frac{z}{z_0}\right)^n \\ &= \frac{2}{\beta_0}\sum_{n=0}^{\infty}\frac{g^{n+1}}{z_0^{n+1}}\int_0^{\infty} dt e^{-t} t^n \\ &= \frac{2}{\beta_0}\sum_{n=0}^{\infty} g^{n+1}\frac{\Gamma(n+1)}{z_0^{n+1}} \\ &= \sum_{n=0}^{\infty} g^{n+1} E^{(n+1)}\,. \end{aligned} \tag{314}$$

Of course one is not claiming we computed the exact perturbative expansion: this is supposed to be the dominant contribution in an asymptotic regime. In view of Eq. (314), the ratio of two consecutive perturbative coefficients, divided by the perturbative order, should approach a constant value, *i.e.*

$$\frac{E^{(n+1)}}{E^{(n)}\cdot n} \sim \frac{\beta_0}{2\sigma}\,, \qquad \text{for} \qquad n >> 1\,. \tag{315}$$

We notice that our calculation doesn't provide any insight about the perturbative order at which the asymptotic scaling sets in: NSPT high-order computations can detect whether and when (asymptotically) the renormalon behavior shows up.

We can also consider two-loop corrections to the Eq. (315). Starting from the two-loop definition of the β-function

$$k\frac{d}{dk}g(k) = -\beta_0 g^2 - \beta_1 g^3 + O(g^4)\,, \tag{316}$$

we get (see App. E for the sketch of the computation)

$$\frac{E^{(n+1)}}{E^{(n)}\cdot n} \sim \frac{\beta_0}{2\sigma}\left(1 + \frac{1}{n}\frac{2\sigma\beta_1}{\beta_0^2}\right), \qquad \text{as} \qquad n \gg 1\,. \tag{317}$$

4.2 Finite volume corrections to renormalons

Eq. (315) and Eq. (317) display the expected scaling in an asymptotic regime. In our computation we integrated over all momenta up to a UV hard cutoff, as in Eq. (306). This scenario is not what typically occurs in a lattice computation, where finite volume effects are inevitably encountered: the finite volume sets an explicit IR cutoff. Notice that different perturbative

orders are differently affected by this cutoff (finite size effects): the coefficients for increasing perturbative order become more and more sensitive to the IR region. Because of this, the effects of finite volume are expected to become increasingly significant.

In the literature, in the detection of renormalons from NSPT computations finite volume effects have been treated differently. When feasible, extrapolations to infinite volume have been considered [20, 22]. It could also be that finite volume effects turn out to be smaller than the statistical errors: various attempts at renormalon detection on different lattice sizes were found to be compatible without any extrapolation in [21]. In the case at hand, we deal with low-dimensional models and we expect finite size effects to be significant. To address this issue, we choose not to attempt any extrapolation of data to $V \to \infty$, but we directly looked at how the factorial growth resulting in Eq. (315) (or Eq. (317)) is corrected by an IR cutoff. In a sense, our calculation is a first-principles one and in particular it will contain no free parameters to fine-tune: we will directly compare our data to a given expression.

For simplicity, we discuss IR corrections sticking to one-loop (the two-loop calculation is presented in App. E). We consider a lattice of finite volume $V = (a \cdot N)^d$ where a is the lattice spacing, N is the number of lattice sites in each direction (we consider for simplicity only cubic lattices) and d is the number of dimensions (in our case $d = 2$). We used Periodic Boundary Conditions. In this lattice setting, one gets the following maximum and minimum momenta (keep in mind that magnitude of momentum enters our integral in Eq. (306))

$$Q = \frac{2\pi}{a}\sqrt{d}\,, \qquad Q_{\rm ir} = \frac{2\pi}{aN}\,. \tag{318}$$

Q is, as before, the UV cutoff, while now an IR cutoff is there as well, which we now plug into the integral in Eq. (306)

$$W = \int_{Q_{\rm ir}^2}^{Q^2} \frac{dk^2}{k^2} \left(\frac{k}{Q}\right)^{2\sigma} g(k)\,. \tag{319}$$

After the change of variable in Eq. (311), we get

$$W = \frac{2}{z_0\beta_0}\int_0^{z_{ir}} dz \frac{e^{-\frac{z}{g}}}{1-\frac{z}{z_0}} = \frac{2}{\beta_0 z_0}\int_0^{z_{ir}} dz\; e^{-\frac{z}{g}} \sum_{n=0}^{\infty}\left(\frac{z}{z_0}\right)^n, \tag{320}$$

where the lower limit stays the same as before (this is coming from the upper limit Q of the original integral), while the upper limit is now (remember $g = g(Q)$)

$$z_{ir} = -z_0 g\beta_0 \ln\frac{Q_{\rm ir}}{Q} = z_0 g\beta_0 \ln N\sqrt{d}\,. \tag{321}$$

Considering Eq. (320), the asymptotic scaling reads

$$\begin{aligned} W &= \frac{2}{\beta_0}\sum_{n=0}^{\infty} g^{n+1}\frac{1}{z_0^{n+1}}\int_0^{z_0\beta_0\ln\sqrt{d}N} dt e^{-t}t^{(n+1)-1} \\ &= \frac{2}{\beta_0}\sum_{n=0}^{\infty} g^{n+1}\frac{1}{z_0^{n+1}}\Gamma_{\rm ir}(n+1)\,, \end{aligned} \tag{322}$$

where $\Gamma_{\rm ir}(n+1)$ is the lower incomplete gamma function. Integrating by parts the incomplete gamma function

$$\Gamma_{\rm ir}(n+1) = \int_0^A dt e^{-t}t^{(n+1)-1} = \left[-e^{-t}t^{(n+1)-1}\right]_0^A + n\int_0^A dt e^{-t}t^{n-1}\,, \tag{323}$$

we recover the well-known property

$$\Gamma_{\rm ir}(n+1) = n\Gamma_{\rm ir}(n) - e^{-A}A^n\,. \tag{324}$$

In the above equation, we use the notation

$$A = z_0\beta_0\ln\sqrt{d}N \tag{325}$$

for brevity. Using Eq. (324) we can rewrite the incomplete gamma function as

$$\Gamma_{\rm ir}(n+1) = n!\left(1 - e^{-A}\sum_{n=0}^{n}\frac{A^k}{k!}\right), \tag{326}$$

so that the ratio in Eq. (315) can be expressed as

$$\frac{E^{(n+1)}}{E^{(n)}\cdot n} \sim \frac{\beta_0}{2\sigma}\frac{\Gamma_{\rm ir}(n+1)}{n\Gamma_{\rm ir}(n)} = \frac{\beta_0}{2\sigma}\frac{1-e^{-A}\sum_{k=0}^{n}\frac{A^k}{k!}}{1-e^{-A}\sum_{k=0}^{n-1}\frac{A^k}{k!}}\,, \qquad \text{as} \qquad n \gg 1\,. \tag{327}$$

Notice that, from Eq. (327), in the limit of infinite volume $N \to \infty$, $A \to \infty$ so that volume corrections are exponentially suppressed restoring the pure factorial growth. However, at finite volume, the series in Eq. (326) approach the exponential e^A for increasing loop order n, so in the asymptotic limit $n \gg 1$ the finite volume effects completely kill the signals. It is worth noting that finite volume corrections to the factorial growth depend on the dimension of the composite operator σ and the dimension of the lattice d by means of Eq. (325).

If we consider finite volume correction with two-loop contribution, the following equation holds(see App. E for more details)

$$\frac{E^{(n+1)}}{E^{(n)}\cdot n} \to \frac{1}{z_0}\left(1+\frac{\gamma}{n}\right)\frac{\left[\left(1-e^{-A}\sum_{k=0}^{n}\frac{A^k}{k!}\right) - \frac{\beta_1 z_0}{\beta_0(\gamma+1)}\left(1-e^{-A}\sum_{k=0}^{n-1}\frac{A^k}{k!}\right)\right]}{\left[\left(1-e^{-A}\sum_{k=0}^{n-1}\frac{A^k}{k!}\right) - \frac{\beta_1 z_0}{\beta_0(\gamma+1)}\left(1-e^{-A}\sum_{k=0}^{n-2}\frac{A^k}{k!}\right)\right]}\,, \tag{328}$$

where

$$\gamma = \frac{2\sigma\beta_1}{\beta_0^2}\,. \tag{329}$$

4.3 Probing renormalons for $O(N)$ at large N

Being the theory asymptotically free, $O(N)$ should admit perturbative expansions displaying renormalons. If we want to detect them we need to probe perturbative orders $n >> 1$. Since we want to prevent the onset of fluctuations, we know that it is a good idea to compute at large N. We selected $O(80)$ on a 20×20 lattice. In this discussion we analyze the asymptotic scaling of the observable

$$W = E - 1 = \sum_{n \geq 0} g^{n+1} E^{(n+1)} \tag{330}$$

where the energy E is defined by Eq. (287). Since the energy density has mass dimension $d = 2$, we will have $\sigma = 1$.

Eqs. (315)-(317)-(327)-(328) require to know the value of the perturbative β-function. The first two coefficients are universal and are given by [81]

$$\beta_0 = \frac{N-2}{2\pi} \qquad \beta_1 = \frac{N-2}{4\pi^2} \tag{331}$$

Notice that, differently from the Principal Chiral Models [22], here the renormalon asymptotic depends on the value of N. In other words, different $O(N)$ models have different values of the ratio $E^{(n+1)}/(E^{(n)}n)$.

In Fig. 20 we plot the ratio $\frac{E^{(n+1)}}{E^{(n)}n}$ for the coefficients in Eq. (330), as evaluated by our NSPT computations. The renormalon ratios in Eqs. (315)-(317)-(327)-(328) are depicted as solid and dashed lines. As expected, the finite volume effects are not at all negligible. The infrared corrected ratio in Eq. (327) (or Eq. (328); the two are hard to distinguish) fits data very well for $n \gtrsim 10$.

It is pretty clear that finite size corrections are crucial to describe data; there is no sign of flattening on the infinite volume value for the ratio; there is indeed quite some distance to cover. We stress that we are trying to make contact with a first-principles calculation modeling finite size effects on top of the renormalon behavior: the model has no fine-tuning of any additional free parameter. Given this, the agreement within errors of our data with the theoretical prediction is very good. Can this be a pure numerical accident? First of all, we would like to have data with less errors. Moreover (and more important) we are pursuing the computation on a 32×32 lattice, to check that the ratio of subsequent coefficients indeed moves to fit the different curve that the model predicts for this larger volume.

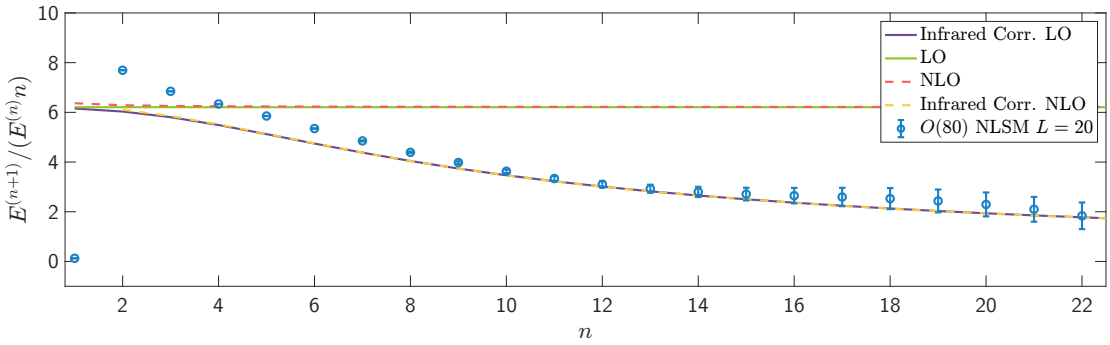

Figure 20: Renormalon asymptotics for the $O(80)$ non-linear sigma model. The ratios obtained from our NSPT computations are depicted as blue markers. The values of the ratio as predicted by renormalon analysis in infinite volume at the leading order (Eq. (315)) and next to leading order (Eq. (317)) are plotted as a solid green line and a dashed red line. Additionally, the ratios computed from renormalon analysis including finite volume corrections for a 20×20 lattice volume are plotted as a solid purple line (leading order, Eq. (327)) and a dashed yellow line (next to leading order, Eq. (328)).

5 | Conclusions

In this thesis we analyzed a couple of different applications of NSPT. In Sec. 2 we pursued NSPT perturbative computations around instanton-like vacua, probing the energy splitting for the double-well potential in 1D Quantum Mechanics. The underlying idea is that NSPT can, in principle, circumvent the complications of diagrammatic perturbation theory around non-trivial vacua. The first non-trivial coefficients were computed in the continuum limit, with a decent accuracy. This *per se* encouraging result has however highlighted that going to higher loops is extremely hard. Not only our computational strategy ended up in subtle cancellations. More importantly, the emergence of severe fluctuations hinders the path to high-order perturbative calculations. This was not really unexpected, given an already available warning, *i.e.* when applied to *small* systems, NSPT produces huge fluctuations (not normally distributed) at orders that the method can successfully manage to compute for *larger* ones. The challenge of confronting large fluctuations for low-dimensional systems thus became the main subject of this work.

In Sec. 3 we discussed high-order NSPT computations in the $O(N)$ Non Linear Sigma Models. This model has proven to be an ideal testing ground for studying the emergence and taming of fluctuations while varying the number of degrees of freedom. In particular, we have shown that in the large N limit, NSPT simulations are not affected by fluctuations at high perturbative orders. Our conclusions are supported by extensive numerical simulations and analyses. For the $O(N)$ NLSM, the larger the value of N, the more perturbative orders we can calculate with NSPT. Indeed the perturbative energy calculation has been extended from the previously known fourth loop-order first up to the fourteenth perturbative order and then to even higher orders.

In Sec. 4 we explored large N NSPT computations in $O(N)$ NLSM to hunt for renormalons. Low-dimensional models are more affected by finite size effects, so the renormalon asymptotic

behavior had to be corrected to incorporate finite volume effects from first-principles. Once finite volume effects are properly modeled, our results show full agreement between high-order NSPT computations and the predicted renormalon behavior. As a byproduct, this study provided an opportunity to discuss the subtleties connected to the removal of the systematic effects connected to the finite stochastic time step used in the numerical integration of the (order-by-order) Langevin equation. To gain confidence with high-order results, we tried an unconventional approach to $\Delta\tau \to 0$ extrapolations, in which we made use of both Euler and Runge Kutta schemes.

Remarkably, the $CP(N-1)$ model represents an ideal extension for this work. For these theories, in a safe large N limit, we plan to go back to expansions around non-trivial saddle points. Quite interestingly, these models were among the very first related to resurgence scenarios [82] which we could in principle try to probe.

References

[1] F. Di Renzo et al. Four-loop result in SU(3) lattice gauge theory by a stochastic method: lattice correction to the condensate. In: *Nuclear Physics B* 426.3 (Sept. 1994), pp. 675–685.

[2] F. Di Renzo et al. Lattice Perturbation Theory by Langevin Dynamics. In: *arXiv e-prints*, hep-lat/9308006 (Aug. 1993). arXiv: hep-lat/9308006 [hep-lat].

[3] F. Di Renzo et al. Lattice perturbation theory on the computer. In: *Nuclear Physics B - Proceedings Supplements* 34 (Apr. 1994), pp. 795–798.

[4] F. Di Renzo et al. High-loop perturbative renormalization constants for lattice QCD (I): finite constants for Wilson quark currents. In: *The European Physical Journal C* 51.3 (June 2007), pp. 645–657.

[5] F. Di Renzo et al. Four-loop lattice-regularized vacuum energy density of the three-dimensional SU(3) + adjoint Higgs theory. In: *Journal of High Energy Physics* 2008.09 (Sept. 2008), pp. 061–061.

[6] F. Di Renzo et al. Two-point functions of quenched Lattice QCD in Numerical Stochastic Perturbation Theory. (I) The ghost propagator in Landau gauge. In: *Nuclear Physics B* 831.1–2 (May 2010), pp. 262–284.

[7] F. Di Renzo et al. Two-point functions of quenched lattice QCD in Numerical Stochastic Perturbation Theory. (II) The gluon propagator in Landau gauge. In: *Nuclear Physics B* 842.1 (Jan. 2011), pp. 122–139.

[8] M. Dalla Brida and M. Lüscher. SMD-based numerical stochastic perturbation theory. In: *The European Physical Journal C* 77.5 (May 2017).

[9] F. Di Renzo and L. Scorzato. Numerical Stochastic Perturbation Theory for full QCD. In: *Journal of High Energy Physics* 2004.10 (Oct. 2004), pp. 073–073.

[10] R. Kitano, H. Takaura, and S. Hashimoto. Stochastic computation of g − 2 in QED. In: *Journal of High Energy Physics* 2021.5 (May 2021).

[11] A. González-Arroyo et al. Numerical stochastic perturbation theory applied to the twisted Eguchi-Kawai model. In: *Journal of High Energy Physics* 2019.6 (June 2019).

[12] A. González-Arroyo et al. Perturbative study of large N principal chiral model with twisted reduction. In: *International Journal of Modern Physics A* 37.36 (Dec. 2022).

[13] M. Dalla Brida, M. Garofalo, and A. D. Kennedy. Investigation of new methods for numerical stochastic perturbation theory in φ^4 theory. In: *Physical Review D* 96.5 (Sept. 2017).

[14] G. Catumba, A. Ramos, and B. Zaldivar. Stochastic automatic differentiation for Monte Carlo processes. In: *arXiv e-prints* (July 2023). arXiv: 2307.15406 [hep-lat].

[15] R. Alfieri et al. Understanding stochastic perturbation theory: toy models and statistical analysis. In: *Nuclear Physics B* 578.1-2 (July 2000), pp. 383–401.

[16] D. Hesse et al. The Schrödinger Functional in Numerical Stochastic Perturbation Theory. In: *Proceedings of 31st International Symposium on Lattice Field Theory — PoS (LATT2013)*. LATTICE 2013. Sissa Medialab, Apr. 2014.

[17] M. Beneke. Renormalons. In: *Physics Reports* 317.1–2 (Aug. 1999), pp. 1–142.

[18] C. Bauer, G. S. Bali, and A. Pineda. Compelling Evidence of Renormalons in QCD from High Order Perturbative Expansions. In: *Physical Review Letters* 108.24 (June 2012).

[19] G. S. Bali et al. Perturbative expansion of the energy of static sources at large orders in four-dimensional SU(3) gauge theory. In: *Physical Review D* 87.9 (May 2013).

[20] G. S. Bali, C. Bauer, and A. Pineda. Perturbative expansion of the plaquette to $\mathcal{O}(\alpha^{35})$ in four-dimensional SU(3) gauge theory. In: *Physical Review D* 89.5 (Mar. 2014).

[21] L. Del Debbio, F. Di Renzo, and G. Filaci. Large-order NSPT for lattice gauge theories with fermions: the plaquette in massless QCD. In: *The European Physical Journal C* 78.11 (Nov. 2018).

[22] F. Bruckmann and M. Puhr. Universal renormalons in principal chiral models. In: *Physical Review D* 101.3 (Feb. 2020).

[23] W. J. Zakrzewski. Low-dimensional Sigma Models. CRC Press, 1989.

[24] P. Baglioni and F. Di Renzo. Numerical Stochastic Perturbation Theory around instantons. In: *Proceedings of The 39th International Symposium on Lattice Field Theory — PoS(LAT2022)*. LATTICE2022. Sissa Medialab, Jan. 2023.

[25] P. Baglioni and F. Di Renzo. NSPT for $O(N)$ non-linear sigma model: the larger N the better. In: *arXiv e-prints* (Jan. 2024). arXiv: 2401.11833 [hep-lat].

[26] P. Baglioni and F. Di Renzo. Large fluctuations in NSPT computations: a lesson from $O(N)$ non-linear sigma models. In: *arXiv e-prints* (Feb. 2024). arXiv: 2402.01322 [hep-lat].

[27] P. Baglioni and F. Di Renzo. *Large order computations in $O(N)$ non-linear sigma models: renormalons, finite size effects and all that - In preparation*. 2024.

[28] P. Baglioni et al. Predictive power of a Bayesian effective action for fully-connected one hidden layer neural networks in the proportional limit. In: *arXiv e-prints* (Jan. 2024). arXiv: 2401.11004 [cond-mat.dis-nn].

[29] G. Parisi and Yong-shi Wu. Perturbation Theory Without Gauge Fixing. In: *Sci. Sin.* 24 (1981), p. 483.

[30] D. Zwanziger. Local and renormalizable action from the gribov horizon. In: *Nuclear Physics B* 323.3 (Sept. 1989), pp. 513–544.

[31] P. H. Damgaard and H. Hüffel. Stochastic quantization. In: *Physics Reports* 152.5-6 (Aug. 1987), pp. 227–398.

[32] G. Jona-Lasinio and P. K. Mitter. Large deviation estimates in the stochastic quantization of ϕ_2^4. In: *Communications in Mathematical Physics* 130.1 (May 1990), pp. 111–121.

[33] V.S. Borkar, R.T. Chari, and S.K. Mitter. Stochastic quantization of field theory in finite and infinite volume. In: *Journal of Functional Analysis* 81.1 (Nov. 1988), pp. 184–206.

[34] E. Floratos and J. Iliopoulos. Equivalence of stochastic and canonical quantization in perturbation theory. In: *Nuclear Physics B* 214.3 (Apr. 1983), pp. 392–404.

[35] W. Grimus and H. Hüffel. Perturbation theory from stochastic quantization of scalar fields. In: *Zeitschrift für Physik C Particles and Fields* 18.2 (June 1983), pp. 129–134.

[36] M. E. Peskin. An Introduction To Quantum Field Theory. CRC Press, May 2018.

[37] P. J. Rossky, J. D. Doll, and H. L. Friedman. Brownian dynamics as smart Monte Carlo simulation. In: *The Journal of Chemical Physics* 69.10 (Nov. 1978), pp. 4628–4633.

[38] G. O. Roberts and R. L. Tweedie. Exponential Convergence of Langevin Distributions and Their Discrete Approximations. In: *Bernoulli* 2.4 (Dec. 1996), p. 341.

[39] G. O. Roberts and J. S. Rosenthal. Optimal Scaling of Discrete Approximations to Langevin Diffusions. In: *Journal of the Royal Statistical Society Series B: Statistical Methodology* 60.1 (Jan. 1998), pp. 255–268.

[40] G. G. Batrouni et al. Langevin simulations of lattice field theories. In: *Physical Review D* 32.10 (Nov. 1985), pp. 2736–2747.

[41] A. S. Kronfeld. Dynamics of Langevin Simulations. In: *Progress of Theoretical Physics Supplement* 111 (1993), pp. 293–311.

[42] C. Davies et al. Langevin simulations of lattice field theories using Fourier acceleration. In: *Journal of Statistical Physics* 43.5–6 (June 1986), pp. 1073–1075.

[43] K. Binder and D. W. Heermann. Monte Carlo Simulation in Statistical Physics. Springer Berlin Heidelberg, 2002.

[44] A. Barbu and S.C. Zhu. Monte Carlo Methods. Springer Singapore, 2020.

[45] N. Metropolis et al. Equation of State Calculations by Fast Computing Machines. In: *The Journal of Chemical Physics* 21.6 (June 1953), pp. 1087–1092.

[46] W. K. Hastings. Monte Carlo sampling methods using Markov chains and their applications. In: *Biometrika* 57.1 (Apr. 1970), pp. 97–109.

[47] S. Duane et al. Hybrid Monte Carlo. In: *Physics Letters B* 195.2 (Sept. 1987), pp. 216–222.

[48] D. M. Young and R. T. Gregory. A survey of numerical mathematics. Dover Books on Mathematics. Mineola, N: Dover Publications, Aug. 1989.

[49] A. Ramos. Automatic differentiation for error analysis of Monte Carlo data. In: *Computer Physics Communications* 238 (May 2019), pp. 19–35.

[50] A. Ramos. *aderrors.jl: A Julia package for automatic differentiation error propagation.* 2023.

[51] F. Joswig et al. *pyerrors: a python framework for error analysis of Monte Carlo data.* `https://github.com/fjosw/pyerrors`. 2023.

[52] A. Sokal. Monte Carlo Methods in Statistical Mechanics: Foundations and New Algorithms. In: *NATO ASI Series*. Springer US, 1997, pp. 131–192.

[53] C. Gattringer and C. B. Lang. Quantum Chromodynamics on the Lattice: An Introductory Presentation. Springer Berlin Heidelberg, 2010.

[54] U. Wolff. Monte Carlo errors with less errors. In: *Computer Physics Communications* 156.2 (Jan. 2004), pp. 143–153.

[55] I.P. Omelyan, I.M. Mryglod, and R. Folk. Symplectic analytically integrable decomposition algorithms: classification, derivation, and application to molecular dynamics, quantum and celestial mechanics simulations. In: *Computer Physics Communications* 151.3 (Apr. 2003), pp. 272–314.

[56] A. D. Kennedy, P. J. Silva, and M. A. Clark. Shadow Hamiltonians, Poisson brackets, and gauge theories. In: *Physical Review D* 87.3 (Feb. 2013).

[57] A. M. Horowitz. The second order Langevin equation and numerical simulations. In: *Nuclear Physics B* 280 (Jan. 1987), pp. 510–522.

[58] A. M. Horowitz. A generalized guided Monte Carlo algorithm. In: *Physics Letters B* 268.2 (Oct. 1991), pp. 247–252.

[59] S. Duane. Stochastic quantization versus the microcanonical ensemble: Getting the best of both worlds. In: *Nuclear Physics B* 257 (Jan. 1985), pp. 652–662.

[60] P. B. Mackenze. An improved hybrid Monte Carlo method. In: *Physics Letters B* 226.3–4 (Aug. 1989), pp. 369–371.

[61] M. Lüscher and S. Schaefer. Non-renormalizability of the HMC algorithm. In: *Journal of High Energy Physics* 2011.4 (Apr. 2011).

[62] E.V. Shuryak. The role of instantons in quantum chromodynamics. In: *Nuclear Physics B* 203.1 (Aug. 1982), pp. 93–115.

[63] J. Ecalle. Les fonctions résurgentes, Vol. 1: Algèbres de fonctions résurgentes. In: *Publ. Math. Orsay* (1981).

[64] J. Ecalle. Les fonctions résurgentes, Vol. 2: Les fonctions résurgentes appliquées à l'itération. In: *Publ. Math. Orsay* (1981).

[65] J. Ecalle. Les fonctions résurgentes, Vol. 3: L'équation du pont et la classification analytique des objets locaux. In: *Publ. Math. Orsay* (1981).

[66] D. Dorigoni. An introduction to resurgence, trans-series and alien calculus. In: *Annals of Physics* 409 (Oct. 2019), p. 167914.

[67] M. Mariño. Instantons and Large N: An Introduction to Non-Perturbative Methods in Quantum Field Theory. Cambridge University Press, Sept. 2015.

[68] A.M. Polyakov. Quark confinement and topology of gauge theories. In: *Nuclear Physics B* 120.3 (Mar. 1977), pp. 429–458.

[69] C. F. Wöhler and E. Shuryak. Two-loop correction to the instanton density for the double well potential. In: *Physics Letters B* 333.3–4 (Aug. 1994), pp. 467–470.

[70] M. A. Escobar-Ruiz, E. Shuryak, and A. V. Turbiner. Three-loop correction to the instanton density. I. The quartic double well potential. In: *Physical Review D* 92.2 (July 2015).

[71] M. Creutz and B. Freedman. A statistical approach to quantum mechanics. In: *Annals of Physics* 132.2 (Apr. 1981), pp. 427–462.

[72] H. B. Curry. The method of steepest descent for non-linear minimization problems. en. In: *Quart. Appl. Math.* 2.3 (1944), pp. 258–261.

[73] A. A. Alei-brevenikov and E. V. Shuryak. Instantons in quantum mechanics. Two-loop effects. In: *Sov. J. Nucl. Phys. (Engl. Transl.);* (1987).

[74] M. Pepe. MA thesis. University of Milano, 1996.

[75] J. Zinn-Justin. Quantum Field Theory and Critical Phenomena. Oxford University Press, June 2002.

[76] S. Elitzur. The applicability of perturbation expansion to two-dimensional goldstone systems. In: *Nuclear Physics B* 212.3 (Feb. 1983), pp. 501–518.

[77] N. D. Mermin. Absence of Ordering in Certain Classical Systems. In: *Journal of Mathematical Physics* 8.5 (May 1967), pp. 1061–1064.

[78] A. Jevicki. Perturbation theory in terms of currents and restoration of continuous symmetry in two dimensions. In: *Nuclear Physics B* 146.1 (Dec. 1978), pp. 77–89.

[79] B. Allés, A. Buonanno, and G. Cella. Perturbation theory predictions and Monte Carlo simulations for the $2D$ $O(n)$ non-linear σ-models. In: *Nuclear Physics B* 500.1–3 (Sept. 1997), pp. 513–543.

[80] F. Di Renzo, E. Onofri, and G. Marchesini. Renormalons from eight-loop expansion of the gluon condensate in lattice gauge theory. In: *Nuclear Physics B* 457.1–2 (Dec. 1995), pp. 202–216.

[81] S. Caracciolo and A. Pelissetto. Four-loop perturbative expansion for the lattice N-vector model. In: *Nuclear Physics B* 455.3 (Sept. 1995), pp. 619–647.

[82] G. V. Dunne and M. Unsal. Resurgence and Trans-series in Quantum Field Theory: The $CP(N-1)$ Model. In: *JHEP* 11 (2012), p. 170. arXiv: 1210.2423 [hep-th].

[83] H.A. Kramers. Brownian motion in a field of force and the diffusion model of chemical reactions. In: *Physica* 7.4 (Apr. 1940), pp. 284–304.

[84] J. E. Moyal. Stochastic Processes and Statistical Physics. In: *Journal of the Royal Statistical Society. Series B (Methodological)* 11.2 (1949), pp. 150–210.

[85] U. D. Jentschura and J. Zinn-Justin. Multi-instantons and exact results IV: Path integral formalism. In: *Annals of Physics* 326.8 (Aug. 2011), pp. 2186–2242.

Appendix A: Kramers-Moyal expansion

A discrete Langevin stochastic dynamics can be summarized by the equation

$$\varphi_{\boldsymbol{i}}(\tau + \Delta\tau) = \varphi_{\boldsymbol{i}}(\tau) - F_{\boldsymbol{i}}(\tau)\,, \tag{332}$$

where $\varphi_{\boldsymbol{i}}(\tau)$ denotes the field at lattice site $\boldsymbol{i}$ and stochastic time τ and the function $F_{\boldsymbol{i}}(\tau)$ is an integrator-dependent function (see for example Eq. (82)). At the stochastic time $\tau + \Delta\tau$ the probability of generating a certain configuration φ is

$$\begin{aligned} P[\varphi, \tau + \Delta\tau] &= \int D\varphi'\; W(\varphi' \to \varphi)\; P[\varphi', \tau] \\ &= \int D\varphi' D\eta\; [\prod_{\boldsymbol{i}} \delta(\varphi_{\boldsymbol{i}} - \varphi'_{\boldsymbol{i}} + F_{\boldsymbol{i}})]\; P[\varphi', \tau]\,. \end{aligned} \tag{333}$$

The function $F_{\boldsymbol{i}}$ is typically a quantity of $O(\Delta\tau^{\frac{1}{2}})$ so that we can think of expanding the Dirac delta function for each degree of freedom in Taylor series:

$$\prod_{\boldsymbol{i}} \delta(\varphi_{\boldsymbol{i}} - \varphi'_{\boldsymbol{i}} + F_{\boldsymbol{i}}) = \prod_{\boldsymbol{i}} \Big[\sum_{n_{\boldsymbol{i}}=0}^{\infty} \frac{1}{n_{\boldsymbol{i}}!} \delta^{n_{\boldsymbol{i}}}(\varphi_{\boldsymbol{i}} - \varphi'_{\boldsymbol{i}}) F_{\boldsymbol{i}}^{n_{\boldsymbol{i}}} \Big]\,. \tag{334}$$

By integrating by parts with respect to the variable $\varphi'_{\boldsymbol{i}}$ and rearranging all terms, one realizes that it is always possible to integrate over all fields with the Dirac delta functions $\delta(\varphi_{\boldsymbol{i}} - \varphi'_{\boldsymbol{i}})$ to get the expression

$$\begin{aligned} P[\varphi, \tau + \Delta\tau] &= P[\varphi, \tau] + \sum_{n=1}^{\infty} \frac{1}{n!} \int D\eta \frac{\partial}{\partial\varphi_{\boldsymbol{i}_1}} \cdots \frac{\partial}{\partial\varphi_{\boldsymbol{i}_n}} \Big(F_{\boldsymbol{i}_1} \ldots F_{\boldsymbol{i}_n} P[\varphi] \Big) \\ &= P[\varphi, \tau] + \sum_{n=1}^{\infty} \frac{1}{n!} \frac{\partial}{\partial\varphi_{\boldsymbol{i}_1}} \cdots \frac{\partial}{\partial\varphi_{\boldsymbol{i}_n}} \Big(\langle F_{\boldsymbol{i}_1} \ldots F_{\boldsymbol{i}_n} \rangle P[\varphi] \Big)\,. \end{aligned} \tag{335}$$

Eq. (335) is the Kramers-Moyal expansion [83, 84] for the Langevin discrete dynamics.

Appendix B: Complete expression for the energy splitting (continuum theory)

In what follows, we explicitly express the dependence of the solution in Eq. (184) on the transition parameter t_0 as $x_c^{\pm}(t-t_0)$. Furthermore, we note that the solution in Eq. (184) has constant energy $E = T + W$, where

$$T = \frac{1}{2}\dot{x}^2 \qquad \text{and} \qquad W = -\lambda(x^2 - x_0^2)^2 \tag{336}$$

and this is also a solution in the zero-energy shell, such that we have $T = V$. We can therefore note that the following holds

$$\begin{aligned} ||\dot{x}_c^+|| &= \sqrt{\int_{-\infty}^{+\infty} \dot{x}_c^+(t-t_0)^2 dt} \\ &= \sqrt{\int_{-\infty}^{+\infty} \left[\frac{1}{2}\dot{x}_c^+(t-t_0)^2 + \lambda(x_c^+(t-t_0)^2 - x_0^2)^2\right] dt} \\ &= \sqrt{S[x_c^+]}\,. \end{aligned} \tag{337}$$

Consider the twisted partition function

$$Z_a(\beta) = \int_{ABC} Dx\; e^{-S[x]}\,. \tag{338}$$

We can implement a useful rewriting of the identity

$$1 = \int dt_0\; \delta(t_0 - t_0^*) = \int dt_0\; \delta(f(t_0))|f'(t_0)|\,, \tag{339}$$

where we have used the well-known property of the Dirac delta function and t_0^* is a zero of the function $f(t_0)$. An appropriate choice of the function $f(t_0)$ leads to the regularization of the zero-mode: this must be done by projecting the fluctuations onto the subspace without a zero-mode component, namely:

$$f(t_0) = \int dt (x(t) - x_c^+(t)) \frac{\dot{x}_c^+(t-t_0)}{\sqrt{S[x_c^+]}}\,. \tag{340}$$

We notice that the last term in the previous equation is exactly the zero-mode profile. We can compute the derivative of the function in the following way

$$\begin{aligned} f'(t_0) &= \int dt\ \Big(\dot{x}_c^+(t-t_0)\frac{\dot{x}_c^+(t-t_0)}{\sqrt{S[x_c^+]}}\Big) - \int dt\ (x(t)-x_c^+(t-t_0))\frac{\ddot{x}_c^+(t-t_0)}{\sqrt{S[x_c^+]}} \\ &= \int dt\ \Big(\dot{x}_c^+(t-t_0)\frac{\dot{x}_c^+(t-t_0)}{\sqrt{S[x_c^+]}}\Big) - \int dt\ x(t)\frac{\ddot{x}_c(t-t_0)}{\sqrt{S[x_c^+]}} + \int dt\ x_c^+(t-t_0)\frac{\ddot{x}_c(t-t_0)}{\sqrt{S[x_c^+]}} \\ &= \int dt\ \Big(\dot{x}_c^+(t-t_0)\frac{\dot{x}_c^+(t-t_0)}{\sqrt{S[x_c^+]}}\Big) - \int dt\ x(t)\frac{\ddot{x}_c^+(t-t_0)}{\sqrt{S[x_c^+]}} - \int dt\ \dot{x}_c^+(t-t_0)\frac{\dot{x}_c^+(t-t_0)}{\sqrt{S[x_c^+]}} \\ &= \int dt\ \dot{x}(t)\frac{\dot{x}_c^+(t-t_0)}{\sqrt{S[x_c^+]}}\,. \end{aligned} \tag{341}$$

It can be shown that this derivative, at least for small values of the coupling constant, is always positive. So in practice we do not have to apply the absolute value on it. Furthermore, since the derivative with respect to the transition time is positive, if the function vanishes, it vanishes at only one point, justifying the use of the aforementioned property of the Dirac delta. Using the Dirac delta propriety with the choice in Eq. (340) we obtain

$$Z_a = \int_{ABC} Dx \int dt_0 \Big[\int dt\ \dot{x}(t)\frac{\dot{x}_c^+(t-t_0)}{\sqrt{S[x_c^+]}}\Big]\delta\Big[\int dt\ (x(t)-x_c^+(t-t_0))\frac{\dot{x}_c^+(t-t_0)}{\sqrt{S[x_c^+]}}\Big]e^{-S[x]}\,. \tag{342}$$

Since we are integrating over all possible configurations, we can make use of the shift $t \to t+t_0$, which in any case can be reabsorbed in the definition of the integral measure. So we have [11]

$$\begin{aligned} Z_a &= \int_{ABC} Dx \int dt_0 \Big[\int dt\ \dot{x}(t)\frac{\dot{x}_c^+(t)}{\sqrt{S[x_c^+]}}\Big]\delta\Big[\int dt\ (x(t)-x_c^+(t))\frac{\dot{x}_c^+(t)}{\sqrt{S[x_c^+]}}\Big]e^{-S[x]} \\ &= \beta \int_{ABC} Dx \Big[\int dt\ \dot{x}(t)\frac{\dot{x}_c^+(t)}{\sqrt{S[x_c^+]}}\Big]\delta\Big[\int dt\ (x(t)-x_c^+(t))\frac{\dot{x}_c^+(t)}{\sqrt{S[x_c^+]}}\Big]e^{-S[x]}\,. \end{aligned} \tag{343}$$

We can introduce the fluctuation ξ by setting

$$x(t) = x_c^+(t) + \xi(t)\,, \tag{344}$$

and we obtain

$$Z_a = \beta \int_{ABC} D\xi \Big[\int dt\ (\dot{x}_c^+(t)+\dot{\xi}(t))\frac{\dot{x}_c^+(t)}{\sqrt{S[x_c^+]}}\Big]\delta\Big[\int dt\ \xi(t)\frac{\dot{x}_c^+(t)}{\sqrt{S[x_c^+]}}\Big]e^{-S[x]}\,. \tag{345}$$

[11] This is similar to the shift that is discussed for the quartic theory in [85].

We now make use of the decomposition of the fluctuation in the components of the zero-mode and the modes that are orthogonal to it:

$$\xi(t) = c_0 \frac{\dot{x}_c(t)}{\sqrt{S[x_c^+]}} + \xi_\perp \tag{346}$$

and we obtain the following relations

$$D\xi = \int \frac{dc_0}{\sqrt{2\pi}} \int D\xi_\perp \,, \tag{347}$$

$$\int dt(\dot{x}_c^+(t) + \dot{\xi}(t)) \frac{\dot{x}_c^+(t)}{\sqrt{S[x_c^+]}} = \int dt\ (\dot{x}_c(t) + \dot{\xi}_\perp(t)) \frac{\dot{x}_c(t)}{\sqrt{S[x_c^+]}} \,, \tag{348}$$

$$\delta\Big[\int dt\ \xi(t) \frac{\dot{x}_c^+(t)}{\sqrt{S[x_c^+]}}\Big] = \delta\Big[\int dt\ \Big(c_1 \frac{\dot{x}_c^+(t)}{\sqrt{S[x_c^+]}} + \xi_\perp(t)\Big) \frac{\dot{x}_c^+(t)}{\sqrt{S[x_c^+]}}\Big] = \delta(c_0) \,, \tag{349}$$

where we used

$$\int dt\ \dot{x}_c^+(t)\ddot{x}_c^+(t) = 0 \qquad \text{and} \qquad \int dt\ \dot{x}_c^+(t)\xi_\perp(t) = 0 \,. \tag{350}$$

Then the twisted partition function can be expressed as

$$\begin{aligned}
Z_a &= e^{-S[x_c^+]}\beta \int_{ABC} D\xi_\perp \int \frac{dc_1}{\sqrt{2\pi}} \Big[\int dt\ (\dot{x}_c^+(t) + \dot{\xi}_\perp(t)) \frac{\dot{x}_c^+(t)}{\sqrt{S[x_c^+]}}\Big] \delta(c_1) e^{-S[\xi]} \\
&= \frac{\beta e^{-S[x_c^+]}}{\sqrt{2\pi}} \int_{ABC} D\xi_\perp \Big[\int dt\ (\dot{x}_c^+(t) + \dot{\xi}_\perp(t)) \frac{\dot{x}_c^+(t)}{\sqrt{S[x_c^+]}}\Big] e^{-S[\xi_\perp]} \\
&= \frac{\beta e^{-S[x_c^+]}\sqrt{S[x_c^+]}}{\sqrt{2\pi}} \int_{ABC} D\xi_\perp \Big[1 + \int dt\ \frac{\dot{\xi}_\perp(t)\dot{x}_c^+(t)}{S[x_c^+]}\Big] e^{-S[\xi_\perp]} \\
&= \frac{\beta e^{-S[x_c^+]}\sqrt{S[x_c^+]}}{\sqrt{2\pi}} \langle 1 + S[x_c^+]^{-1} \int dt\ \dot{\xi}_\perp(t)\dot{x}_c^+(t)\rangle_{a,\perp} Z_{a,\perp} \,,
\end{aligned} \tag{351}$$

where $\langle \ldots \rangle_{a,\perp}$ indicates the expectation value in the theory with antiperiodic boundary conditions and without zero-mode. In addition $Z_{a,\perp}$ is the twisted partition function for the theory without zero-mode. It is always possible to write the partition functions as

$$Z_a(\lambda) = Z_{a,\perp}^{(0)} e^{W_{a,\perp}} \,, \tag{352}$$

$$Z(\lambda) = Z^{(0)} e^{W} \,, \tag{353}$$

where $Z_{a,\perp}^{(0)}$ and $Z^{(0)}$ are respectively the free partition functions for anti-symmetric theory without zero mode and for the usual theory with periodic boundary conditions. Additionally, $W_{a,\perp}$ and W are perturbative series coming from the evaluation of the interacting part of the action (we refer to the discussion in Sec. 2.3 for details).

Finally, using also the relations in Eq. (201), we obtain

$$\frac{Z_a}{Z} = \frac{\beta e^{-\frac{1}{12\lambda}}}{\sqrt{2\pi\lambda}} \langle 1 + S[x_c^+]^{-1} \int dt\ \dot{\xi}_\perp(t)\dot{x}_c(t)\rangle_{a,\perp} e^{W_{a,\perp}-W} \,. \tag{354}$$

Appendix C: First-order correction to the propagator

Here we will show how the corrections to the propagator up to the first perturbative order can be calculated. This will provide the perturbation theory at the second-order for the energy - see Eq. (288). We note that the interacting terms of the action in Eq. (285) can be expanded in a Taylor series up to $O(g^2)$

$$\log\left(1-g\boldsymbol{\pi}_x^2\right) = -g\boldsymbol{\pi}_x^2 + O(g^2)\,, \tag{355}$$

$$\begin{aligned} -\frac{1}{2g}\Big[(\Delta_\mu)\sqrt{1-g\boldsymbol{\pi}_x^2}\Big]^2 &= -\frac{1}{2g}\Big[\sqrt{1-g\boldsymbol{\pi}_{x+\mu}^2}-\sqrt{1-g\boldsymbol{\pi}_x^2}\Big]^2 \\ &= -\frac{1}{2g}\Big[1-\frac{g}{2}\boldsymbol{\pi}_{x+\mu}^2-\Big(1-\frac{g}{2}\boldsymbol{\pi}_x^2\Big)\Big]^2 + O(g^2) \\ &= -\frac{g}{4}\Big(\boldsymbol{\pi}_x^4-\boldsymbol{\pi}_x^2\boldsymbol{\pi}_{x+\mu}^2\Big) + O(g^2)\,. \end{aligned} \tag{356}$$

The standard approach in perturbation theory then requires the Taylor expansion in terms of the weak coupling of the partition function written in Eq. (285). We have

$$\begin{aligned} Z &= \lim_{\lambda\to 0}\int\prod_x d\boldsymbol{\pi}_x\; e^{-\frac{1}{2}\sum_{x,\mu}\left[(\Delta_\mu\boldsymbol{\pi}_x)^2+\lambda^2\boldsymbol{\pi}_x^2\right]} e^{-\sum_{x,\mu}\frac{1}{2g}(\Delta_\mu\sqrt{1-g\boldsymbol{\pi}_x^2})^2-\frac{1}{2}\sum_x\log(1-g\boldsymbol{\pi}_x^2)} \\ &= \lim_{\lambda\to 0}\int\prod_x d\boldsymbol{\pi}_x\; e^{-\frac{1}{2}\sum_{x,\mu}\left[(\Delta_\mu\boldsymbol{\pi}_x)^2+\lambda^2\boldsymbol{\pi}_x^2\right]} e^{-\sum_{x,\mu}\frac{g}{4}\left(\boldsymbol{\pi}_x^4-\boldsymbol{\pi}_x^2\boldsymbol{\pi}_{x+\mu}^2\right)+\frac{g}{2}\sum_x\boldsymbol{\pi}_x^2+O(g^2)} \\ &= \lim_{\lambda\to 0}\int\prod_x d\boldsymbol{\pi}_x\; e^{-\frac{1}{2}\sum_{x,\mu}\left[(\Delta_\mu\boldsymbol{\pi}_x)^2+\lambda^2\boldsymbol{\pi}_x^2\right]}\Big(1-\sum_{x,\mu}\frac{g}{4}\Big(\boldsymbol{\pi}_x^4-\boldsymbol{\pi}_x^2\boldsymbol{\pi}_{x+\mu}^2\Big)+\frac{g}{2}\sum_x\boldsymbol{\pi}_x^2+O(g^2)\Big)\,. \end{aligned} \tag{357}$$

By taking into account Eq. (357) we obtain the following expression for the propagator $\boldsymbol{\pi}\boldsymbol{\pi}$ up to $O(g^2)$

$$\begin{aligned} \langle\boldsymbol{\pi}_0\boldsymbol{\pi}_x\rangle &= \frac{1}{Z}\int\prod_x d\boldsymbol{\pi}_x\; e^{-\frac{1}{2}\sum_{x,\mu}\left[(\Delta_\mu\boldsymbol{\pi}_x)^2+\lambda^2\boldsymbol{\pi}_x^2\right]}\Big(1-\sum_{x,\mu}\frac{g}{4}\Big(\boldsymbol{\pi}_x^4-\boldsymbol{\pi}_x^2\boldsymbol{\pi}_{x+\mu}^2\Big) \\ &\qquad + \frac{g}{2}\sum_x\boldsymbol{\pi}_x^2+O(g^2)\Big)\boldsymbol{\pi}_0\boldsymbol{\pi}_x \qquad (358) \\ &= \langle\boldsymbol{\pi}_0\boldsymbol{\pi}_x\rangle^{(0)} + g\Big\langle-\Big(\sum_{y,\mu}\frac{1}{4}\Big(\boldsymbol{\pi}_y^4-\boldsymbol{\pi}_y^2\boldsymbol{\pi}_{y+\mu}^2\Big)+\frac{1}{2}\sum_y\boldsymbol{\pi}_y^2\Big)\boldsymbol{\pi}_0\boldsymbol{\pi}_x\Big\rangle_c^{(0)} + O(g^2)\,, \end{aligned}$$

where in the last line we are considering only connected Wick contraction (the disconnected contributions are canceled out by the partition function contribution). At the leading order, we have

$$\langle\boldsymbol{\pi}_0\boldsymbol{\pi}_x\rangle^{(0)} = (N-1)G(x) = (N-1)\int_{-\pi}^{+\pi}\frac{d^2k}{(2\pi)^2}\frac{e^{ik\cdot(x-y)}}{4\sum_\mu\sin^2\left(\frac{k\cdot\mu}{2}\right)+\lambda^2}\,, \tag{359}$$

getting thus the result provided in Eq. (286). Concerning the first-order correction, we apply the Wick contractions and we get the following results

$$\begin{aligned}\Big\langle \boldsymbol{\pi}_0\boldsymbol{\pi}_x \sum_y \boldsymbol{\pi}_y^2 \Big\rangle_c^{(0)} &= \sum_y \langle \boldsymbol{\pi}_0\boldsymbol{\pi}_y\rangle^{(0)}\langle \boldsymbol{\pi}_x\boldsymbol{\pi}_y\rangle^{(0)} + \sum_y \langle \boldsymbol{\pi}_0\boldsymbol{\pi}_y\rangle^{(0)}\langle \boldsymbol{\pi}_x\boldsymbol{\pi}_y\rangle^{(0)} \\ &= 2(N-1)\sum_y G(y)G(y-x)\,,\end{aligned} \tag{360}$$

$$\begin{aligned}\Big\langle \boldsymbol{\pi}_0\boldsymbol{\pi}_x \sum_y \boldsymbol{\pi}_y^2\boldsymbol{\pi}_{y+\mu}^2 \Big\rangle_c^{(0)} &= (N-1)\sum_y \Big[2G(y)G(y-x)G(0) + 4G(y)G(y+\mu-x)G(\mu) \\ &\quad + 4G(y+\mu)G(y-x)G(\mu) + 2G(y+\mu)G(y-\mu-x)G(0)\Big] \\ &= (N-1)\sum_y \Big[2G(y)G(y-x)G(0) + 4G(y)G(y+\mu-x)G(\mu) \\ &\quad + \underbrace{4G(y)G(y-\mu-x)G(\mu)}_{4G(y)G(y-\mu-x)G(-\mu)} + 2G(y+\mu)G(y-\mu-x)G(0)\Big]\,,\end{aligned} \tag{361}$$

$$\begin{aligned}\Big\langle \boldsymbol{\pi}_0\boldsymbol{\pi}_x \sum_y \boldsymbol{\pi}_y^2\boldsymbol{\pi}_y^2 \Big\rangle_c^{(0)} &= (N-1)\sum_y \Big[2G(y)G(y-x)G(0) + 4G(y)G(y-x)G(0) \\ &\quad + 4G(y)G(y-x)G(0) + 2G(y)G(y-x)G(0)\Big]\,.\end{aligned} \tag{362}$$

Hence we obtain

$$\begin{aligned}-\frac{g}{4}\Big\langle \sum_{y,\mu}\Big(\boldsymbol{\pi}_y^4 - \boldsymbol{\pi}_y^2\boldsymbol{\pi}_{y+\mu}^2\Big)\boldsymbol{\pi}_0\boldsymbol{\pi}_x\Big\rangle_c^{(0)} &= (N-1)\sum_{y,\mu}\Big(G(y)G(y+\mu-x)G(\mu) \\ &\quad + G(y)G(y-\mu-x)G(-\mu) - 2G(y)G(y-x)G(0)\Big) \\ &= (N-1)\sum_y G(y)\Delta_z\Big[G(x-z)G(z-y)\Big]_{z=y}\,,\end{aligned} \tag{363}$$

where we used the notation

$$\Delta_z f(x) = \sum_\mu \Big(f(x+\mu) + f(x-\mu) - 2f(x)\Big)\,. \tag{364}$$

The first-order correction reads

$$g\langle \boldsymbol{\pi}_0\boldsymbol{\pi}_x\rangle^{(1)} = (N-1)\sum_y G(y)G(y-x) + (N-1)\sum_y G(y)\Delta_z\Big[G(x-z)G(z-y)\Big]_{z=y}\,. \tag{365}$$

We note that

$$\begin{aligned}\Delta_x G(x) &= \sum_\mu G(x+\mu) + G(x-\mu) - 2G(x) = \int_{-\pi}^{+\pi} \frac{d^2k}{(2k)^2} \frac{e^{ik(x+\mu)} + e^{ik(x-\mu)} - 2e^{ikx}}{4\sum_\mu \sin^2(k_\mu/2) + \lambda^2} \\ &= \int_{-\pi}^{+\pi} \frac{d^2k}{(2k)^2} e^{ikx} \underbrace{\frac{\sum_\mu (2\cos(k_\mu/2) - 2 - \lambda^2)}{4\sum_\mu \sin^2(k_\mu/2) + \lambda^2}}_{=-1} + \int_{-\pi}^{+\pi} \frac{d^2k}{(2k)^2} e^{ikx} \frac{\lambda^2}{4\sum_\mu \sin^2(k_\mu/2) + \lambda^2} \\ &= -\delta_{x,0} + \lambda^2 G(x)\,.\end{aligned} \tag{366}$$

In addition, we have

$$\begin{aligned}\Delta_z \Big[G(x-z)G(z-y)\Big]_{z=y} &= \sum_\mu \Big[G(x-z-\mu)G(z+\mu-y) + G(x-z+\mu)G(z-\mu-y) - \\ &\quad - 2G(x-z)G(0)\Big]_{z=y} \\ &= \sum_\mu \Big[G(x-y-\mu)G(\mu) + G(x-y+\mu)G(-\mu) - 2G(x-y)G(0)\Big] \\ &= G(1)\sum_\mu \Big[G(x-y+\mu) + G(x-y-\mu)\Big] - 4G(x-y)G(0) \\ &= G(1)\sum_\mu \Big[G(x-y+\mu) + G(x-y-\mu) - 2G(x-y)\Big] \\ &\quad + 4G(1)G(x-y) - 4G(0)G(x-y) \\ &= G(1)\Delta_y G(x-y) - 4(G(0)-G(1))G(x-y)\,.\end{aligned} \tag{367}$$

The last term can be evaluated using the property of Eq. (366) in $x = 0$, namely

$$\Delta_x G(x)|_{x=0} = \sum_\mu \Big[G(x+\mu) + G(x-\mu) - 2G(x)\Big]|_{x=0} = 4G(1) - 4G(0) = -\delta_{0,0} + \lambda^2 G(0)\,, \tag{368}$$

from which it follows that

$$G(0) - G(1) = \frac{1}{4} - \frac{\lambda^2}{4} G(0)\,. \tag{369}$$

In the end, we obtain the first-order correction to the propagator, which is given by

$$\begin{aligned}\langle \boldsymbol{\pi}_0 \boldsymbol{\pi}_1 \rangle^{(1)} &= -(N-1)G(1)G(x) + \mu^2 (N-1)(G(1)-G(0)) \sum_y G(y)G(x-y) \\ &= -(N-1)G(1)G(x) + O(\lambda^2)\,.\end{aligned} \tag{370}$$

Appendix D: Leading-order zero-mode regularization

In this Appendix we will show that at the leading order Eq. (290) can also be computed using configurations without zero-mode. In the Fourier representation we have

$$\pi_n^j = \sum_p e^{ip\cdot n}\ \tilde{\pi}_p^j\,, \tag{371}$$

so that we can calculate

$$\begin{aligned}\langle \pi_n^j \pi_m^j\rangle &= \sum_{k'}\sum_{k''} e^{i(k'\cdot n + k''\cdot m)}\langle \pi_{k'}^j \pi_{k''}^j\rangle \\ &= \sum_{k'}\sum_{k''} e^{i(k'\cdot n + k''\cdot m)}\frac{\delta_{k',-k''}}{f(k')} \\ &= \sum_k e^{ik\cdot(n-m)}\frac{1}{f(k)}\,.\end{aligned} \tag{372}$$

In the previous equation, $f(k)$ is the propagator that is given in Eq. (286).
The $O(N)$ invariant leading order propagator reads

$$\begin{aligned}\langle \pi_n^j \pi_m^j\rangle - \langle \pi_n^j \pi_n^j\rangle &= \sum_{k'}\sum_{k''} e^{i(k'\cdot n + k''\cdot m)}\langle \pi_{k'}^j \pi_{k''}^j\rangle - \sum_{k'}\sum_{k''} e^{i(k'\cdot n + k''\cdot n)}\langle \pi_{k'}^j \pi_{k''}^j\rangle \\ &= \sum_k e^{ik\cdot(n-m)}\frac{1}{f(k)} - \sum_k e^{ik\cdot 0}\frac{1}{f(k)} \\ &= \sum_k e^{ik\cdot(n-m)}\frac{1}{f(k)} - \sum_k \frac{1}{f(k)} \\ &= \sum_k \Big(e^{ik\cdot(n-m)} - 1\Big)\frac{1}{f(k)} \\ &= \sum_k e^{ik\cdot(n-m)}\underbrace{\frac{1-e^{-ik\cdot(n-m)}}{f(k)}}_{=g(k)} \\ &= \sum_k e^{ik\cdot(n-m)}\frac{1}{g(k)}\,,\end{aligned} \tag{373}$$

where it is easy to notice that the new signal does not have the zero mode, namely

$$g(0) = 0\,. \tag{374}$$

We observe that in such a case, cancellation occurs only in a statistical sense, that is, after calculating $\langle ...\rangle$.

On the other hand, in NSPT simulations we are aiming at calculating propagators by em-

ploying configurations free of zero-modes. In that case we have

$$\begin{aligned}
&\langle(\pi_n^j - \frac{1}{V}\sum_{n'}\pi_{n'}^j)(\pi_m^j - \frac{1}{V}\sum_{m'}\pi_{m'}^j)\rangle \\
&= \langle\pi_n^j\pi_m^j\rangle - \frac{1}{V}\sum_{n'}\langle\pi_{n'}^j\pi_m^j\rangle - \frac{1}{V}\sum_{m'}\langle\pi_n^j\pi_{m'}^j\rangle + \frac{1}{V^2}\sum_{m'}\sum_{n'}\langle\pi_{n'}^j\pi_{m'}^j\rangle \\
&= \sum_k e^{ik\cdot(n-m)}\frac{1}{f(k)} - \sum_k e^{-ik\cdot m}\frac{\delta_{k,0}}{f(k)} \\
&\qquad - \sum_k e^{ik\cdot n}\frac{\delta_{k,0}}{f(k)} + \frac{1}{V}\sum_{m'}\sum_k e^{-ik\cdot m'}\frac{\delta_{k,0}}{f(k)} \\
&= \sum_k e^{ik\cdot(n-m)}\frac{1}{f(k)} - \frac{1}{f(0)}\,.
\end{aligned} \tag{375}$$

As expected, this signal does not have a zero-mode, even before performing the subtraction with its counterpart as in Eq. (290). The $O(N)$ invariant leading order propagator, using configurations without zero-more reads

$$\begin{aligned}
&\langle(\pi_n^j - \frac{1}{V}\sum_{n'}\pi_{n'}^j)(\pi_m^j - \frac{1}{V}\sum_{m'}\pi_{m'}^j)\rangle - \langle(\pi_n^j - \frac{1}{V}\sum_{n'}\pi_{n'}^j)(\pi_n^j - \frac{1}{V}\sum_{m'}\pi_{m'}^j)\rangle \\
&= \sum_k e^{ik\cdot(n-m)}\frac{1}{f(k)} - \frac{1}{f(0)} - \Big(\sum_k e^{ik\cdot 0}\frac{1}{f(k)} - \frac{1}{f(0)}\Big) \\
&= \sum_k e^{ik\cdot(n-m)}\frac{1}{f(k)} - \sum_k e^{ik\cdot 0}\frac{1}{f(k)} \\
&= \sum_k e^{ik\cdot(n-m)}\frac{1}{f(k)} - \sum_k \frac{1}{f(k)} \\
&= \langle\pi_n^j\pi_m^j\rangle - \langle\pi_n^j\pi_n^j\rangle\,.
\end{aligned} \tag{376}$$

Thus the result of Eq. (376) demonstrates the assertion we made in the discussion of Sec. 3.4.

Appendix E: Infrared corrections to the renormalon scaling at two-loops

We are interested in calculating the integral

$$\int_0^{Q^2} \frac{dk^2}{k^2}\left(\frac{k}{Q}\right)^{2\sigma} g(k) \tag{377}$$

at two-loop. We take into account the definition of the β-function at second-order

$$k\frac{d}{dk}g(k) = -\beta_0 g^2 - \beta_1 g^3 + O(g^4)\,. \tag{378}$$

Integrating the previous equation we obtain

$$-\beta_0(\ln k - \ln k_0) = -\left(\frac{1}{g(k)} - \frac{1}{g(k_0)}\right) - \frac{\beta_1}{\beta_0}\ln\frac{g(k)}{g(k_0)}\,, \tag{379}$$

so that

$$\left(\frac{k}{k_0}\right)^{2\sigma} = e^{\frac{2\sigma}{\beta_0}\left(\frac{1}{g(k)}-\frac{1}{g(k_0)}\right)}\left(\frac{g(k)}{g(k_0)}\right)^{\frac{2\sigma\beta_1}{\beta_0^2}}\,. \tag{380}$$

We set

$$\frac{2\sigma}{\beta_0} = z_0 \qquad z = z_0\left(1 - \frac{g(k_0)}{g(k)}\right). \tag{381}$$

In this way, the following holds

$$\left(\frac{k}{k_0}\right)^{2\sigma} = e^{-\frac{z}{g(k_0)}}\left(1 - \frac{z}{z_0}\right)^{-\gamma}\,, \tag{382}$$

where

$$\gamma = \frac{2\sigma\beta_1}{\beta_0^2}\,. \tag{383}$$

The integral measure changes to

$$dz = z_0\left(-\frac{d}{dk}\frac{g(k_0)}{g(k)}\right)dk = z_0\left(\frac{1}{g(k)^2}\frac{dg(k)}{dk}g(k_0)\right)\frac{dk}{k} = -z_0\beta_0\left(1 + \frac{\beta_1}{\beta_0}g(k)\right)g(k_0)\frac{dk}{k}\,. \tag{384}$$

Inserting Eq. (384) and Eq. (382) in Eq. (377), we obtain the equation

$$\int_0^{k_0}\frac{dk^2}{k^2}\left(\frac{k}{k_0}\right)^{2\sigma} g(k) = 2\int_0^{\infty}\frac{dz}{z_0\beta_0}e^{-\frac{z}{g(k_0)}}\left(1 - \frac{z}{z_0}\right)^{-\gamma-1}\left(1 - \frac{\beta_1}{\beta_0}g(k)\right) = C + B\,, \tag{385}$$

where

$$C = 2\int_0^{\infty}\frac{dz}{z_0\beta_0}e^{-\frac{z}{g(k_0)}}\left(1 - \frac{z}{z_0}\right)^{-\gamma-1}\,, \tag{386}$$

$$B = -2\int_0^{\infty}\frac{dz\beta_1 g(k_0)}{z_0\beta_0^2}e^{-\frac{z}{g(k_0)}}\left(1 - \frac{z}{z_0}\right)^{-\gamma-2}\,. \tag{387}$$

The first integral can be computed by setting

$$\frac{z}{g(k_0)} = t\,, \tag{388}$$

so that we get

$$C = 2\int_0^\infty \frac{g(k_0)dt}{z_0\beta_0} e^{-t}\left(1-\frac{tg(k_0)}{z_0}\right)^{-1-\gamma}. \tag{389}$$

We note that using the Taylor expansion

$$\begin{aligned}\left(1-\frac{tg(k_0)}{z_0}\right)^{-1-\gamma} &= 1+\frac{tg(k_0)}{z_0}(\gamma+1)+\frac{1}{2}\frac{t^2g(k_0)^2}{z_0^2}(\gamma+1)(\gamma+2)+\\ &\quad+\frac{1}{3!}\frac{t^3g(k_0)^3}{z_0^3}(\gamma+1)(\gamma+2)(\gamma+3)+\ldots\\ &= \sum_{n=0}^\infty \frac{t^n g(k_0)^n}{z_0^n}\frac{\Gamma(\gamma+n+1)}{\Gamma(\gamma+1)\Gamma(n+1)}\,,\end{aligned} \tag{390}$$

we obtain

$$\begin{aligned}C &= 2\int_0^\infty \frac{g(k_0)dt}{z_0\beta_0}e^{-t}\sum_{n=0}^\infty \frac{t^n g(k_0)^n}{z_0^n}\frac{\Gamma(\gamma+n+1)}{\Gamma(\gamma+1)\Gamma(n+1)}\\ &= \frac{2}{\beta_0}\sum_{n=0}^\infty \frac{g(k_0)^{n+1}}{z_0^{n+1}}\frac{\Gamma(\gamma+n+1)}{\Gamma(\gamma+1)\Gamma(n+1)}\int_0^\infty dte^{-t}t^{(n+1)-1}\\ &= \frac{2}{\beta_0}\sum_{n=0}^\infty \frac{g^{n+1}}{z_0^{n+1}}\frac{\Gamma(\gamma+n+1)}{\Gamma(\gamma+1)}\,.\end{aligned} \tag{391}$$

In a similar way we work for the integral B; we have

$$B = -2\int_0^\infty \frac{\beta_1 g(k_0)^2 dt}{z_0\beta_0^2}e^{-t}\left(1-\frac{tg(k_0)}{z_0}\right)^{-2-\gamma}. \tag{392}$$

The Taylor expansion of $(1-tg(k_0)/z_0)^{-2-\gamma}$ is derived from Eq. (390) by considering $\gamma\to\gamma+1$ and thus

$$\left(1-\frac{tg(k_0)}{z_0}\right)^{-2-\gamma} = \sum_{n=0}^\infty \frac{t^n g(k_0)^n}{z_0^n}\frac{\Gamma(\gamma+n+2)}{\Gamma(\gamma+2)\Gamma(n+1)}\,. \tag{393}$$

Inserting the previous identity in Eq. (392) we get

$$\begin{aligned}B &= -\frac{2\beta_1}{\beta_0^2}\int_0^\infty \frac{g(k_0)^2dt}{z_0}e^{-t}\sum_{n=0}^\infty \frac{t^n g(k_0)^n}{z_0^n}\frac{\Gamma(\gamma+n+2)}{\Gamma(\gamma+2)\Gamma(n+1)}\\ &= -\frac{2\beta_1 z_0}{\beta_0^2}\sum_{n'=0}^\infty \frac{g(k_0)^{n'+2}}{z_0^{n'+2}}\frac{\Gamma(\gamma+n'+2)}{\Gamma(\gamma+2)}\,.\end{aligned} \tag{394}$$

To sum order-by-order C and B, it is necessary to consider only the terms that satisfy $n+1=n'+2$, where n is the perturbative order of the series C and n' is the perturbative order of the

series B, which means that $n' = n - 1$. So we get

$$\begin{aligned} C + B &= \sum_{n=0}^{\infty} g(k_0)^{n+1} \left\{ \frac{2}{\beta_0} \frac{\Gamma(\gamma+n+1)}{\Gamma(\gamma+1) z_0^{n+1}} - \frac{2\beta_1 z_0}{\beta_0^2} \frac{\Gamma(\gamma+n+1)}{\Gamma(\gamma+2) z_0^{n+1}} \right\} \\ &= \sum_{n=0}^{\infty} g(k_0)^{n+1} \frac{\Gamma(\gamma+n+1)}{z_0^{n+1}} \underbrace{\left(\frac{2}{\beta_0 \Gamma(\gamma+1)} - \frac{2 z_0 \beta_1}{\beta_0 \Gamma(\gamma+2)} \right)}_{=\chi} \\ &= \chi \sum_{n=0}^{\infty} g(k_0)^{n+1} \frac{\Gamma(\gamma+n+1)}{z_0^{n+1}} \,. \end{aligned} \tag{395}$$

In this case we obtain the two-loop renormalon asymptotic, *i.e.*

$$E^{(n+1)} = \frac{\Gamma(\gamma+n+1)}{z_0^{n+1}} \qquad \to \qquad \frac{E^{(n+1)}}{E^{(n)} \cdot n} = \frac{1}{z_0} \left(1 + \frac{\gamma}{n} \right), \tag{396}$$

recovering Eq. (317). We consider finite volume effects as for the one-loop case. This amounts to adjusting the limits of the integrals C and B, namely

$$C = \frac{2}{\beta_0} \sum_{n=0}^{\infty} \frac{g(k_0)^{n+1}}{z_0^{n+1}} \frac{\Gamma(\gamma+n+1)}{\Gamma(\gamma+1)\Gamma(n+1)} \int_0^{z_0 \beta_0 \ln \sqrt{2} N} dt e^{-t} t^{(n+1)-1} \,, \tag{397}$$

$$B = -\frac{2\beta_1}{\beta_0^2} \sum_{n=0}^{\infty} \frac{g(k_0)^{n+2}}{z_0^{n+1}} \frac{\Gamma(\gamma+n+2)}{\Gamma(\gamma+2)\Gamma(n+1)} \int_0^{z_0 \beta_0 \ln \sqrt{2} N} dt e^{-t} t^{(n+1)-1} \,. \tag{398}$$

From now on, we set $A = z_0 \beta_0 \ln \sqrt{2} N$. The calculation of the first integral yields

$$\begin{aligned} C &= \frac{2}{\beta_0} \sum_{n=0}^{\infty} \frac{g(k_0)^{n+1}}{z_0^{n+1}} \frac{\Gamma(\gamma+n+1)}{\Gamma(\gamma+1)\Gamma(n+1)} \int_0^{A} dt e^{-t} t^{(n+1)-1} \\ &= \frac{2}{\beta_0} \sum_{n=0}^{\infty} \frac{g(k_0)^{n+1}}{z_0^{n+1}} \frac{\Gamma(\gamma+n+1)}{\Gamma(\gamma+1)\Gamma(n+1)} n! \left(1 - e^{-A} \sum_{k=0}^{n} \frac{A^k}{k!} \right) \\ &= \frac{2}{\beta_0} \sum_{n=0}^{\infty} \frac{g(k_0)^{n+1}}{z_0^{n+1}} \frac{\Gamma(\gamma+n+1)}{\Gamma(\gamma+1)} \left(1 - e^{-A} \sum_{k=0}^{n} \frac{A^k}{k!} \right), \end{aligned} \tag{399}$$

while for the integral B we have

$$\begin{aligned} B &= -\frac{2\beta_1}{\beta_0^2} \sum_{n=0}^{\infty} \frac{g(k_0)^{n+2}}{z_0^{n+1}} \frac{\Gamma(\gamma+n+2)}{\Gamma(\gamma+2)\Gamma(n+1)} \int_0^{z_0 \beta_0 \ln \sqrt{2} N} dt e^{-t} t^{(n+1)-1} \\ &= -\frac{2\beta_1 z_0}{\beta_0^2} \sum_{n'=0}^{\infty} \frac{g(k_0)^{n'+2}}{z_0^{n'+2}} \frac{\Gamma(\gamma+2+n')}{\Gamma(\gamma+2)\Gamma(n'+1)} n'! \left(1 - e^{-A} \sum_{k=0}^{n'} \frac{A^k}{k!} \right) \\ &= -\frac{2\beta_1 z_0}{\beta_0^2} \sum_{n'=0}^{\infty} \frac{g(k_0)^{n'+2}}{z_0^{n'+2}} \frac{\Gamma(\gamma+2+n')}{\Gamma(\gamma+2)} \left(1 - e^{-A} \sum_{k=0}^{n'} \frac{A^k}{k!} \right). \end{aligned} \tag{400}$$

Finally we consider the sum of integrals C and B, *i.e.*

$$\begin{aligned} C+B &= 2\sum_{n=0}^{\infty}\frac{g(k_0)^{n+1}}{z_0^{n+1}}\Bigg(\frac{\Gamma(\gamma+n+1)\big(1-e^{-A}\sum_{k=0}^{n}\frac{A^k}{k!}\big)}{\beta_0\Gamma(\gamma+1)} \\ &\qquad - \frac{\beta_1 z_0}{\beta_0^2}\frac{\Gamma(\gamma+n+1)\big(1-e^{-A}\sum_{k=0}^{n-1}\frac{A^k}{k!}\big)}{\Gamma(\gamma+2)}\Bigg) \\ &= \frac{2}{\beta_0\Gamma(\gamma+1)}\sum_{n=0}^{\infty}\frac{g(k_0)^{n+1}}{z_0^{n+1}}\Gamma(\gamma+n+1)\Bigg[\Bigg(1-e^{-A}\sum_{k=0}^{n}\frac{A^k}{k!}\Bigg) \\ &\qquad - \frac{\beta_1 z_0}{\beta_0(\gamma+1)}\Bigg(1-e^{-A}\sum_{k=0}^{n-1}\frac{A^k}{k!}\Bigg)\Bigg]. \end{aligned} \tag{401}$$

In this case, the perturbative coefficients read

$$E^{(n+1)} = \frac{1}{z_0^{n+1}}\Gamma(\gamma+n+1)\Bigg[\Bigg(1-e^{-A}\sum_{k=0}^{n}\frac{A^k}{k!}\Bigg)-\frac{\beta_1 z_0}{\beta_0(\gamma+1)}\Bigg(1-e^{-A}\sum_{k=0}^{n-1}\frac{A^k}{k!}\Bigg)\Bigg]. \tag{402}$$

The asymptotic behavior can be computed considering the ratio

$$\frac{E^{(n+1)}}{E^{(n)}\cdot n} = \frac{1}{z_0}\Bigg(1+\frac{\gamma}{n}\Bigg)\frac{\Bigg[\Bigg(1-e^{-A}\sum_{k=0}^{n}\frac{A^k}{k!}\Bigg)-\frac{\beta_1 z_0}{\beta_0(\gamma+1)}\Bigg(1-e^{-A}\sum_{k=0}^{n-1}\frac{A^k}{k!}\Bigg)\Bigg]}{\Bigg[\Bigg(1-e^{-A}\sum_{k=0}^{n-1}\frac{A^k}{k!}\Bigg)-\frac{\beta_1 z_0}{\beta_0(\gamma+1)}\Bigg(1-e^{-A}\sum_{k=0}^{n-2}\frac{A^k}{k!}\Bigg)\Bigg]}, \tag{403}$$

which is the form of Eq. (328).